Top-Down Analysis of High-Capacity Fiber-Optic Transmission

vorgelegt von
Diplom - Ingenieur
Hadrien Louchet
aus Berlin

Von der Fakultät IV - Elektrotechnik und Informatik -
der Technischen Universität Berlin
zur Erlangung des akademischen Grades

Doktor der Ingenieurwissenschaften
Dr.-Ing.
genehmigte Dissertation

Promotionsausschuss:
Vorsitzender: Prof. Dr. Dr. Holger Boche
Berichter: Prof. Dr.-Ing. Klaus Petermann
Berichter: Prof. Dr.-Ing. Norbert Hanik

Tag der wissenschaftliche Aussprache: 22. Mai 2006

Berlin 2006
D 83

Acknowledgments

Contents

Chapter 1

Introduction

1.1 An overview of fiber-optic communication

1.1.1 Historical background

History of modern lightwave communication began in 1960 with the first demonstrations of lasers. At this time, the huge bandwidth potentially offered by optical transmission appeared as a promising solution to keep pace with the rapid development of the telecommunication industry. In 1966, Kao and Hockham predicted that the loss of the fibers available at this time ($1000\,\mathrm{dB/km}$) could be reduced to $20\,\mathrm{dB/km}$, making optical fiber a real alternative to copper cable [1]. The announcement four years later by the Corning Glass Works company of such a fiber led to an explosion of research and development in this field. The first commercial fiber-optic transmission systems appeared in the late seventies. In 1988, the first transatlantic fiber-optic cable was installed, but it is only with the introduction of Erbium-doped optical amplifier (EDFA) and wavelength-division multiplexing in early nineties that fiber-optic technology stood out as the best solution for long-haul high-capacity transmission. Since then, demand for more capacity has been driven by the phenomenal growth of the Internet (Internet traffic is doubling approximately each year [2]). Today about 500 million km of optical fiber are deployed around the world.

capacity	unregenerated reach	spectral efficiency	company	year
10.9 Tb/s	117 km	0.8 b/s/Hz	NEC	2001
6 Tb/s	6000 km	0.8 b/s/Hz	Alcatel	2002
5 Tb/s	1280km	0.8 b/s/Hz	Lucent	2002
10.2 Tb/s	100km	1.28 b/s/Hz	Alcatel	2001
320 Gb/s	200km	1.6 b/s/Hz	Siemens	2003

Table 1.1: Transmission records: Striving towards high capacity & high spectral efficiency (from the proceedings of *Optical Fiber Communication Conference* and *European Conference on Optical Communication*).

1.1.2   State of the art in fiber-optic communication

Fiber-optic transmission is by far the technology offering the largest bandwidth for telecommunication. A convenient way to share this huge bandwidth between several users is Wavelength-Division Multiplexing (WDM) [3]. WDM technology enables an easy upgrade of the system capacity either by increasing the utilized bandwidth (e.g. the number of channels) or by using the available bandwidth more efficiently (e.g. by increasing the bit-rate per channel). These two approaches present both advantages and drawbacks so that the best solution depends on the network's specific requirements. For that reason, tremendous efforts have been made in both directions and today several Tb/s can be transmitted over a single optical fiber (see Table 1.1).

Basic system components and available technologies

The basic building blocks of a fiber-optic transmission system are the transmitter, the transmission line and the receiver. The electrical signal is first converted to an optical signal at the transmitter and then sent into the transmission line, which consists of optical fibers, optical amplifiers (compensating for the fiber loss) and eventually of passive or active optical components such as optical filters, add-drop multiplexers, wavelength converters etc. At the receiver, the optical signal is converted back into electrical form in order to recover the original message.

The optical signal is generated in the **optical transmitter** by modulation of an optical carrier. In fiber-optic communication, the optical carrier is usually generated by a semicon-

ductor laser (e.g. Distributed Feedback (DFB) or Vertical Cavity Surface Emitting Laser (VCSEL) [4], [5]). Besides this classical single optical carrier generation, a frequency-comb (or supercontinuum) [6], [7] can be used as a multiple optical carrier source for WDM transmission. The optical carrier is modulated by a Mach-Zehnder interferometer [3] (enabling phase and/or amplitude modulation) or by an electro-absorption modulator [8]. For low bit-rate transmission over short distances, the laser can be directly modulated via its driving current.

An **optical fiber** consists of a cylindrical core of silica glass surrounded by a cladding with lower refractive index to enable light confinement in the fiber. The difference of refractive index is realized by doping the core, the cladding or both. Fiber characteristics depend on the concentration of doping elements and on the fiber geometry[1]. For example, loss and chromatic dispersion of commercially available transmission fibers (E.g. standard single mode fibers -SSMF-, dispersion-shifted fibers -DSF- or non-zero dispersion shifted fibers -NZDSF-) vary in the range 0.2...0.25 dB/km and -8...20 ps/(nm-km) in the 1550 nm region. For comparison, dispersion compensating fibers exhibit about 0.5 dB/km loss and -80 ps/(nm-km) chromatic dispersion in this region.

Most commonly used **optical amplifiers** are Erbium-Doped Fiber Amplifiers (EDFAs) [9]. They consist of optical fibers doped with Erbium ions (Er^{3+}), which are operated as an active laser medium: Erbium ions are excited to a higher energy level by a pump signal. Amplification (or stimulated emission) occurs when photons from the signal make excited Erbium ions to relax to the ground level by emission of a photon. Conversely, spontaneous relaxation of excited ions degrades the transmitted signal.

Recently intensively investigated Raman amplifiers [10], [11] represent a good opportunity for the realization of distributed amplification. The advantages of Distributed Raman Amplification (DRA) with respect to EDFAs are that amplification can be provided at any frequency by simply changing the pump wavelength and that it provides better OSNR performance and reduced nonlinear impairments [12].

The main component of an **optical receiver** is a photodetector (usually a PIN or avalanche

---

[1]See section 2.2.

Vendor	System	WDM channels	channel rate	unregenerated reach
Marconi	Multihaul 3000™	80	10Gb/s	3000 km
		80	40Gb/s	3000 km
Siemens	SURPASS hiT 7500™	160	10Gb/s	3000 km
Lucent	LambdaXtreme™	128	10Gb/s	4000 km
		64	40Gb/s	1000 km
Alcatel	1626 Light Manager™	96	10Gb/s	2600 km
Fujitsu	FLASHWAVE 7700 ™	80	10Gb/s	2000 km
Nortel	Optical Long Haul 1600™	640	1.25Gb/s	1500 km
		320	2.5Gb/s	1500 km
		80	10Gb/s	1500 km

Table 1.2: Some characteristics of commercial long-haul transmission systems available in 2005.

photodiode [4]), that converts the power of the incoming optical signal into current through photo-electric effect. Not only the amplitude, but also the phase of the signal can be detected with the help of passive optical components like a Mach-Zehnder interferometer [3]. The photodetector is followed by a lowpass filter and by the sampling and decision circuits.

1.1.3   A push forward for more bandwidth?

With the advent of Internet, applications like e-mail, e-commerce and data-transfer among others have boosted the demand for more bandwidth. So far, the access-network (from which end-users access the global network) has been dominated by copper and wireless technologies, creating a bottleneck for future broadband applications. However, solutions like Fiber-To-The-Home (FTTH) or 10Gb Ethernet are about to provide business and private users several hundreds of Mb/s, enabling new broadband services like high-speed Internet, video-conferencing, video-on-demand, teleworking, etc. Today's commercial transmission systems already offer capacity of several Tb/s (see Table 1.2) but since the demand for more bandwidth is expected to continue to grow [13], transmission rates of a few tens of Tb/s may be required in the core network in the next decades.

1.2 Motivation for a top-down analysis

The telecom crash of 2000 has increased the need to exploit legacy fiber plant and to reduce the cost and enhance the flexibility of novel optical transmission systems. These are very challenging tasks for three reasons: First, a capacity upgrade necessitates additional power to be launched in the fiber, leading to stronger nonlinear effects, that limit the ultimate capacity of optical transmission systems [14]. The second difficulty originates from the multi-dimensional nature of the optimization problem. Indeed, system designers are faced with a bewildering array of options for modulation format, rate and fiber type, making the search for an optimum system design through numerical simulations extremely time-consuming. Finally, the current approach for system design, which is mostly based on incremental improvement of existing solutions, may become obsolete as novel prospects like multi-level modulation formats [15], electrical dispersion compensation [16] or receivers implementing adaptive filtering or maximum likelihood sequence estimation [17] become available.

In this context, only a top-down analysis may help to target the best solutions and to define universal design rules. Analytical models offering insights into fiber nonlinearities exist but are restricted to single-fiber [18] or non-dispersion-managed transmission [19–22] or require the use of numerical calculations [23] and are therefore not suitable for a high-level analysis.

1.3 Outline

The purpose of the present work is to provide a comprehensive understanding of fiber nonlinearities in dispersion-managed WDM transmission systems. The goal is to derive universal design rules and to determine the ultimate capacity of fiber-optic transmission systems.

The theoretical framework required for this top-down analysis is briefly reviewed in **chapter 2**. A generic approach for the characterization of fiber nonlinearities in dispersion-managed transmission systems as well as an analytical model for the assessment of nonlinearly-induced impairments in WDM systems are presented in **chapter 3**. Some design guidelines for the reduction of nonlinear impairments are proposed in **chapter 4**. Not only the trans-

5

mission link design, but also the impact of information distribution in frequency and of fiber birefringence are investigated. In **chapter 5**, the issue of fiber nonlinearities is tackled from an "information theory" point of view: The maximal achievable capacity of fiber-optic transmission systems in presence of linear noise and fiber nonlinearities is derived and spectral efficiencies achievable with current technologies are discussed. Finally, some conclusions regarding the design of future high-capacity transmission systems are drawn in **chapter 6**.

Chapter 2

Wave Propagation in Optical Fibers

In the following chapter[1], the main characteristics of signal propagation in optical fibers are reviewed. Linear and nonlinear aspects are considered. Finally, the nonlinear Schrödinger equation describing the propagation of the slowly varying envelope of the electric field in single-mode optical fibers is derived.

2.1   Theoretical framework

Like all electromagnetic phenomena, propagation of light is governed by Maxwell's equations [24]. In a nonmagnetic, dielectric medium like silica, the electric field verifies the following wave equation [25]:

$$\nabla^2 \overrightarrow{E}(t) + \frac{1}{c^2}\frac{\partial^2 \overrightarrow{E}(t)}{\partial t^2} + \mu_0 \frac{\partial^2 \overrightarrow{P}(t)}{\partial t^2} = 0 \tag{2.1}$$

The 3-dimensional vectors $\overrightarrow{E}(t)$ and $\overrightarrow{P}(t)$ describe the electric field and the induced electric polarization. $c = 1/\sqrt{\epsilon_0 \mu_0}$ is the velocity of light in vacuum, ϵ_0 and μ_0 being the vacuum permittivity and permeability. The induced electric polarization results from the interaction of the propagating wave with the medium: Indeed, when a dielectric is subjected to an

---

[1]In the following, the Fourier Transform of the time-dependent complex variable $X(t)$ is noted $\tilde{X}(\omega)$ and its complex conjugate $X^*(t)$.

applied electric field, the internal charge distribution is distorted, leading to the generation of electric dipole moments. The resultant dipole moment per unit volume is the induced electric polarization $\overrightarrow{P}(t)$. Since $\overrightarrow{P}(t)$ depends on $\overrightarrow{E}(t)$, it can be expanded in a Taylor series as follows [26]:

$$\overrightarrow{P} = \epsilon_0(\chi^{(1)} * \overrightarrow{E} + \chi^{(2)} * \overrightarrow{E}\,\overrightarrow{E} + \chi^{(3)} * \overrightarrow{E}\,\overrightarrow{E}\,\overrightarrow{E} + \cdots) \tag{2.2}$$

Where * is the convolution operator. $\chi^{(1)}(t)$ is the first-order susceptibility tensor[2] and $\chi^{(1)}(t)\overrightarrow{E}(t)$ represents the principal component of the induced polarization. Because the S_iO_2 molecule is symmetric, $\chi^{(2)}(t) = 0$ for silica glasses [25]. As a consequence, most nonlinear effects originate from the third-order[3] susceptibility $\chi^{(3)}(t)$. Therefore, $\overrightarrow{P}(t)$ can be written as the sum of its linear, $\overrightarrow{P}_L(t)$, and nonlinear, $\overrightarrow{P}_{NL}(t)$, parts given as

$$\overrightarrow{P} = \overrightarrow{P}_L + \overrightarrow{P}_{NL} \tag{2.3}$$

with

$$\overrightarrow{P}_L = \epsilon_0(\chi^{(1)} * \overrightarrow{E}) \tag{2.4}$$

$$\overrightarrow{P}_{NL} \approx \epsilon_0(\chi^{(3)} * \overrightarrow{E}\,\overrightarrow{E}\,\overrightarrow{E}) \tag{2.5}$$

2.2 Linear characteristics

The wave propagation can be expressed in the frequency domain by taking the Fourier Transform of Eq. (2.1). For a linear medium ($\overrightarrow{P}_{NL}(t) = 0$), one obtains:

$$\nabla^2 \overrightarrow{\tilde{E}}(\omega) + \epsilon(\omega)\frac{\omega^2}{c^2}\overrightarrow{\tilde{E}}(\omega) = 0 \tag{2.6}$$

---

[2]$\chi^{(1)}$ is a 3×3 matrix. In a nonmagnetic isotropic medium like silica, $\chi^{(1)}$ is reduced to its diagonal components, $\chi_{(x,x,x)}$, which are all equal.

[3]$\chi^{(3)}$ is a cubic matrix with a 3×3 matrix at each lattice point.

with the frequency-dependent dielectric constant $\epsilon(\omega)$ defined as:

$$\epsilon(\omega) = 1 + \tilde{\chi}_{(x,x,x)}(\omega) \tag{2.7}$$

The real and imaginary parts of $\epsilon(\omega)$ can be related to the fiber refractive index $n(\omega)$ and absorption coefficient $\alpha(\omega)$ using the following definition [25]:

$$\epsilon(\omega) = \left(n(\omega) + i\frac{\alpha(\omega)c}{2\omega} \right)^2 \tag{2.8}$$

A solution of the wave equation Eq. (2.6) is easily obtained for a one-dimensional problem[4]. For a particular frequency, ω, it comes:

$$\overrightarrow{\tilde{E}}(z,\omega) = \overrightarrow{\tilde{E}}(0,\omega) \exp\left((-\alpha/2 + i\beta)z\right) \tag{2.9}$$

with the phase propagation constant $\beta = n\omega/c$ in this case. In the above equation, as well as in the rest of the analysis, z denotes the direction of propagation of the electrical field.

2.2.1 Fiber modes

More generally, the solutions of Eq. (2.6) have to satisfy the boundary conditions imposed by the optical fiber (fiber geometry, index profile, etc). The form of these solutions can be guessed by using the method of separation of variables:

$$\overrightarrow{\tilde{E}}(z,\omega) = F(x,y)\overrightarrow{\tilde{E}}(0,\omega) \exp\left(i\bar{\beta}z\right) \tag{2.10}$$

where $F(x,y)$ describes the transversal field distribution and $\bar{\beta}$ the propagation constant of a particular mode . These solutions are referred to as guided[5] modes of the fiber. Conditions to satisfy for these solutions to exist are obtained by substituting Eq. (2.10) in Eq. (2.6). A comprehensive study of fiber modes can be found in [3]. Important results for our analysis can be summarized as follows: When the so-called effective index of a particular mode

---

[4]I.e. for a single polarization propagating in an isotropic medium.
[5]Unlike leaky modes and radiation modes [27], guided modes effectively propagate in the fiber.

(or mode index) defined as $\bar{n} = \bar{\beta}c/\omega$ is lower than the refractive index of the cladding n_2, this mode ceases to be guided. Thus, it is possible to design fibers supporting only the fundamental mode[6]. The single-mode condition is met when the normalized frequency $V = \frac{\omega}{c}a\sqrt{n_1^2 - n_2^2} < 2.4$, a and n_1 being the core radius and refractive index. Single-mode fibers are of particular interest in fiber-optic communications because signal distortion resulting from the different mode velocities is avoided. For a single-mode fiber, each frequency component of the optical field propagates as:

$$\overrightarrow{\tilde{E}}(z,\omega) = \overrightarrow{x}F(x,y)\tilde{E}(0,\omega)\exp\left((-\alpha/2 + i\beta)z\right) \tag{2.11}$$

where $\overrightarrow{x}$ is the polarization unit vector and $F(x,y)$ the field distribution of the fundamental mode that can be approximated by a Gaussian:

$$F(x,y) \approx \exp\frac{-(x^2 + y^2)}{\rho_m^2} \tag{2.12}$$

where ρ_m is the mode field radius. In the following, we restrict our approach to single-mode fibers.

2.2.2 Optical losses

In today's standard fibers, the loss is around $0.2\,\mathrm{dB/km}$ in the $1.55\,\mu m$ region. The fiber attenuation coefficient α is defined as:

$$P_{out} = P_{in}\exp\left(-\alpha L\right) \tag{2.13}$$

where P_{in} is the power at the input of the fiber of length L and P_{out} the output power. Difference with the definition for α proposed in Eq. (2.8) is that not only material absorption but also other sources of power attenuation are considered. Material absorption is caused by electronic (in the ultraviolet region, $\lambda < 0.4\mu m$) and molecular (in the infrared region, $\lambda > 1.7\mu m$) resonance of pure silica and by the impurities included in the fiber. In today's

---

[6]The mode HE_{11} always exists.
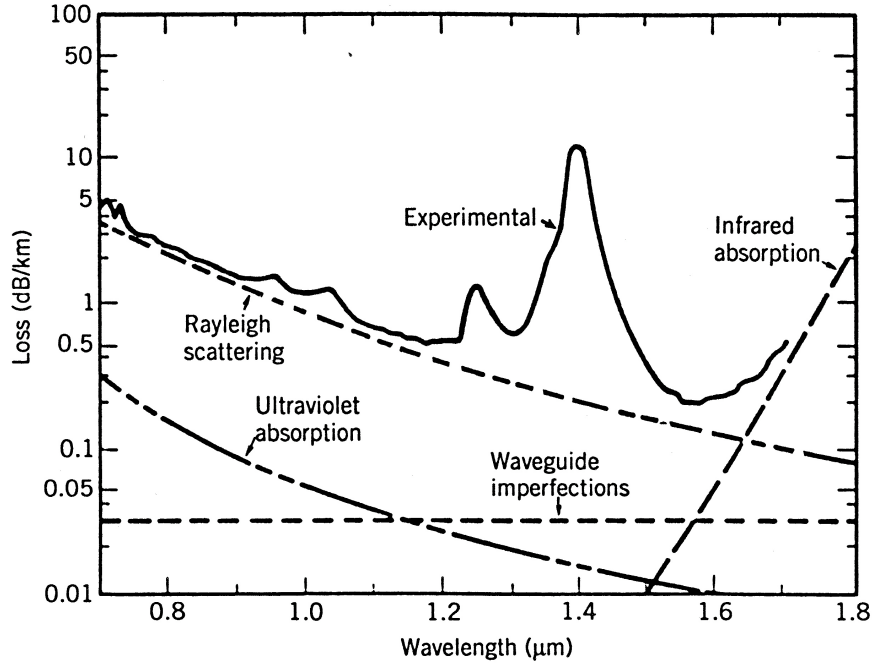
Figure 2.1: Spectral loss profile of a single-mode fiber (from [3]).

silica fibers, the vibrational resonance of ions OH^- is the main source of absorption due to impurities. It produces strong absorption peaks at the 2.73, 1.39, 1.24 and $0.95\mu m$ wavelengths as displayed in Fig. 2.1. Another major loss mechanism is Rayleigh scattering [28]. It arises from the random fluctuations of the refractive index[7]. The losses related to these phenomena are wavelength dependent[8]. Fiber bending [30] and microbending [31] losses are other kinds of loss mechanisms that have to be considered especially during the cabling. Power-dependent losses finding their origin in the nonlinear nature of the fiber (see section 2.3.3) also exist. The loss profile of single-mode silica fibers, together with the properties of EDFAs, enable an optimal transmission of optical signal in the so-called C-band (1.53 to 1.57 μm), L-band (1.565 to 1.625 μm). For optical amplification in the S-band (1.46 to 1.53 μm) other kinds of amplifier (e.g. fluoride fibers, [32]) must be employed.

---

[7]These fluctuations are due to small variations of the molecular density on a scale smaller than the optical wavelength.

[8]UV absorption $\sim 10^{1/\lambda}$, IR absorption $\sim 10^{-1/\lambda}$, Rayleigh scattering $\sim 1/\lambda^4$, see [29].
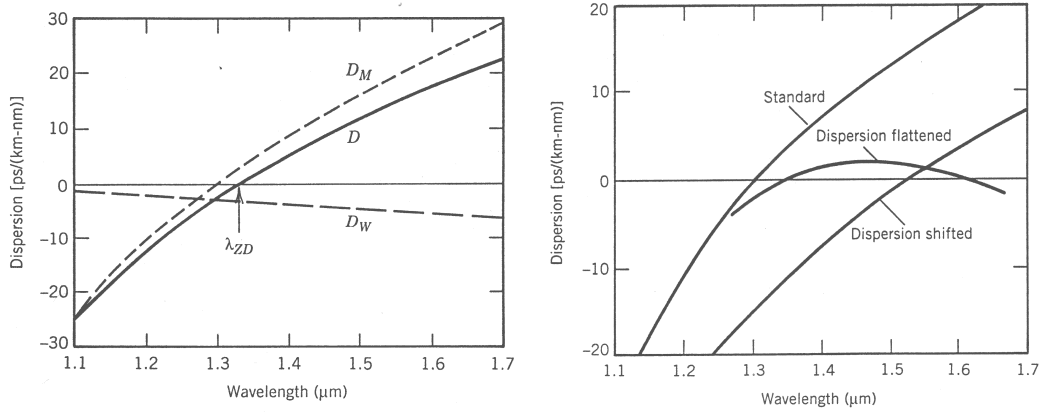
Figure 2.2: Left: material D_M and waveguide D_W dispersion. Right: total dispersion $(D_M + D_W)$ of various optical fibers (from [3]).

2.2.3 Chromatic dispersion

Similarly to α, the phase propagation constant β is also frequency-dependent and can be expanded in a Taylor series around the center frequency ω_0. Noting $\beta_i = \frac{\partial^i \beta}{\partial \omega^i}$, β can be written as:

$$\beta(\omega) \approx \beta_0 + \beta_1 \Delta\omega + \frac{1}{2}\beta_2 \Delta\omega^2 + \frac{1}{6}\beta_3 \Delta\omega^3 \cdots \qquad (2.14)$$

with $\Delta\omega = \omega - \omega_0$ and $\beta_1 = 1/v_g$, where v_g is the group velocity, i.e. the speed of the energy propagating at frequency ω_0. β_2 describes the frequency dependence of $1/v_g$, a phenomenon called chromatic dispersion or group-velocity dispersion (GVD) giving rise to pulse broadening for example. β_3 is known as the slope of GVD or second order GVD and should be considered when $\beta_2 \approx 0$ or in wide-band transmission systems. It is common to describe GVD with the dispersion parameter D (typically expressed in $ps/(nm - km)$) accounting for the dependence of $1/v_g$ on the wavelength rather than on frequency:

$$D = \frac{d}{d\lambda}\frac{1}{v_g} = -\frac{2\pi c}{\lambda^2}\beta_2 \qquad (2.15)$$

D can be written as the sum of two terms called material dispersion D_M and waveguide dispersion D_W (see Fig. 2.2). Whereas only n_2 appears in D_M, D_W depends on n_1, n_2 and V, i.e. on the fiber geometry. As a consequence, it is possible to modify D_W (and thus the

overall fiber dispersion) by changing the fiber index profile [3]. Dispersion compensating fibers (DCF), which present a negative value for D, rely on this principle.

2.2.4   Birefringence and polarization-mode dispersion

Polarization mode dispersion (PMD) is another dispersion phenomenon. It arises from the anisotropy of silica-fibers, which is due to a non-circular waveguide geometry or a non-symmetrical stress (see Fig. 2.3). This asymmetry induces a difference between the refractive index experienced by the orthogonally polarized HE_{11} modes[9]. As a consequence, single-mode fibers are not really single mode but support two distinct HE_{11} polarization modes, which do not travel at the same velocity (see Fig. 2.4). They are referred to as *fast* and *slow* modes (or Principal States of Polarization, PSP). This feature of the fiber is called birefringence [33], [34]. Birefringence is difficult to characterize for the whole fiber because stress, bending, vibration and temperature make the refractive index difference as well as the PSP evolve in time and along the fiber. However, it is possible to derive two coupled equations describing the local propagation of the orthogonal modes (see section 2.4 and [35]). These equations will be used to investigate the propagation of optical signals in birefringent, nonlinear ($\chi^{(3)} \neq 0$) fibers.

Although the arrival delay between [10] the slow and fast mode can be a major source of degradation in high-bit rate transmission systems (40 Gbit/s and higher), PMD and other polarization-dependent effects like polarization-dependent loss (PDL) will not be considered in this work. Extensive studies on the impact of polarization effects in optical-fiber transmission system are available in [36] and [37] .

---

[9]These modes are indistinguishable in a ideal fiber and are called degenerate modes, see Eq. (2.11).

[10]Also called differential group delay (DGD).
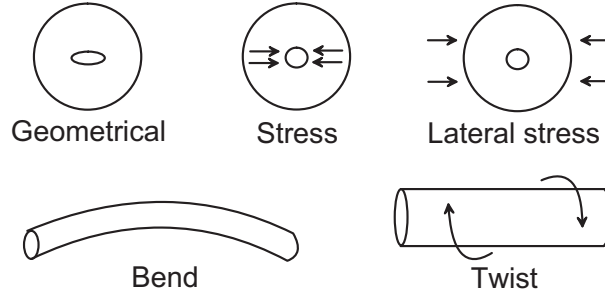
Figure 2.3: Intrinsic (a) and extrinsic (b) mechanisms of fiber birefringence.
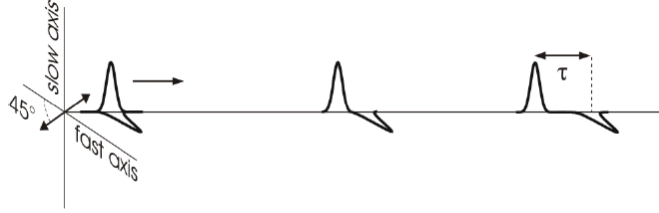
Figure 2.4: Pulse splitting due to birefringence.

2.3 Fiber nonlinearities

2.3.1 Origin of nonlinearities

Fiber nonlinearities arise from the nonlinear dependence of the induced polarization $\overrightarrow{P}$ on the propagating electrical field $\overrightarrow{E}$ (see Eq. (2.2)). This dependence is governed by the third-order susceptibility of silica fibers, $\chi^{(3)}$ which has a real, $\chi^{(3)}_{re}$, and an imaginary, $\chi^{(3)}_{im}$, part. Similarly to what was done for the first-order susceptibility $\chi^{(1)}$ (see Eq. (2.8)), $\chi^{(3)}_{re}$ can be related to a refractive index and $\chi^{(3)}_{im}$ to a loss mechanism. As a consequence, silica fibers present a signal-dependent refractive index, a phenomenon called Kerr-effect and signal-dependent loss mechanisms (Raman and Brillouin scattering).

Note: Examples treated in the following sections are limited to linearly co-polarized optical signals propagating in non-birefringent fibers.

2.3.2 Kerr-effect

Kerr nonlinearities are characterized by the power-dependent refractive index (for the fundamental mode) of the fiber [25]:

$$n = n_0 + \frac{3}{8n_0}\chi_{re}^{(3)}I = n_0 + n_2 I \tag{2.16}$$

n_2 is the nonlinear-index coefficient[11] and I the optical intensity in the fiber. Using Eq. (2.16) in Eq. (2.8) and Eq. (2.6) and assuming that n_2 can be treated as a small perturbation to n_0, the modified phase propagation constant accounting for the Kerr-effect [25] becomes:

$$\beta' = \beta + \gamma P \tag{2.17}$$

where β is the propagation constant in the linear case, $P(t) = |E(t)|^2$ the optical power and γ the fiber nonlinear coefficient defined as:

$$\gamma = \frac{n_2\omega}{cA_{eff}} \tag{2.18}$$

with A_{eff} the fiber effective area:

$$A_{eff} = \frac{\left(\int\limits_{-\infty}^{+\infty}\int |F(x,y)|^2 dxdy\right)^2}{\int\limits_{-\infty}^{+\infty}\int |F(x,y)|^4 dxdy} \tag{2.19}$$

Depending on whether the intensity fluctuations are caused by the channel itself, by one or several neighboring channels, one distinguishes between self-phase modulation (SPM), cross-phase modulation (XPM) or four-wave mixing (FWM).

---

[11]$n_2 \approx 3 \times 10^{-20} m^2/W$ for silica fibers.

Self-phase modulation (SPM)

SPM gives rise to a time-dependent phase modulation of the optical signal leading to spectral broadening. Neglecting GVD and loss and noting $P(t)$ the pulse power, L the fiber length, the SPM-induced phase shift approximated as:

$$\Delta\varphi_{SPM} = -\gamma P(t)L \tag{2.20}$$

In presence of GVD, SPM leads to amplitude distortions because chromatic dispersion converts the nonlinear phase shift into amplitude variations. In Soliton transmission systems [36], [38], this nonlinear chirp is used to balance the effects of chromatic dispersion. A major drawback of Soliton systems is that they require careful dispersion management, especially at high-bit-rates. Moreover, they are very complex to realize in a multi-channel configuration [3], and are thus rarely used for high-capacity transmission systems.

Cross-phase modulation (XPM)

In XPM, the modulation of the fiber refractive index is caused by power variations of adjacent channels. Similarly to SPM, XPM-induced phase modulations are partially converted to intensity distortions of the optical signal by chromatic dispersion. XPM-interaction between two channels can be characterized by the walk-off parameter, d:

$$d = \frac{1}{v_{g1}} - \frac{1}{v_{g2}} = D\Delta\lambda \tag{2.21}$$

with v_{g1} and v_{g2} the group velocities of the two interacting channels and $\Delta\lambda$ the channel spacing. Since XPM occurs only when pulses overlap, it is reduced in general with increased dispersion or channel spacing (so that channels propagate faster through each-other).

Four wave mixing (FWM)

FWM describes a process in which three frequency components (f_i, f_j, f_k) interact through the medium to generate new spectral components at the frequencies [25]:

$$f_{ijk} = f_i + f_j - f_k \tag{2.22}$$

Since i, j, k are interchangeable, nine[12] new spectral components are generated. SPM ($i = j = k$) and XPM ($i \neq j = k$ and $ik \neq j$) are special cases of FWM. For transmission over a single fiber, the power of the generated spectral component is [39]:

$$P_{ijk} = \eta(\gamma LD/2)^2 P_i P_j P_k \tag{2.23}$$

where P_i is the input power of the spectral component f_i and D is a degeneracy factor which amounts 1,3 or 6 depending on whether 3, 2 or none of the interacting spectral components are equal. η is the FWM efficiency, [39]:

$$\eta = \frac{\alpha^2}{\alpha^2 + \Delta\beta^2} \left(1 + \frac{4 \exp{(-\alpha L)} \sin{(\Delta\beta L/2)}}{(1 - \exp{(-\alpha L)})^2} \right) \tag{2.24}$$

with $\Delta\beta = \beta_{ijk} + \beta_k - \beta_j - \beta_i$ the phase matching coefficient. Neglecting the second order GVD ($\beta_3 = 0$), $\Delta\beta$ is given with respect to the fiber dispersion:

$$\Delta\beta(\omega) \approx -(\omega_i - \omega_k)(\omega_j - \omega_k)\beta_2(\omega_0) \tag{2.25}$$

FWM is a major limitation in DWDM transmission systems [40] leading to amplitude and phase jitter in the optical signal. A general treatment of FWM including polarization effects can be found in [41].

---

[12]Assuming f_i, f_j and f_k are different.

2.3.3 Stimulated light scattering

Contrary to the Kerr-effect, the medium plays an active role in Raman (SRS) and Brillouin (SBS) scattering [3]. These effects can be understood as the scattering of a photon to a lower energy photon[13]. The energy difference appears in the form of an optical phonon [3] in SRS and an acoustic phonon in SBS.

In a WDM transmission system, SRS can couple different channels, leading to the depletion of the shorter wavelength channel, while the longer wavelength channel is amplified. For silica fibers, the maximum power transfer occurs for a frequency difference around $12\,\mathrm{THz}$. This effect is used for optical amplification in Raman-amplifiers [42]. SBS and SRS present a threshold behaviour[14] but in contrast to SRS, the SBS threshold is hardly reached in common optical transmission systems[15]. Conversely, SRS is likely to happen in wide-band WDM transmission systems. However, it has been shown [43–45] that Kerr-effect affects the performance of common optical transmission systems more than SRS (indeed, the tilt in spectrum due to Raman pumping has to be compensated but pattern effects affecting the ones level can be neglected as a consequence of the short walk-off length between interacting channels). As a consequence, SRS-and SBS-induced limitations are not considered in this work.

2.4 Generalized nonlinear Schrödinger equation

In Silica-based fibers, the nonlinear-index coefficient $n_2 I$ is usually much smaller[16] than the linear part of the refractive index n_0. Consecutively, $n_2 I$ can be treated as a small perturbation to n_0. For a single polarization, the solution for Eq. (2.6) (with the modified dielectric constant, $\epsilon = (n_0 + n_2 I + i\alpha c/2\omega)^2$) has the form:

$$E(t,z) = F(x,y)A(t)e^{(-i\omega_0 t)} \exp{(i\beta z)} \tag{2.26}$$

---

[13]Resulting in a loss for the considered spectral component.
[14]I.e. do not happen until a certain power level has been reached.
[15]$5-10mW$ are required within the SBS gain bandwidth (~ 100MHz) [25].
[16]Even at high power levels.

Where A is the slowly varying envelope of the electrical field (i.e. the modulated part of the signal, which is of interest in optical communication systems) and β the propagation constant to be determined. Neglecting β_3 against β_2 and SRS and SBS against Kerr-effect, we find from Eq. (2.26) and Eq. (2.6) that $A(t)$ verifies the following equation:

$$\frac{\partial A}{\partial z} + \beta_1 \frac{\partial A}{\partial t} + \frac{i}{2}\beta_2 \frac{\partial^2 A}{\partial t^2} + \frac{\alpha}{2} A = i\gamma |A|^2 A \qquad (2.27)$$

By making the transformation $T = t - z/v_g$, Eq. (2.27) can be re-written in frame moving at the group velocity (v_g):

$$\frac{\partial A}{\partial z} + \frac{i}{2}\beta_2 \frac{\partial^2 A}{\partial T^2} + \frac{\alpha}{2} A = i\gamma |A|^2 A \qquad (2.28)$$

Eq. (2.28) is known as the *Nonlinear Schrödinger Equation (NLSE)*, which is commonly used to describe the propagation of a single polarization state in optical fibers. The case of birefringent fibers is more complicated since the propagation of one mode is affected by the other through fiber nonlinearities. A derivation of the equations governing evolution of the two polarization components is derived in [25] for linearly birefringent fibers:

$$\frac{\partial A_x}{\partial z} + \frac{i}{2}\beta_2 \frac{\partial^2 A_x}{\partial T^2} + \frac{\alpha}{2} A_x = i\gamma \left(|A_x|^2 + \frac{2}{3}|A_y|^2 \right) A_x + \frac{i\gamma}{3} A_x{}^* A_y{}^2 \exp\left(-2i\Delta\beta z\right) \qquad (2.29)$$

where A_x and A_y are the complex amplitudes of the slowly varying electrical fields of the polarization components and $\Delta\beta = \beta_x - \beta_y$ the wave vector mismatch due to modal birefringence (see section 2.2.4). The last term can be neglected when the beat-length $(L_B = 2\pi/\Delta\beta)$ is much smaller than the propagation distance, more exactly L_B has to be smaller than the fiber effective length L_{eff} (see next section). The solution for A_y is obtained from Eq. (2.29) by inverting A_x and A_y. For elliptically birefringent fibers[17], this equation becomes [35]:

$$\frac{\partial A_x}{\partial z} + \frac{i}{2}\beta_2 \frac{\partial^2 A_x}{\partial T^2} + \frac{\alpha}{2} A_x = i\gamma(|A_x|^2 + B|A_y|^2)A_x \qquad (2.30)$$

---

[17]PSPs vary along the fiber.

where B is a factor depending on the relative disposition of the polarization of incoming light with the PSP. Propagation in randomly birefringent fibers can be described by setting $B = 8/9$ [46], [47].

2.5 Fiber parameters

The following scale lengths can be very helpful to characterize the pulse evolution over a single optical fiber and to give insight into the dominant system limitations.

Effective fiber length, L_{eff}

The effective length is the length of a loss-less fiber causing the same nonlinear impact as a lossy fiber of length L and attenuation coefficient α:

$$L_{eff} = \int_0^L \exp(-\alpha z) dz = \frac{1 - \exp(-\alpha L)}{\alpha} \tag{2.31}$$

For example 80km of standard single-mode Fiber (SSMF with $\alpha = 0.2 dB/km$ [3]) correspond to an effective length of about 20km.

Dispersion length, L_D

The dispersion length defines the distance over which a chirp-free Gaussian pulse ($A(t) \sim \exp -(T/T_0)^2$) broadens by a factor of $\sqrt{2}$ due to chromatic dispersion [3]:

$$L_D = \frac{T_0^2}{|\beta_2|} \tag{2.32}$$

with T_0 a measure of the pulse width (typically the half width at $1/e$ intensity point).

Nonlinear length, L_{NL}

The nonlinear length defines the distance over which the phase change due to Kerr nonlinearities becomes one radian[18] [3]:

$$L_{NL} = \frac{1}{\gamma P_0} \qquad (2.33)$$

with P_0 the pulse peak power.

Insight into pulse propagation regimes

The above defined parameters enable us to distinguish between different propagation regimes:

• $L \ll L_{NL}$ and $L \ll L_D$: The fiber length is much shorter than the dispersion and nonlinear length so that neither GVD nor Kerr-effect affect the signal.

• $L \ll L_{NL}$ and $L \geqslant L_D$: Pulse evolution is governed by dispersion. Nonlinearities can be neglected.

• $L \geqslant L_{NL}$ and $L \ll L_D$: Pulse evolution is governed by nonlinear effects.

• $L \geqslant L_{NL}$ and $L \geqslant L_D$: Dispersion and nonlinearities act together. Transmission performance is limited by dispersion-nonlinearities interplay.

---

[18]Fiber loss is neglected.

Chapter 3

Nonlinearities in Fiber-Optic Transmission Systems

The aim of this chapter is to provide a comprehensive understanding of fiber nonlinearities and a simple characterization of their impact on the transmitted signal. An analytical method to characterize fiber nonlinearities in dispersion-managed transmission systems is presented. Finally, we introduce the concept of the *nonlinear diffusion bandwidth*, a simple metric for understanding and predicting nonlinear degradation in single-channel and Wavelength-Division Multiplexed (WDM) transmission systems.

3.1 Frequency domain analysis

3.1.1 Motivation

The nonlinear Schrödinger equation (NLSE) as given in Eq. (2.28) can not be solved analytically for the case of an arbitrary signal launched into the fiber (an analytical solution only exists for Soliton transmission). Therefore, a numerical approach[1] is often necessary to predict the signal evolution along the fiber. Unfortunately, simulations involving a high number of channels are prohibitively time consuming and do not provide any general guide-

---

[1]See appendix A

line for the design of high-capacity transmission systems. For that reason, an alternative to numerical simulation is necessary.

As we will show in the following, linear propagation (i.e. loss and dispersion) is described by a simple attenuation and phase rotation in the frequency domain. It follows from that, that the impact of Kerr nonlinearities can be described by a single additional term, a key simplification in our analysis.

3.1.2 Methodology

The NLSE can be expressed in the frequency domain by taking the Fourier-transform [2] of its time-domain counterpart (see Eq. (2.28)):

$$
\begin{aligned}
\frac{\partial \tilde{A}(\omega, z)}{\partial z} &= \frac{i}{2}\omega^2 \beta_2 \tilde{A}(\omega, z) - \frac{\alpha}{2}\tilde{A}(\omega, z) \\
&\quad + i\gamma \int \int \tilde{A}(\omega_1, z)\tilde{A}(\omega_2, z)\tilde{A}^*(\omega - \omega_1 + \omega_2, z)d\omega_1 d\omega_2
\end{aligned}
\tag{3.1}
$$

In the frequency domain, loss and chromatic dispersion are described by a simple attenuation and a phase rotation. Setting $\tilde{A}(\omega, z) = \tilde{U}(\omega, z)e^{(\frac{-\alpha + i\beta_2\omega^2}{2})z}$ so that $\tilde{U}(\omega, z)$ is independent of distance for linear transmission and is only affected by fiber nonlinearities, Eq. (3.1) becomes:

$$
\begin{aligned}
\frac{\partial \tilde{U}(\omega, z)}{\partial z} &= i\gamma \int \int \exp\left(-\alpha z - i\beta_2 \Delta\Omega z\right) \\
&\quad \times \tilde{U}(\omega_1, z)\tilde{U}(\omega_2, z)\tilde{U}^*(\omega - \omega_1 + \omega_2, z)d\omega_1 d\omega_2
\end{aligned}
\tag{3.2}
$$

with $\Delta\Omega = (\omega - \omega_1)(\omega - \omega_2)$.

Volterra Series

The NLSE (and its frequency counterpart, Eq. 3.2) are characteristic of nonlinear systems with memory. In the frequency domain, linear systems with memory are described by the following relationship between the Fourier-transform of the input signal $\tilde{X}(\omega)$ and the

---

[2] $F(\omega) = \int_{-\infty}^{\infty} f(d)\exp -i\omega t dt$

Fourier-transform of the output signal $\tilde{Y}(\omega)$:

$$\tilde{Y}(\omega) = H(\omega)\tilde{X}(\omega) \tag{3.3}$$

with $H(\omega, z)$ the transfer function of the system. Similarly, a memoryless nonlinear system can be described by an expansion in Taylor series:

$$\tilde{Y}(\omega) = \sum_{n=1}^{\infty} a_n \tilde{X}(\omega_1)\tilde{X}(\omega_2)...\tilde{X}(\omega_n)\tilde{X}(\omega - \omega_1...\omega_n) \tag{3.4}$$

with a_n the Taylor series coefficients. Expansion in Volterra Series Transfer Function (VSTF) [48, 49], combines these two approaches. In the frequency domain a VSTF is obtained as:

$$\begin{aligned}
\tilde{Y}(\omega) = \quad & \sum_{n=1}^{\infty} \quad \int \cdot \cdot \int H_n(\omega_1, ..., \omega_{n-1}, \omega - \omega_1 - ... - \omega_{n-1}) \\
& \times \tilde{X}(\omega_1)...\tilde{X}(\omega_{n-1}) \\
& \times \tilde{X}(\omega - \omega_1 - ... - \omega_{n-1})d\omega_1 \cdots d\omega_{n-1} \tag{3.5}
\end{aligned}$$

where $H_n(\omega_1, ..., \omega_n)$ is the nth-order frequency domain Volterra kernel. The VSTF related to Eq. (3.2) is then:

$$\begin{aligned}
\tilde{U}(\omega, z) \quad = \quad & H_1(\omega, z)\tilde{U}(\omega) \\
& + \int\int H_3(\omega_1, \omega_2, \omega - \omega_1 + \omega_2, z)\tilde{U}(\omega_1)\tilde{U}^*(\omega_2)\tilde{U}(\omega - \omega_1 + \omega_2)d\omega_1 d\omega_2 \\
& + \int\int\int\int H_5(\omega_1, \cdots, \omega_4, \omega - \omega_1 + \omega_2 - \omega_3 + \omega_4, z) \\
& \times \tilde{U}(\omega_1)\tilde{U}^*(\omega_2)\tilde{U}(\omega_3)\tilde{U}^*(\omega_4)\tilde{U}(\omega - \omega_1 + \omega_2 - \omega_3 + \omega_4)d\omega_1 d\omega_2 d\omega_3 d\omega_4 \\
& + \cdots \tag{3.6}
\end{aligned}$$

where $\tilde{U}(\omega)$ stands for $\tilde{U}(\omega, z = 0)$. Note that $\tilde{U}(\omega)$ is equal to $\tilde{A}(\omega)$. In Eq. (3.6) all even order kernels are set to zero due to the absence of even order nonlinearities in silica fibers (see section 2.1). The above VSTF can be evaluated numerically to predict system

performance. Results obtained by retaining only the 3 or 5 first order terms were shown to be at least as good as the ones obtained with the SSF method with regard to the accuracy of the results and computation time [23], [50].

Perturbation approach

In Eq. (3.6), H_1 is the operator for linear propagation and H_3 is related to the "first order nonlinearities" (generated by the linear evolution, $H_1\tilde{A}$, of the signal). Higher order terms represent nonlinear interferences between $H_1\tilde{A}$ and already generated nonlinear spectral components $(H_3, H_5, \cdots)$. Exact solution of the NLSE is obtained for $n \to \infty$. However, when nonlinear effects are small compared to the signal, [19], higher order terms can be neglected so that the Volterra series expansion can be truncated after H_3. The derivative over z of Eq. (3.6) truncated after H_3 is:

$$
\begin{aligned}
\frac{\partial \tilde{U}(\omega, z)}{\partial z} &= \frac{\partial H_1(\omega, z)}{\partial z}\tilde{U}(\omega) + \\
&\quad \int\int \frac{\partial H_3(\omega_1, \omega_2, \omega, z)}{\partial z}\tilde{U}(\omega_1)\tilde{U}(\omega_2)\tilde{U}^*(\omega - \omega_1 + \omega_2)d\omega_1 d\omega_2
\end{aligned} \tag{3.7}
$$

so that H_1 is then easily obtained by identifying the first order terms of Eq. (3.1) and Eq. (3.7):

$$
\frac{\partial H_1(\omega, z)}{\partial z} = 0 \Rightarrow H_1(\omega, z) = C_1(\omega) \tag{3.8}
$$

Similarly, one obtains for H_3:

$$
\frac{\partial H_3(\omega_1, \omega_2, \omega, z)}{\partial z} = i\gamma \exp\left(-\left(\alpha + i\Delta\Omega\beta_2\right)z\right) \Rightarrow
$$
$$
H_3(\omega_1, \omega_2, \omega, z) = \int_0^z i\gamma \exp\left(-\left(\alpha + i\Delta\Omega\beta_2\right)z'\right)dz' + C_2 \tag{3.9}
$$

C_2 is set to 0 so that boundary condition for $z = 0$ is verified. Constant $C_1(\omega)$ ensures energy conservation so that:

$$
\int |U(\omega, L)|^2 d\omega = \int \left| C_1(\omega)U(\omega) + \int\int H_3 \cdots d\omega_1 d\omega_2 \right|^2 d\omega \tag{3.10}
$$

For weak nonlinearities, we can assume $C_1(\omega) \approx 1$ (see (3.6)). The signal after propagation over a single fiber of length L is obtained by integrating Eq. (3.7) over z:

$$
\begin{aligned}
\tilde{U}(\omega, L) = & \ \tilde{U}(\omega) + \int\int \left(\int_0^L i\gamma \exp\left(-(\alpha + i\Delta\Omega\beta_2)z\right)dz \right) \\
& \times \tilde{U}(\omega_1)\tilde{U}\omega_2)\tilde{U}^*(\omega - \omega_1 + \omega_2)d\omega_1 d\omega_2 \\
= & \ \tilde{U}(\omega) + \ \delta_{NL}(\omega, L)
\end{aligned}
\tag{3.11}
$$

This last result notably simplifies the considered problem, since it reduces the description of the signal propagation in optical fibers to an additional term, $\delta_{NL}(\omega, L)$, representing the impact of fiber nonlinearities on the transmitted signal.

3.1.3 General analytical expression for the nonlinear perturbation

The above results have been derived for the case of a transmission over a single optical fiber. The case of real transmission systems is more complex to describe because transmission lines usually consist of many sections, each comprising a transmission fiber and one or several optical amplifiers and dispersion compensation modules to compensate (totally or partially) for loss and chromatic dispersion accumulated in the line. In this configuration, the definition for H_3 proposed in Eq. (3.9) has to be reviewed since neither α nor β_2 are constant over z. For that reason, it is much more convenient to consider the gain and dispersion profiles, $G(z)$ and $D(z)$, of the transmission line rather than α and β_2 for the case of a signal propagating over a complex transmission line. $G(z)$ and $D(z)$ are defined as follows (see Fig. 3.1):

$$
\frac{\partial G(z)}{\partial z} = -\alpha(z) + g(z) + \sum_i g_i \delta_i(z - z_i) \tag{3.12}
$$

$$
\frac{\partial D(z)}{\partial z} = \beta_2(z) + \sum_j d_j \delta(z - z_j) \tag{3.13}
$$

with $g(z)$ accounting for distributed amplification (e.g. Distributed Raman Amplification). g_i is the gain of the bulked amplifiers and $\delta(z)$ the Dirac function so that $g_i\delta_i(z-z_i)$ describes
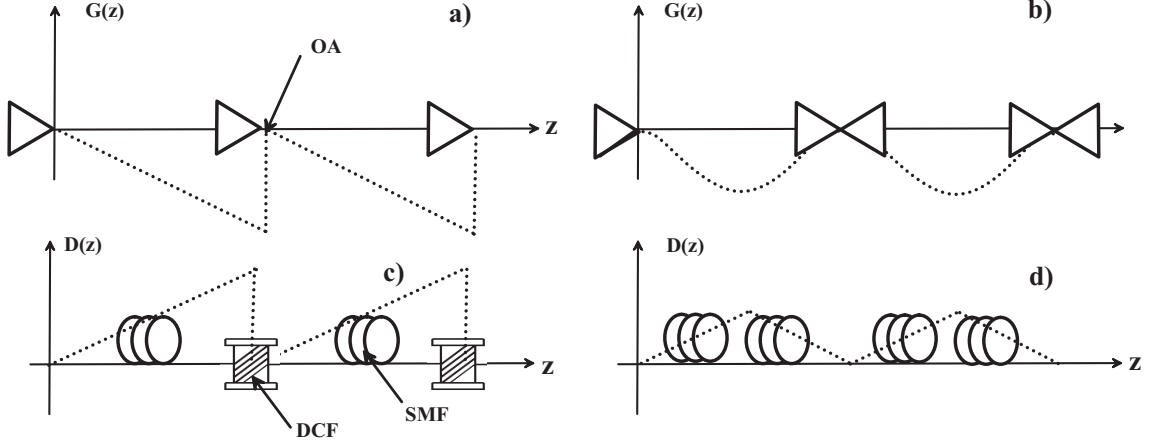
Figure 3.1: Example of gain, $G(z)$, and dispersion, $D(z)$, profiles in transmission lines: Amplification maps with EDFAs (a) and forward and backward Raman pumping (b). Dispersion maps with (c) or without (d) bulked dispersion compensation.

the effect of the ith lumped amplifier (at position z_i). Identically $d_j\delta_i(z - z_j)$ accounts for the jth bulk dispersion-compensation module. $H_3(\omega_1, \omega_2, \omega, z)$ can be re-expressed as a function of $G(z)$ and $D(z)$:

$$H_3(\Delta\Omega, z) = \int_0^z i\gamma \exp\big(G(z') - i\Delta\Omega D(z')\big)dz' \qquad (3.14)$$

This result is of particular interest for our study, since it allows us to consider the impact of the amplification and dispersion map on the fiber nonlinearities.

3.1.4 Validity domain

Nonlinear interferences between amplifier noise and signal (Gordon-Mollenauer effect [51]) are not taken into account by the present approach. Usually, they can be neglected for non-Soliton systems if the amplifier noise is weak. Raman and Brillouin scattering were also neglected for the reason that we expect the Kerr-effect to be the major source of non-linear impairments. Although this perturbation approach may be limited to relatively small nonlinearities, it should yield reliable results within its validity domain and provide reliable trends concerning the impact of transmission line design on Kerr-induced impairments.

3.2 Nonlinear characterization of the transmission line

A closed-form solution for the nonlinear Schrödinger equation for arbitrary signal and transmission line has been reported in Eq. (3.11). This solution is given as the sum of the solution for linear transmission and a perturbation term representing nonlinear effects. After loss and dispersion compensation, the transmitted signal is described by:

$$\tilde{A}(\omega, L) = \tilde{A}(\omega) + \delta_{OA}(\omega, L) + \delta_{NL}(\omega, L) \tag{3.15}$$

where $\tilde{A}(\omega)$ is the Fourier-transform of $A(t, z = 0)$, the slowly varying (compared to the light frequency) envelope of the electrical field. $\delta_{OA}(\omega, L)$ accounts for the noise generated during optical amplification[3] and $\delta_{NL}(\omega, L)$ is a small perturbative term describing the impact of fiber nonlinearities on the signal:

$$
\begin{aligned}
\delta_{NL}(\omega, L) &= i \int\int \overbrace{\left(\int_0^L \gamma(z) e^{(G(z) - i\Delta\Omega D(z))} dz \right)}^{\eta} \\
&\qquad \times \underbrace{\tilde{A}(\omega_1)\tilde{A}(\omega_2)\tilde{A}^*(\omega - \omega_1 + \omega_2)}_{\tilde{S}} d\omega_1 d\omega_2 \\
&= i \int\int \eta(\Delta\Omega)\tilde{S}(\omega, \omega_1, \omega_2) d\omega_1 d\omega_2
\end{aligned}
\tag{3.16}
$$

$G(z)$ and $D(z)$, defined in Eq. (3.13), represent the gain and dispersion profiles of the transmission line: $G(z)$ accounts on the one hand for fiber loss and on the other hand for lumped or distributed optical amplification. $D(z)$ is the dispersion accumulated by the signal in the transmission line and $\gamma(z)$ takes the values of the fibers' nonlinear coefficients. The condition for this closed form to be valid is $|\delta_{NL}(\omega, L)| \ll |A(\omega)|$, i.e. for weak nonlinearities.

3.2.1 Nonlinear transfer function of the transmission line

In Eq. (3.16) fiber and signal contributions are clearly separated so that the nonlinear characteristics of the transmission line can be determined independently of the propagating

---

[3] Amplified Spontaneous Emission (ASE) [9].

signal. In the following, we refer to $\eta(\Delta\Omega)$ as the *nonlinear transfer function* of the transmission line.

Single-fiber transmission

For single-fiber transmission, the dispersion and gain profiles are given as:

$$G(z) = -\alpha z + \int_0^z g(z')dz' \qquad (3.17)$$

$$D(z) = D_0 + \beta_2 z \qquad (3.18)$$

where α and β_2 are the loss and dispersion parameter of the transmission fiber, D_0 is the amount of pre-compensation and $g(z)$ describes the gain of a distributed optical amplification. In most common systems, lumped amplifiers like EDFAs are used for optical amplification and $g(z) = 0$. In that simple case, the *nonlinear transfer function* of the transmission line is easily derived from Eq. (3.16):

$$\eta(\Delta\Omega) = -\gamma \left(\frac{1 - e^{(-\alpha - i\Delta\Omega\beta_2)L}}{\alpha + i\Delta\Omega\beta_2} \right) e^{-i\Delta\Omega D_0} \qquad (3.19)$$

For $e^{-(\alpha L)} << 1$, i.e. when the fiber length is much larger than its effective length L_{eff}, the *nonlinear transfer function* can be approximated by:

$$\eta(\Delta\Omega) \approx -\frac{\gamma}{\alpha\sqrt{1 + \left(\frac{\Delta\Omega\beta_2}{\alpha}\right)^2}} e^{-i(\Delta\Omega D_0 + \varphi(\Delta\Omega))} \qquad (3.20)$$

with

$$\varphi(\Delta\Omega) = atan(\Delta\Omega\beta_2/\alpha) \qquad (3.21)$$

Besides EDFAs, another way to compensate for fiber loss is to distribute the optical amplification along the fiber. Recently intensively investigated Raman amplifiers [10, 11] represent a good opportunity for the realization of distributed amplification, which is of particular interest for the reduction of nonlinearities [12, 52] (see also the impact of Raman amplification
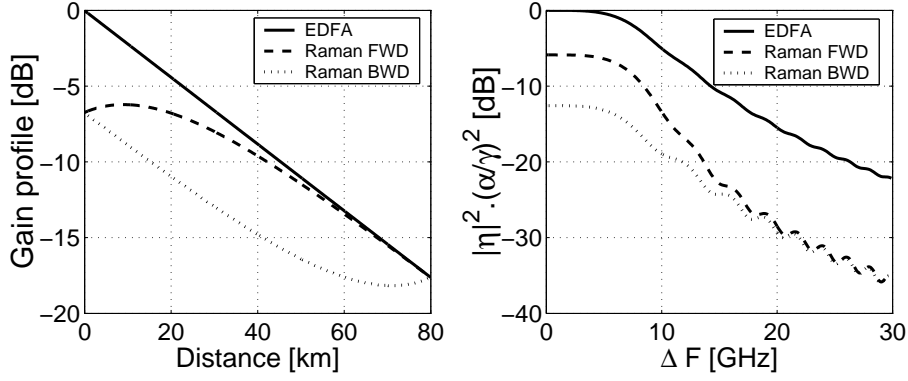
Figure 3.2: Gain profiles (-16dB) over 80 km SSMF and normalized nonlinear transfer function η (according to Eq. (3.16)) for the case of lumped (EDFA) and distributed amplification (forward and backward Raman pumping). For Raman amplification, $g_{r,b}$=0.8 /W/m and $P_o = 100$ mW. $\Delta F = \sqrt{\frac{|\Delta\Omega|}{4\pi^2}}$

on the magnitude of the *nonlinear transfer function* in Fig. 3.2). In Raman amplification, optical channels are amplified by a pump signal at shorter wavelength. This technique makes use of the Raman scattering process occurring in silica-fiber (see section 2.3.3). When the pump depletion can be neglected[4], $g(z)$ is given as [3]:

$$g(z) = g_{rf}P_0 e^{-\alpha z} \tag{3.22}$$

$$g(z) = g_{rb}P_0 e^{-\alpha(L-z)} \tag{3.23}$$

g_{rf} and g_{rb} are the gains for forward and backward Raman pumping and P_0 the input power of the pump laser. In that case, there is no simple analytical expression for $\eta(\Delta\Omega)$, which has to be assessed numerically (see Fig. 3.2). Because EDFA is considered as the state-of-the-art technology for optical amplification, this work mainly focuses on systems with lumped amplification (i.e. $g(z) = 0$). However, the concepts presented so far and those to be introduced can be easily extended to the case of distributed amplification.

---

[4]I.e. for small signal amplification.

Multi-span transmission

In real transmission systems, the optical signal is usually amplified every 50-100km and the dispersion compensation is often performed in line[5] to avoid large signal distortion (especially before amplification). In order to account for these complex amplification and dispersion schemes, η has to be derived for n consecutive fiber-sections:

$$\eta(\Delta\Omega) = \sum_{j=1}^{n} \int_0^{L_j} \gamma_j e^{(G_j - \alpha_j z - i[\Delta\Omega(D_j + \beta_{2,j}z)])} dz = \sum_{j=1}^{n} \eta_j(\Delta\Omega) \qquad (3.24)$$

where G_j and D_j are the signal accumulated gain and dispersion at the input of the jth fiber-section. It is helpful to describe the transmission line as a concatenation of *spans* rather than as a concatenation of fiber-sections. We refer to span as a basic building-block of a transmission line. It may comprise several fiber-sections and optical amplifiers so that loss and chromatic dispersion compensation are (totally or partially) performed in the span (see Fig. 3.3). For N spans, the *nonlinear transfer function* of the transmission line can be rewritten as:

$$\eta(\Delta\Omega) = \sum_{k=1}^{N} \eta_{s,k}(\Delta\Omega) e^{(G_{s,k} - i\Delta\Omega D_{s,k})} \qquad (3.25)$$

where $\eta_{s,k}$, $D_{s,k}$ and $G_{s,k}$ are now related to the spans and not to the fiber-sections. $\eta_{s,k}$ is the *nonlinear transfer function* of the kth span taken taken individually. For a transmission line consisting of N identical spans ($\eta_{s,k} = \eta_{s,l}$) performing full loss and dispersion compensation (i.e. $D_{s,j} = D_{s,k} = D_0$ and $G_{s,j} = G_{s,j} = G_0$ set arbitrarily to $G_0 = 0$), the nonlinear transfer function is given by:

$$\eta(\Delta\Omega) = N\eta_s(\Delta\Omega) e^{-i(\Delta\Omega D_0)} \qquad (3.26)$$

where η_s is the span *nonlinear transfer function* and D_0 the amount of pre-compensation performed at the transmitter side. When dispersion is not totally compensated within the

---

[5]I.e. not at the transmitter or receiver side, but within the transmission line by means of optical fibers exhibiting appropriate chromatic dispersion.
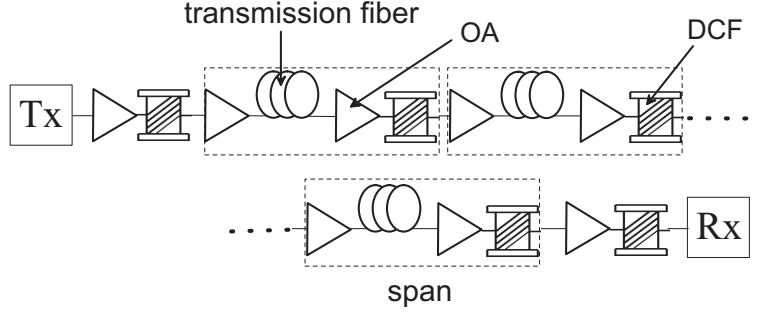
Figure 3.3: Schematic of a transmission line: Each span comprises transmission fibers, optical amplifiers (OA) and dispersion compensating fibers (DCF). Additional DCF can be used for pre- and post dispersion compensation.

spans, $D_{s,k} = D_0 + (k-1)D_{res}$, where D_{res} is the amount of residual dispersion per span in ps^2. In that case, the *nonlinear transfer function* becomes:

$$
\begin{aligned}
\eta(\Delta\Omega) &= \eta_s(\Delta\Omega)e^{-i(\Delta\Omega D_0)} \overbrace{\sum_{k=1}^{N} e^{-i(\Delta\Omega(k-1)D_{res})}}^{\left(\frac{1-e^{(i\Delta\Omega N D_{res})}}{1-e^{(i\Delta\Omega D_{res})}}\right)} \\
&= |\eta_s(\Delta\Omega)|\frac{\sin\left(N\Delta\Omega D_{res}/2\right)}{\sin\left(\Delta\Omega D_{res}/2\right)}e^{-i\left(\left(\frac{1}{2}(N-1)D_{res}+D_0\right)\Delta\Omega+\varphi_s(\Delta\Omega)\right)}
\end{aligned}
\tag{3.27}
$$

with φ_s defined as in Eq. (3.21). Eq. (3.26) and Eq. (3.27) provide useful information regarding the influence of the dispersion map on nonlinear effects: They show (see Fig. 3.4) that introducing a certain amount of residual dispersion per span modifies the *nonlinear transfer function* and consequently the nonlinear perturbation.

3.2.2 A simple metric: the nonlinear diffusion bandwidth

In this section, the concept of *the nonlinear diffusion bandwidth* is introduced. It is a simple metric for the characterization of the *nonlinear transfer function*, that simplifies the description of fiber nonlinearities and offers useful insight into the impact of the dispersion map on nonlinear effects.
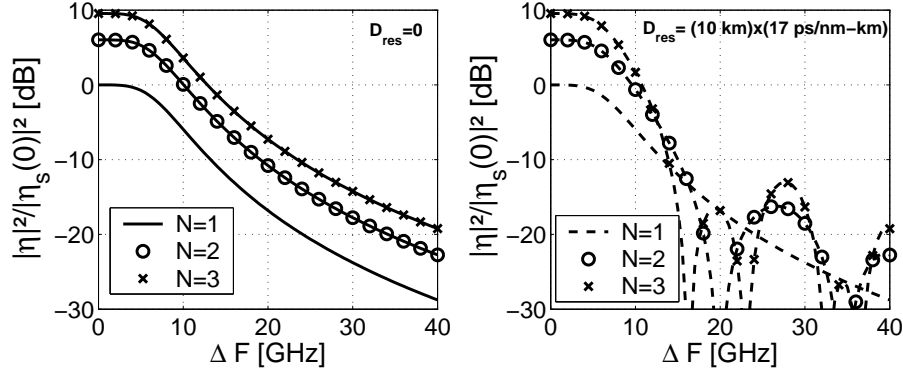
Figure 3.4: $|\eta|^2$ normalized with $|\eta_s(0)|^2$ (see Eq. (3.27)) for N=1,2 or 3 identical spans. Each span consists of an EDFA followed by 80 km of SSMF and a linear dispersion compensating module $\left(\Delta F = \sqrt{\frac{|\Delta\Omega|}{4\pi^2}}\right)$.

Single-fiber transmission

Setting $f_{3dB} = \frac{1}{2\pi}\sqrt{\frac{\alpha}{|\beta_2|}}$ and $f_d = \sqrt{\frac{\alpha}{4\pi|\beta_2|}}$, the magnitude of the *nonlinear transfer function* for single-fiber transmission (with lumped optical amplification) reported in Eq. (3.20) can be rewritten as follows:

$$|\eta(\Delta\Omega)| = \frac{\eta_o}{\sqrt{1 + \left(\frac{\Delta\Omega}{4\pi^2 f_{3dB}^2}\right)^2}} = \frac{\eta_o}{\sqrt{1 + \left(\frac{\Delta\Omega}{4\pi f_d^2}\right)^2}} \qquad (3.28)$$

with $\eta_o = \gamma/\alpha$. Thus, $|\eta(\Delta\Omega)|^2$ is reduced by a factor of 2 for $|\Delta\Omega| = (\omega - \omega_1)(\omega - \omega_2) = 4\pi^2 f_{3dB}^2$. Identically, $|\eta(\Delta\Omega)|^2$ is reduced by about a factor of 10 when $|\Delta\Omega| = 4\pi^2 f_d^2$. $|\eta|$ is maximized when the phase-matching condition ($\Delta\Omega = 0$) is verified. This maximum is equal to η_o. Since f_d and f_{3dB} are scalable, they can be used indifferently. In the following, we opt for f_d, which is referred to as *nonlinear diffusion*[6] *bandwidth*. f_d is a powerful metric, because it fully characterizes the magnitude of the *nonlinear transfer function* for single-fiber transmission.

---

[6]Fiber Kerr effect can be described by analogy with a *diffusion* process (see Fig 3.9). In fact, the nonlinear impact of a given spectral component is restricted to a 2-dimensional frequency space (see Fig. 3.5) delimited by f_d (analog to a *diffusion length*). The nonlinear interactions occurring within this space are responsible for the main nonlinear perturbations.
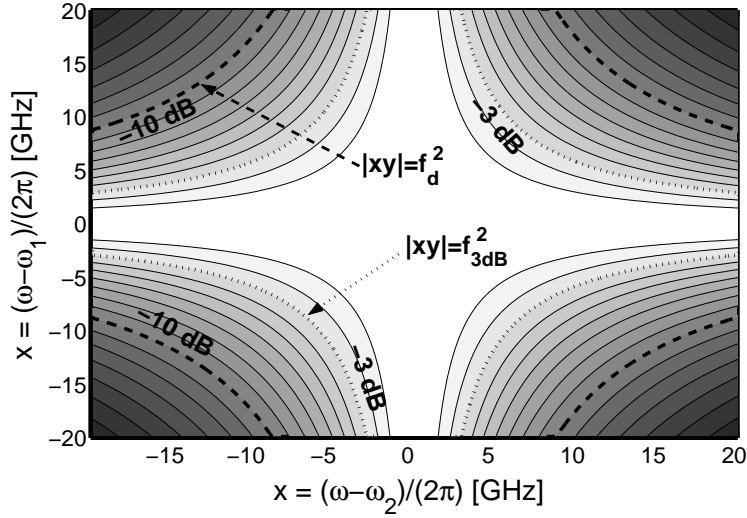
Figure 3.5: $|\eta(\Delta\Omega)|^2$ for single-span transmission (e.g. $g(z) = 0$, $\alpha = 0.2dB/km$, $\beta_2 = -20ps^2/km$ and $L > L_{eff}$). f_{3dB} and f_d ($\sim 13GHz$) delimit the -3dB and -10dB domains respectively.

Multi-span transmission

For complex transmission links, η and f_d have to be evaluated numerically. However, a simple analytical expression for η has been derived in Eq. (3.27) for transmission lines consisting of N identical spans. When chromatic dispersion is fully compensated within a span ($D_{res} = 0$), the nonlinear transfer function is simply characterized by $\eta_o = N\eta_{o,s}$ and $f_d = f_{d,s}$, where $\eta_{o,s}$ and $f_{d,s}$ are related to the nonlinear transfer function of the span (η_s). When $D_{res} \neq 0$, destructive interferences take place at $\Delta\Omega D_{res} = k2\pi/N$ so that η can not be fully characterized by f_d and η_o any more. However, it is possible to approximately describe a multi-span transmission link with an equivalent single-fiber model having the following *equivalent nonlinear transfer function* (η_{eq}) giving rise to the same amount of nonlinear power W_{NL} as η for the case of an AWGN propagating in the line (see Eq. (3.44)):

$$|\eta_{eq}(\Delta\Omega)| = \frac{N\eta_{o,s}}{\sqrt{1 + \left(\frac{\Delta\Omega}{4\pi f_{d,eq}^2}\right)^2}} \tag{3.29}$$
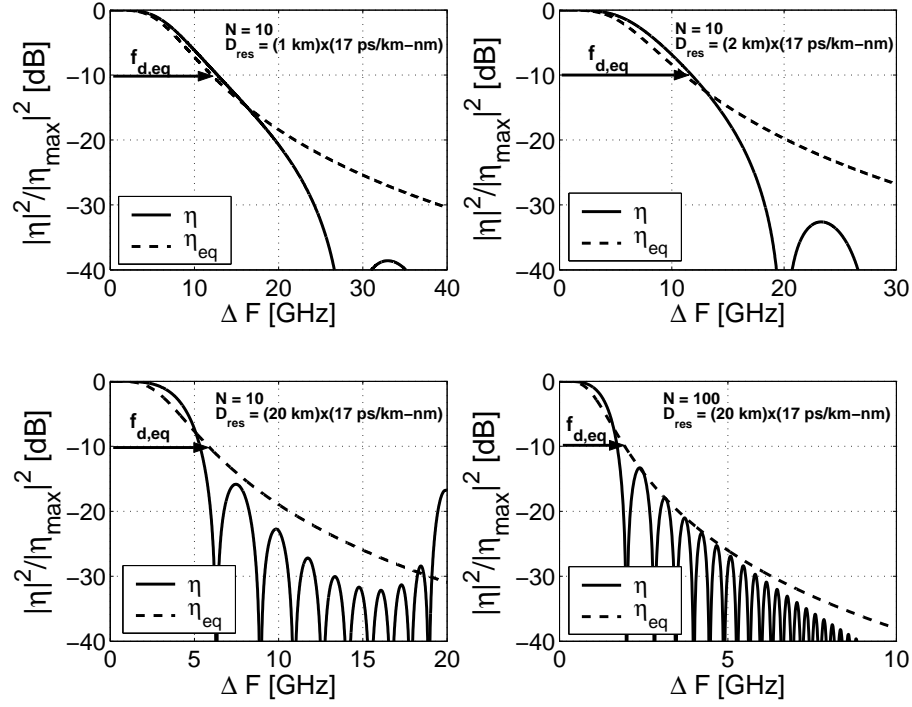
Figure 3.6: $|\eta(\Delta\Omega)|^2$ and $|\eta_{eq}(\Delta\Omega)|^2$ for different transmission lines with identical transmission fiber. Each span consists of an EDFA followed by 80km SSMF and a ideal (linear) dispersion compensating module. $\Delta F = \sqrt{\frac{|\Delta\Omega|}{4\pi^2}}$. Note that the accumulated dispersion D_{res} is indicated in ps/nm and not in ps^2.

with $f_{d,eq}$ the *equivalent nonlinear diffusion bandwidth* of the transmission line, which is well approximated by the following formula[7]:

$$f_{d,eq} \approx \frac{1}{\sqrt{\frac{1}{f_{d,s}^2} + 2\pi(N-1)|D_{res}|}} \tag{3.30}$$

$f_{d,eq}$ depends on the span architecture, $f_{d,s}$, on the number of spans, N, as well as on the residual dispersion in the transmission line, D_{res}. As illustrated in Fig. 3.6, $|\eta_{eq}|$ is a relatively good approximation for $|\eta|$.

---

[7]See appendix B.

3.2.3 Equivalent single-span model

Not only the magnitude $|\eta|$ but also the phase $arg(\eta)$ of the nonlinear transfer function can be approximated. In the range $\Delta\Omega \leq f_{d,eq}^2$ (i.e. where the nonlinear interactions are the strongest) the phase of the expression reported in Eq. (3.27) can re-written as follows (see 3.7):

$$arg(\eta) \approx e^{-i\left(\left(\frac{1}{2}(N-1)D_{res}+D_0+\frac{\beta_2}{\alpha}\right)\Delta\Omega\right)}$$

$$e^{i\left(\left(\frac{1}{4\pi}\left(Sign(\beta_2)/f_{d,eq}^2-4\pi D_0\right)\right)\Delta\Omega\right)} \tag{3.31}$$

Eq. (3.31) shows [8] that $arg(\eta)$ can be characterized by $f_{d,eq}$ and D_0. That leads to two key results:

• Transmission lines having identical *nonlinear diffusion bandwidth* $f_{d,eq}$ and pre-compensation D_0 have similar *nonlinear transfer functions* (in phase and amplitude) and thus should lead to similar nonlinear degradations[9].

• The nonlinear transfer function of any multi-span transmission line with *nonlinear diffusion bandwidth* $f_{d,eq}$ can be approximated by the one of a single span with $f_d = f_{d,eq}$ and having the same pre-compensation D_0 as depicted in Fig. 3.8.

To conclude, transmission lines having comparable *nonlinear diffusion bandwidth* and pre-compensation also have similar *nonlinear transfer functions*. Thus, we expect similar nonlinear degradations in these transmission lines. These important issues are addressed in the following sections.

3.3 Nonlinear impairments

3.3.1 Noise loading analysis

The *noise loading analysis* [53], [54] is a simple method to characterize the nonlinear nature of a system. It consists in looking at the systems response to an additive white gaussian

---

[8]In the above expression, it is assumed that D_{res} has the same sign as β_2, i.e. that no over compensation per span is considered.

[9]Assuming they have identical values for η_o
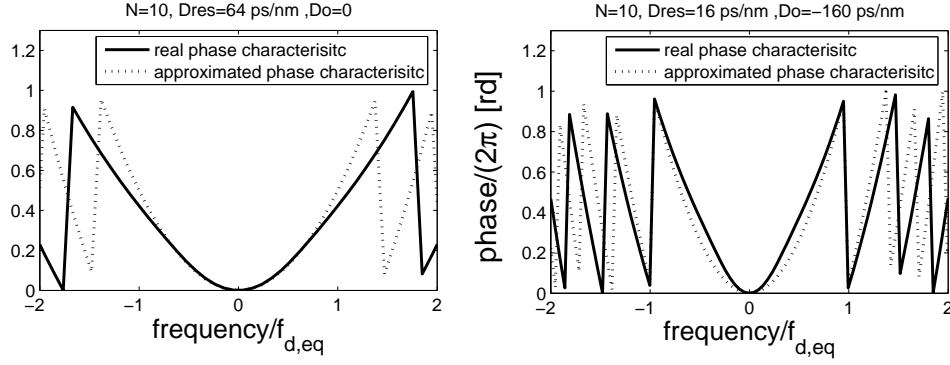
Figure 3.7: Exact and approximated phase characteristic of the *nonlinear transfer function* for two multi-span transmission line, with and without pre-compensation.
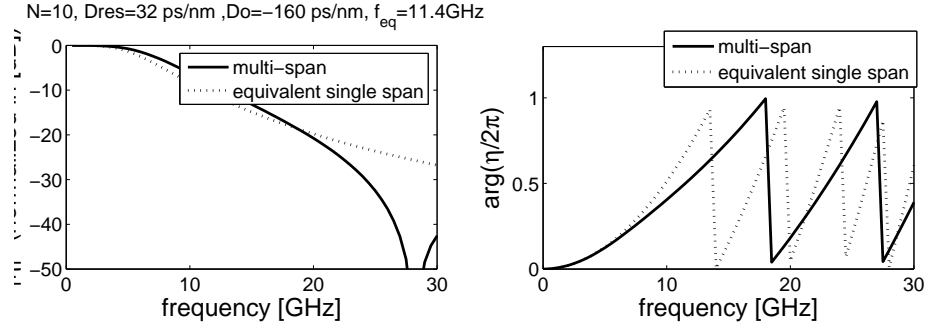
Figure 3.8: *nonlinear transfer function* (magnitude and phase) of a multi-span transmission line and its equivalent single-span model.)

noise [55] (AWGN). This approach is particularly interesting in the present case, because it allows an analytical treatment of fiber nonlinearities. Noting P the power (in Watt), B_{opt} the bandwidth (in Hz) and $W = P/B_{opt}$ the power spectral density of the transmitted noise (see Fig. 3.9), the power spectral density of the nonlinear perturbation at the central

Figure 3.9: Power spectral density of the transmitted AWGN and of the generated nonlinear perturbation.

frequency component $(f = 0)$ is derived from Eq. (3.16) as follows[10]:

$$
\begin{aligned}
W_{NL}(f = 0) &= \left\langle 2\pi \left| \delta_{NL}(\omega = 0) \right|^2 \right\rangle \\
&= \left\langle 2\pi \left| \int_{-\pi B_{opt}}^{\pi B_{opt}} \int_{-\pi B_{opt}}^{\pi B_{opt}} \eta(\Delta\Omega) S(0, \omega_1, \omega_2) d\omega_1 d\omega_2 \right|^2 \right\rangle \\
&= 2\pi \int_{-\pi B_{opt}}^{\pi B_{opt}} \int_{-\pi B_{opt}}^{\pi B_{opt}} \left| \eta(\Delta\Omega) S(0, \omega_1, \omega_2) \right|^2 d\omega_1 d\omega_2 \\
&\approx 2 f_d^2 W^3 \eta_o^2 \ln\left(1 + \frac{\pi}{4} \frac{B_{opt}^2}{f_d^2} \right)
\end{aligned}
\tag{3.32}
$$

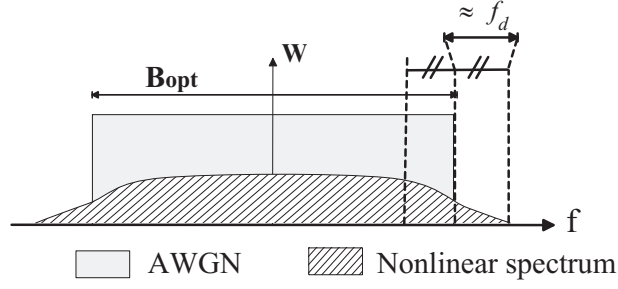The above result is valid for $B_{opt} \gg f_d$. When $B_{opt} \leq f_d$, it comes:

$$
W_{NL}(f = 0) \approx \frac{3}{4} W^3 B_{opt}^2 \eta_0^2
\tag{3.33}
$$

In that simple case, the knowledge of f_d and η_o is sufficient to characterize completely the impact of the transmission line on the nonlinear perturbation. The above formulas hold for other frequency components $(f \neq 0)$ as long as they remain far away from the edges of the signal spectrum.

This approach provides useful information regarding the nonlinear perturbation, δ_{NL}, generated by Kerr effect. In fact, Eq. (3.32) and Eq. (3.33) can be extended to the case of multi-span transmission systems by substituting η_o by $N\eta_{o,s}$ and f_d by $f_{d,eq}$.

---

[10]See appendix C for details.

38

3.3.2 Evaluation criteria

OSNR

Signal to Noise Ratio (SNR) is a common criterion to assess the quality of a communication channel [55]. It is defined as the (average) ratio of the power of the useful signal (i.e. the one containing information) to the power of noise signals. In optical communications, the Optical Signal to Noise Ratio (OSNR) is defined with regard to the noise generated in EDFAs during optical amplification (amplified spontaneous emission or ASE):

$$OSNR = \frac{P_{ch}}{W_{ASE}\Delta_B} \tag{3.34}$$

where P_{ch} is the average channel power, W_{ASE} the power spectral densities of ASE and Δ_B the noise equivalent bandwidth typically set to 0.1nm (12.5GHz), [56]. Usually, both polarizations are considered for the OSNR. However -and at the notable exception of section 4.2.2- this study is restricted to a single polarization for signal and noise. Since Eq. (3.34) does not account for nonlinear impairments, we propose the following definition for the OSNR:

$$OSNR_{nl} = \frac{P_{ch} - B_{ch}W_{NL}}{P_{ASE} + B_{ch}W_{NL}} \tag{3.35}$$

with P_{ch} and B_{ch} the channel power and occupied optical bandwidth and $B_{ch}W_{NL} = P_{NL}$ the power of the nonlinear perturbations (see Eq. (3.32)). The minus term in the numerator ensures energy conservation. The above definition is of great value because it leads to the theoretical maximum achievable capacity[11] of an optical transmission system according to the well-known Shannon theorem [57]. However, for this theorem to be valid, the noise term has to be Gaussian [58]. ASE noise already verifies this condition (before tight filtering and direct detection). If the transmitted signal consists of a large number of uncorrelated (independent) channels, nonlinear noise can also be considered as Gaussian[12] so that the Shannon theorem is applicable.

---

[11]See section 5.3.

[12]See Appendix D.

Q factor

The Q factor is a useful criterion for the performance evaluation of optical transmission systems because it enables rapid assessment of the Bit-Error Rate (BER), [3], [59], [60]. It is obtained in electrical domain (i.e. after signal detection) as follows:

$$Q = \frac{|\mu_1 - \mu_0|}{\sigma_1 + \sigma_0} \tag{3.36}$$

where μ_1, μ_0 and σ_1, σ_0 are the means and standard deviations of marks and zeros respectively. The Q-factor definition presented in Eq. (3.36) has a limited validity and becomes incorrect [61] if excessive pattern effects are present in a bit stream. Because OSNR is not always convenient to assess system performance, analytical formulas have been derived for OOK signals to convert OSNR in Q factor, [62], [63]:

$$Q \approx \frac{2OSNR\sqrt{pM}}{\sqrt{1 + 4OSNR} + 1} \tag{3.37}$$

where $p = 1, 2$ depending if one or two polarizations for the noise are considered. $M = TB_F$ with T the bit-period and B_F the bandwidth of the optical filter. In Eq. (3.37), the channel spacing (Δ_{ch}) is assumed large enough so that linear cross-talks can be neglected ($B_F > \Delta_{ch}$).

In order to account for the system specific features (modulation format, optical and electrical filters, etc), an "OSNR-Q factor conversion table" can be computed for each investigated system with numerical simulation. By doing this, the analytical expression for the OSNR reported in Eq. (3.35) can be turned into Q factor. Indeed, in the limit of very tight optical filtering, coherent WDM crosstalk [64] can be neglected and the nonlinear perturbation can be considered equivalent to ASE. In this case, we can obtain numerically this correspondence table by varying the level of ASE noise at the transmitter in a back-to-back configuration and by evaluating the OSNR and the related Q factor for a given system.

OSNR penalty

The present analytical approach also enables the assessment of the OSNR penalty. It is defined as the difference in OSNR (as defined in Eq. (3.34)) required at the photodiode to achieve a desired BER (e.g. 10^{-9}) after back-to-back (BTB) and nonlinear transmission. The BER is evaluated as proposed in [65]. The required OSNR for BTB transmission is evaluated by means of numerical simulations. Once the maximum allowed power ASE falling on the photodiode has been determined for back-to-back transmission, the analytical derivation of the OSNR penalty is straight-forward:

$$OSNR_p \approx \frac{W_{ASE,BTB}}{W_{ASE,BTB} - W_{NL}} \tag{3.38}$$

where $W_{ASE,BTB}$ is the maximal allowed power spectral density (PSD) of the ASE to obtain the desired BER in linear transmission and W_{NL} the PSD of the nonlinear noise. For this approach to be valid, nonlinear and ASE have to be considered roughly equivalent.

3.3.3 Nonlinear impairments in single-channel transmission

The performance of single-channel transmission systems depends on the pulse evolution in the fiber and particularly on nonlinear interactions with neighboring pulses. Pulse propagation inside a single-mode fiber is governed by the nonlinear Schrödinger equation (NLSE)(see section 2.4):

$$\frac{\partial A}{\partial z} + \frac{i}{2}\beta_2 \frac{\partial^2 A}{\partial T^2} + \frac{\alpha}{2}A = i\gamma |A|^2 A \tag{3.39}$$

with $A(T, z)$ the slowly varying amplitude of the pulse envelope and α, β_2 and γ the fiber loss, dispersion and nonlinear coefficients. In order to make general statements concerning the transmission, it is convenient to normalize this equation. Noting P_0 ($|A_0|^2$) the pulse peak power and B the channel bit-rate[13], we can define the following dimensionless variables:

---

[13]Note that other temporal characteristic of the initial pulse (for example the pulse full width half maximum, T_0) could be used.

$\xi = z\alpha$, $\tau = TB$ and $a = \frac{A}{\sqrt{P_0}}e^{\alpha z/2}$, so that Eq. (3.39) becomes:

$$i\frac{\partial a}{\partial \xi} = x_l\frac{\partial^2 a}{\partial \tau^2} - x_{nl}e^{-\xi}|a|^2 a \qquad (3.40)$$

with $x_{nl} = \frac{\gamma P_0}{\alpha}$ and $x_l = \frac{\beta_2 B^2}{2\alpha}$ or equivalently $x_l = Sign(\beta_2)\frac{B^2}{8\pi f_d^2}$. This normalized form makes the NLSE easier to deal with and gives better insight into pulse propagation, which can be simply characterized with the values for x_l and x_{nl}. It also highlights the fact that at constant power and for identical modulation format, transmission systems with the same same ratio B/f_d exhibit identical performance with regard to nonlinearities. Finally, this normalized form of the NLSE can be intuitively extended to multi-span transmission by replacing f_d by $f_{d,eq}$ in the expression for x_l.

Propagation regimes

When $x_{nl} \ll 1$, Eq. (3.40) describes the classical case of linear propagation. Conversely, when x_{nl} is not negligible, different propagation regimes can be distinguished depending on the value of x_l:

• For $|x_l| \ll 1$, chromatic dispersion does not lead to pulse overlap within the fiber effective length[14] and pulse self phase-modulation is the dominant nonlinear effect. This regime is generally referred to as *solitonic regime*.

• The case $|x_l| \gg 1$ corresponds to the *pseudo-linear regime* [37, 66] where pulses spread very rapidly, leading to a reduction of nonlinear impairments.

• Otherwise (i.e for $|x_l| \sim 1$), pulses overlap but the pseudo-linear regime is not reached. Consequently, nonlinear impairments are maximized (this will be explained later with Fig. 3.11).

3.3.4 Nonlinear impairments in WDM transmission

Contrary to single-channel transmission, more than one parameter is required to characterize the signal in Wavelength-Division Multiplexed (WDM) transmission (e.g. bit-rate,

---

[14]see Eq. (2.31).

number of channels, channel spacing, etc...) and normalizing the NLSE with one of these parameters can not lead to universal conclusions regarding the propagation regime. In order to characterize nonlinear impairments, we start from the analytical expression for the small nonlinear perturbation derived in the preceding section (Eq. (3.16)):

$$\delta_{NL}(\omega) = i \int \int \eta(\Delta\Omega)\tilde{S}(\omega, \omega_1, \omega_2)d\omega_1 d\omega_2 \tag{3.41}$$

where η is the *nonlinear transfer function* of the transmission line and $\tilde{S}$ is a function of the input signal only. Since noise results from the random[15] fluctuations of the received signal, the power spectral density $W_{NL}(\omega)$ of the nonlinear noise is given as the variance of $\delta_{NL}(\omega)$:

$$W_{NL}(\omega) = <|\delta_{NL}(\omega)|^2> - |<\delta_{NL}(\omega)>|^2 \tag{3.42}$$

where $< \, . \, >$ denotes the mean operator over all realization (in our case the detected bits in all possible channel configurations).

Continuum model

In the case of WDM signals, a simple analytical expression for W_{NL} is difficult to derive because of the complexity of the term $\tilde{S}$ in Eq. (3.41). However, it is sometimes possible (see appendix D) to model the aggregate WDM signal by a Gaussian noise. Under this assumption, $<\delta_{NL}> = 0$ and the following simplifications can be done:

$$
\begin{aligned}
W_{NL}(\omega) &= \left\langle \left| \int \int \eta(\Delta\Omega)\tilde{S}(\omega, \omega_1, \omega_2)d\omega_1 d\omega_2 \right|^2 \right\rangle \\
&= \int \int |\eta(\Delta\Omega)|^2 |\tilde{S}(\omega, \omega_1, \omega_2)|^2 d\omega_1 d\omega_2
\end{aligned} \tag{3.43}
$$

For dense WDM systems (DWDM), the transmitted spectrum can be well approximated with a continuum (Fig. 3.10), and the above integral can be approximated as follows (see

---

[15]Indeed deterministic changes (like intra-pulse nonlinear interaction) can not be treated as noise.

Eq. (3.32)):

$$W_{NL}(f = 0) \approx 2f_{d,eq}^2 W^3 \eta_o^2 \ln \left(1 + \frac{\pi}{4} \frac{B_{opt}^2}{f_{d,eq}^2} \right) \qquad (3.44)$$

with B_{opt} the total optical bandwidth of the aggregate WDM signal and W its average power spectral density given in W/Hz. $f_{d,eq}$ is the *equivalent nonlinear diffusion bandwidth* of the transmission line. $\eta_o = |\eta(0)|$ is easily obtained from Eq. (3.24). This result is valid for $B_{opt} >> f_{d,eq}$.

Semi-continuum model

In order to describe WDM systems for which frequency gaps between the channels exist, a semi-continuum rather than a continuum can be used to approximate the signal spectrum (see Fig. 3.10). This semi-continuum is characterized by the channel occupied bandwidth B_{ch}, the number of channels N_{ch} and by the channel spacing Δ_{ch}. This semi-continuum model leads to the following expression (see appendix C) for the amount of nonlinear power, P_{NL}, falling in the channels:

$$P_{NL} \approx 2f_{d,eq}^2 \frac{1}{\rho^{\chi-1}} \frac{P_{ch}^3}{\Delta_{ch}^2} N^2 \eta_0^2 \ln \left(1 + \frac{\pi}{4} \frac{B_{opt}^2}{f_{d,eq}^2} \right) \qquad (3.45)$$

P_{ch} is the channel power, and $\rho = B_{ch}/\Delta_{ch}$, the ratio of occupied bandwidth or *spectral use* (not to be confused with the spectral efficiency). χ is a measure of the granularity [16] with regard to the transmission line nonlinear characteristic, $f_{d,eq}$:

$$\chi = \frac{1}{1 + \frac{f_{d,eq}}{\Delta_{ch}-B_{ch}}} \qquad (3.46)$$

Impact of the system granularity and more generally of the signal distribution in the frequency domain will be discussed in section 4.2.

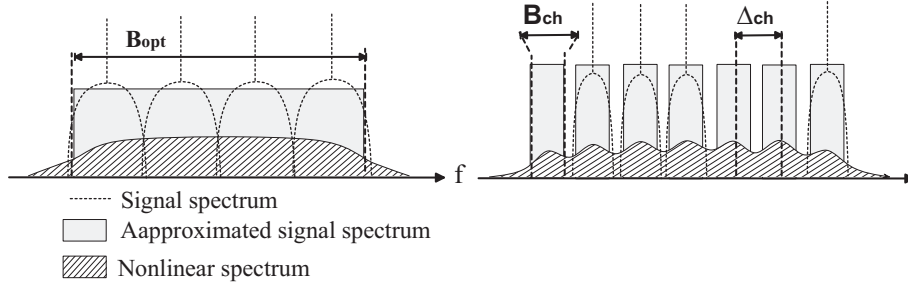[16]χ decreases with the granularity.

Figure 3.10: Continuum (left) and semi-continuum (right, here for $N_{ch} = 7$) models for WDM signals.

Validity domain

Although WDM signals cannot be strictly considered as noise, they often present characteristics, so that the nonlinear perturbation is roughly equivalent to that generated by noise. This is the case when the interacting spectral components have random relative optical phases. This condition is fulfilled when these spectral components belong to different wavelength channels (i.e. for inter-channel effects when optical carriers are generated by independent lasers) or when the accumulated dispersion is large enough, so that their optical phases evolve rapidly within the fiber effective length (e.g. intra-channel effects when $|x_l| \gg 1$). Conversely, intra-pulse interactions can not be properly described by a noise approach, because of their deterministic nature. For that reason, impairments due to intra-pulse interactions (e.g. signal distortion due to SPM and FM-AM conversion) can not be properly described by this approach.

3.3.5 Numerical verification

Numerical simulations reported in this section were realized with the commercially available tool VPItransmissionMaker™ [67], which implements the split-step Fourier algorithm[17].

Single-channel transmission

In this section, the analytical predictions concerning the different propagation regimes for on-off keying signals and their dependence on the normalized parameter B/f_d are verified

---

[17]See section A.

by means of numerical simulations. To that aim, amplitude of an ideal laser source is modulated with a Mach-Zender Interferometer (MZI) by a Pseudo Random Bit Sequence (PRBS) [68] of 2048 bits. Pulses are assumed Gaussian (with 33% duty-cyle[18]). OSNR penalty for a required BER of 10^{-9} is used as the evaluation criterion.

System without pre-compensation

OSNR penalty is displayed in Fig. 3.11 against B/f_d and $B/f_{d,eq}$ for single and multi-span transmission respectively. In order to cover a wide range of values for B/f_d and $B/f_{d,eq}$, 10, 40 and 160 Gbit/s systems have been considered. For single-span transmission (80 km SMF, channel input power = 13dBm), f_d has been modified by changing the fiber chromatic dispersion (from 1 to 22 ps/nm-km), whereas for multi-span transmission (10 spans of 80 km, channel input power = 3dBm), the fiber chromatic dispersion has been set to 2,4 and 10 ps/nm-km and $f_{d,eq}$ has been modified by changing the amount of residual dispersion[19] per span (from 0 to 160 ps/nm). As expected system performance depends only on the dimensionless constant $B/f_{d,eq}$ (rather than on B and $f_{d,eq}$ independently). Similar results have been observed with the help of numerical simulations in [69] and [70], but with the normalized constant DB^2, which is equivalent to $B/f_{d,eq}$ only for the case of single-span[20] transmission.

System with pre-compensation

The analysis made in 3.3.3 shows that pulse propagation is identical in systems with same B/f_d and $B^2 D_0$ (D_0 being the amount of pre-compensation). To verify this prediction, the transmission of a single RZ channel (33% duty-cycle) over a 80 km fiber with ideal (linear and lossless) pre-compensation is considered. The ration B/f_d is varied through the channel bit-rate (10,40 and 160 Gb/s) and the fiber chromatic dispersion. The accumulated dispersion (included pre-compensation) is compensated at the receiver. The results displayed in 3.12

---

[18]The duty-cycle is the ratio of the pulse full width at half maximum over the bit duration.

[19]for the dependence of f_d on chromatic dispersion and of $f_{d,eq}$ on residual dispersion, see Eq. (3.28) and Eq. (3.30).

[20]or equivalently for multi-span transmission without residual dispersion per span.
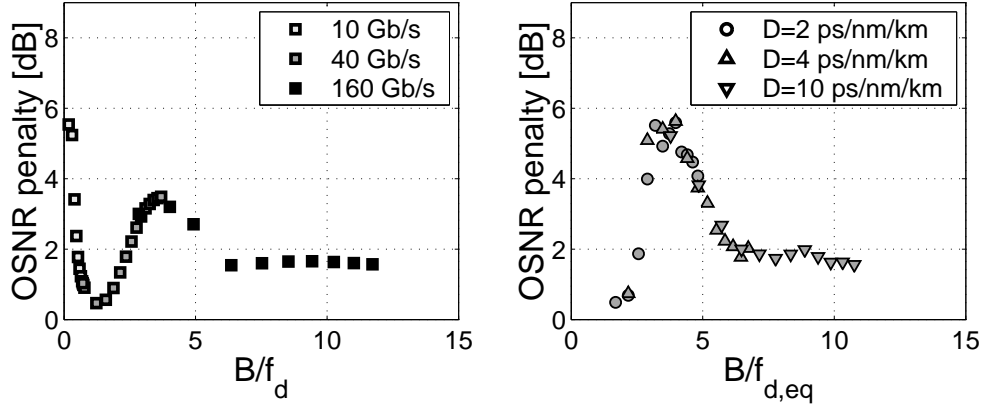
Figure 3.11: OSNR penalty versus B/f_d and $B/f_{d,eq}$ for single (a) and multi-span (b) transmission.
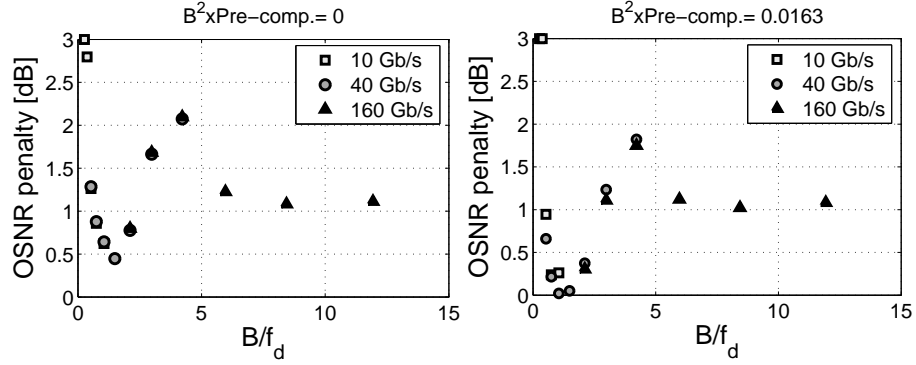
Figure 3.12: OSNR penalty versus the ratio B/f_d without pre compensation (left) and with precompensation (right). Systems with identical B/f_d and $B^2 D_0$ have similar systems performance.

were obtained for a channel input power of 12dBm. As expected, nonlinear impairments are identical in systems with same B/f_d and $B^2 D_0$.

WDM transmission

The goal of this section is to validate our analysis of nonlinear impairments in WDM transmission systems. To that aim, the transmission of a 16x10Gb/s NRZ WDM signal (with 25 GHz channel spacing, i.e. at a spectral efficiency of 0.4 bit/s/Hz) is considered. No precompensation is considered since it is expected to have a limited impact on inter-channels effects. To ensure independence of the WDM channels, optical carriers (lasers) start to emit

Figure 3.13: OSNR penalty for a WDM signal against f_d and $f_{d,eq}$ for single and multi-span transmission respectively. Analytical and numerical predictions show good agreement.

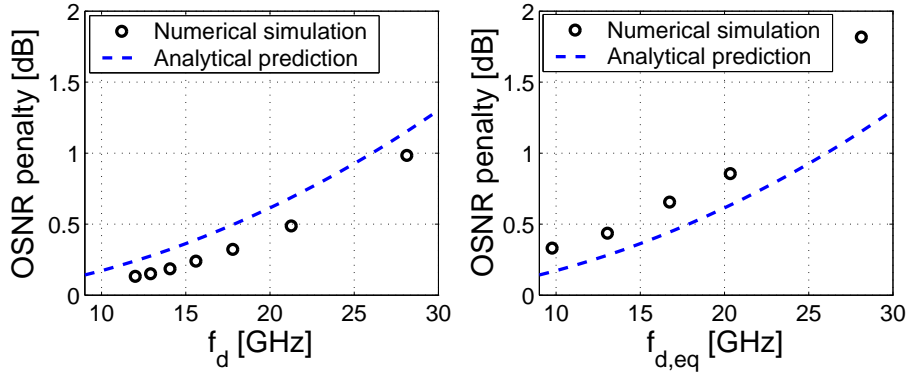with random optical phases and are modulated with different and unsynchronized PRBS sequences of 2048 bits. Optical WDM multiplexer and demultiplexer consist of 2nd order Gaussian filters with 15GHz 3dB bandwidth.

In order to verify the dependence of the system performance on the *nonlinear diffusion bandwidth*, the OSNR penalty (for a required BER of 10^{-9}) of the central channel is displayed against f_d and $f_{d,eq}$ in Fig. 3.13 for the single (channel input power = 3dBm) and multi-span (channel input power = -7dBm) transmission described in the previous section. Transmission lines are identical to the single-channel case: f_d (Eq. 3.28) is varied by changing the local dispersion of the fiber, whereas $f_{d,eq}$ (Eq. 3.30) is modified by changing the amount of residual dispersion per span. Numerical results and analytical predictions derived from the results reported in Eq. (3.45) and Eq. (3.38) agree very well.

3.4 Conclusion

An analytical model for the description of fiber nonlinearities has been reported. It has been shown that nonlinearities in multi-span transmission systems can be characterized with an equivalent single-span model and that transmission lines with identical *nonlinear diffusion bandwidth* lead to similar nonlinear degradation in single channel as well as in WDM transmission systems. Finally, the value of the nonlinear diffusion bandwidth as a simple and universal criterion to predict nonlinear impairments in WDM dispersion-

managed systems has been verified by means of numerical simulations.

Chapter 4

Strategies for the Reduction of Nonlinear Impairment

The goal of this chapter is to derive general guidelines for the reduction of nonlinear impairments in single-channel and WDM transmission systems.

4.1 Transmission link design

The impact of fiber dispersion in single-channel transmission systems has been investigated in [69]. In this pioneering work, it was shown that the performance of single-span, single-channel transmission systems is governed by the product DB^2, B being the channel bit-rate and D the fiber dispersion coefficient. Extensive numerical simulations validating this result have been reported in [70, 71]. Not only fiber chromatic dispersion, but also careful tuning of dispersion compensation at the transmitter (pre- compensation), between the optical amplifiers (in-line compensation) and at the receiver (post-compensation) can reduce the impact of fiber nonlinearities, [72–74].

In the following, an analytical expression for the optimum amount of pre-compensation in single-fiber and multi-span transmission systems is derived and the transmission line design is optimized with the help of the concept of the *nonlinear diffusion bandwidth*.

4.1.1   Optimum nonlinear diffusion bandwidth

Single-channel transmission

In the preceding chapter, a normalized form of the NLSE[1] describing the propagation of amplitude-modulated single-channel has been derived (Eq. (3.40)):

$$i\frac{\partial a}{\partial \xi} = x_l \frac{\partial^2 a}{\partial \tau^2} - x_{nl} e^{-\xi} |a|^2 a \qquad (4.1)$$

with the dimensionless variables $\xi = z\alpha$, $\tau = TB$ and $a = \frac{A}{\sqrt{P_0}} e^{\alpha z/2}$. $x_{nl} = \frac{\gamma P_0}{\alpha}$ and $x_l = Sign(\beta_2) \frac{B^2}{8\pi f_d^2}$. As already discussed in section 3.3.3, two propagation regimes can be distinguished depending on the value of $|x_l|$: When $|x_l| \ll 1$, chromatic dispersion does not lead to pulse overlap and pulse self phase-modulation is the dominant nonlinear effect. In this regime, the pulses (assumed as being identical) experience the same propagation and give rise to the same nonlinear perturbation δ_{NL}, is generally referred to as *solitonic regime*. Since δ_{NL} is deterministic, the generated nonlinear power cannot be considered as noise. For $|x_l| \gg 1$, pulses spread very rapidly within the fiber effective length, leading to stochastic[2] nonlinear perturbations. Under this condition, the deterministic part of δ_{NL} can be neglected and the whole generated nonlinear power can be considered as noise. This case corresponds to the *tedon regime* or *pseudo-linear regime* discussed in [37, 66].

In order to predict system performance, we propose the following approach: We assume that (deterministic) intra-pulse interactions do not lead to any penalty whereas (stochastic) inter-bit interactions (iXPM, iFWM) are equivalent to the nonlinear perturbation generated by an additive white Gaussian noise (AWGN) with the same occupied bandwidth and power as the considered channel. Under these assumptions, the generated noise power P_{noise} can be approximated by the product:

$$P_{noise} \approx RP_{NL} \qquad (4.2)$$

P_{NL} being the power spectral density of the nonlinear perturbation generated by the "equivalent" AWGN (see Eq. (3.44)) and R the ratio of nonlinear power effectively generated by

---

[1] Nonlinear Schrödinger Equation, see Eq. (2.28).
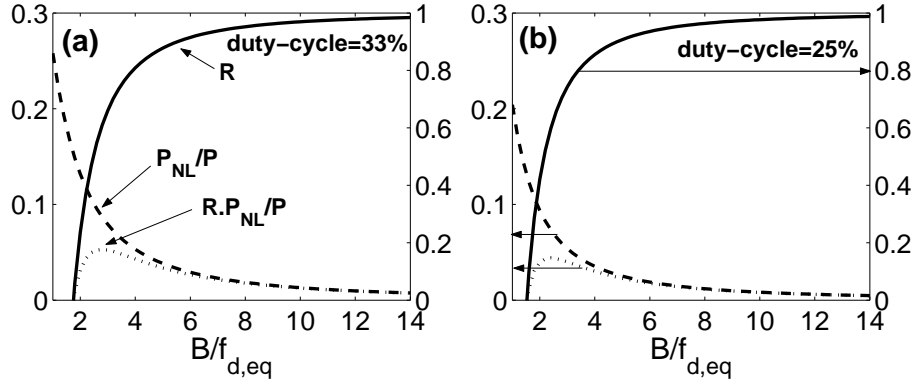[2] Because bit-pattern dependent.

Figure 4.1: Generated nonlinear power, P_{NL} (normalized with the signal average input power, P) and R against B/f_d for unchirped Gaussian pulses with (a) 33% and (b) 25% duty-cycle. No pre-compensation is considered.

inter-bits interactions, which can be roughly approximated as:

$$R \approx \frac{N_{eff} - 1}{N_{eff}} \tag{4.3}$$

where N_{eff} is the number of bits overlapping in the fiber effective length, L_{eff}. For a random pattern of Gaussian pulses, N_{eff} can be readily calculated from the formulas reported in [3]:

$$N_{eff} = \frac{1}{2} \frac{4ln(2)|D_{max}|B}{T_{FWHM}} \tag{4.4}$$

with D_{max} the maximum accumulated dispersion in the effective length (depending on $f_{d,eq}$ and on the amount of pre-compensation), B the channel bit-rate and T_{FWHM} the pulse full width at half maximum. The factor 1/2 accounts for the occurrence probability of the marks. Examples for Gaussian pulses (40 Gb/s, with duty-cycle 33% and 25%) are reported in Fig. 4.1. The system OSNR penalty (for a BER of 10^{-9}) resulting from intra-channel nonlinear effects can be derived from Eq. (4.2) and Eq. (3.38). Analytical predictions show relatively good agreement with numerical results (see Fig. 4.2).
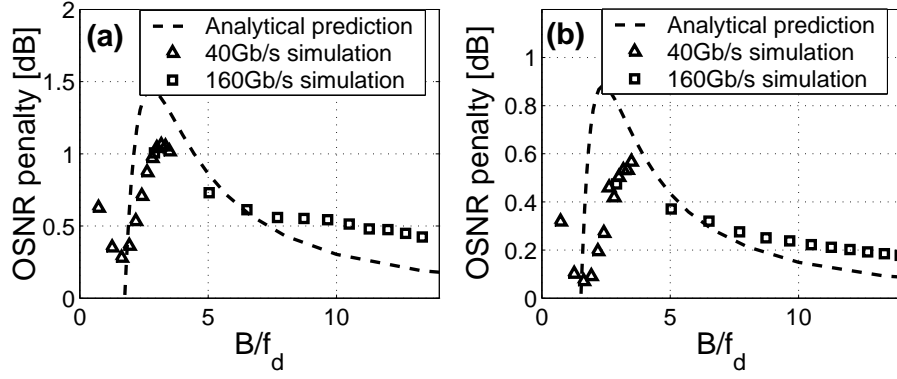
Figure 4.2: Analytically and numerically estimated OSNR penalty against B/fd for RZ transmission (Gaussian pulses with (a) 33% and (b) 25% duty-cycle). Transmission over a single-span (80 km SSMF, γ=1.3 /W/km, α=0.21 dB/km) is considered. Channel input power is set to 11dBm, $B = 40$ and 160 Gb/s and f_d is varied by changing the fiber chromatic dispersion.

WDM transmission

In WDM transmission systems, inter-channel as well as intra-channel nonlinear interactions affect the signal. Using formulas reported in Eq. (3.44) and Eq. (3.33), it is possible to evaluate the ratio, r, of nonlinear power generated by intra-channel interactions:

$$r = \frac{P_{intra}}{P_{inter} + P_{intra}} \approx \frac{P_{NL}(B_{ch})}{P_{NL}(B_{opt}) - P_{NL}(\Delta_{ch}) + P_{NL}(B_{ch})} \tag{4.5}$$

where P_{NL} is obtained from Eq. (3.45). B_{opt}, B_{ch} and Δ_{ch} stand for the total bandwidth of the aggregate WDM signal, the channel occupied bandwidth and the channel spacing. The following results can be derived from Eq. (4.5):

$$\frac{\partial r}{\partial f_d} < 0, \frac{\partial r}{\partial \chi} > 0 \tag{4.6}$$

In other words, the ratio of inter-channel effects increases with the *nonlinear diffusion bandwidth* and with the granularity (see Eq. (3.46)). For $r \approx 1$ (i.e. when intra-channel interactions are the main nonlinear effects), the approach presented in the preceding section can be applied to determine the optimal value for f_d. Conversely, for $r \ll 1$, inter-channel interactions (XPM,FWM) are the dominant nonlinear impairments and the power of the
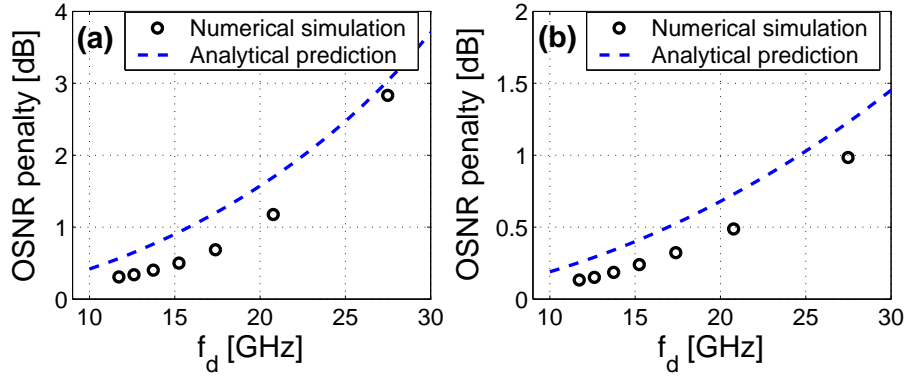
Figure 4.3: Analytically and numerically estimated OSNR penalty against fd for 16x 10Gb/s NRZ at (a) 0.8 bit/s/Hz (0 dBm/Channel, 12.5 GHz channel spacing) and (b) 0.4 bit/s/Hz (3 dBm/Channel, 25 GHz channel spacing). Transmission over a single-span (80 km SSMF, $\gamma=1.3$ /W/km, $\alpha=0.21$ dB/km) is considered. f_d is varied by changing the fiber chromatic dispersion.

nonlinear noise falling in the WDM channels is given as reported in Eq. (3.45):

$$P_{NL} \approx 2f_{d,eq}^2 \rho^{1-\chi} \frac{P_{tot}^3}{B_{opt}^2} N^2 \eta_0^2 \ln \left(1 + \frac{\pi}{4} \frac{B_{opt}^2}{f_{d,eq}^2} \right)$$

In that case, a small value for $f_{d,eq}$ is beneficial (see Fig. 4.3), because it reduces the amount of generated nonlinear noise.

4.1.2 Optimized pre-and residual dispersion

The knowledge of the optimal *nonlinear diffusion bandwidth* is not sufficient for the optimization of the transmission link design. Indeed, some important dispersion-management techniques like pre-compensation (for mitigation of intra-channel nonlinear effects, [75]) or residual dispersion at the receiver side (for mitigation of SPM-induced impairments, [76]) are not taken into account in the expression for $f_{d,eq}$.

It is known that intra-channel nonlinear impairments can be reduced with pre-and in-line dispersion compensation, [75], [74]. Analytical models for the characterization of intra-channel nonlinear effects have been reported in [77], [78] and [79]. For a bit-stream composed

of equally spaced pulses, the amplitude of electrical field $A(T, z)$ is given by:

$$A(T, z) = \sum m_j b_j(T, z) \qquad (4.7)$$

$b_j(T)$ being the amplitude of the pulses in the jth bit-slot and m_j takes the value 0 or 1 depending on whether a mark or a space is transmitted. Pulse propagation is described by setting Eq. (4.7) in the NLSE. For the central pulse ($j = 0$), one obtains:

$$\frac{\partial b_o(T, z)}{\partial z} + \frac{i}{2}\beta_2 \frac{\partial^2 b_o(T, z)}{\partial T^2} + \frac{\alpha}{2} b_o(T, z) = i\gamma \sum_{l+m-n=0} a_{l,m,n} b_l(T, z) b_m(T, z) b_n^*(T, z) \qquad (4.8)$$

with $a_{l,m,n} = m_l m_m m_n$. In the perturbation theory framework[3], the solution of Eq. (4.8) can be approximated as the sum of the solution for linear transmission, B_o, and a perturbation term, δb_0, representing nonlinear effects. After loss and dispersion compensation, the optical signal at the end of the transmission link (of length L) is given as:

$$b_o(T, L) = b_o(T, 0) + \delta b_0(T, L) \qquad (4.9)$$

Following identical steps as in 3.1.2, the nonlinear perturbation at the end of the transmission line (when loss and chromatic dispersion have been compensated) is found to be:

$$\delta b_0(T, L) = \sum_{l,m} a_{l,m,n} \delta b_{l,m}(T, L) \qquad (4.10)$$

with $\delta b_{l,m}(T, L)$ the nonlinear perturbation for b_0 at the end of the transmission line resulting from the interaction of the pulses l,m and $n = l + m$, verifying:

$$\frac{\partial \delta b_{l,m}(T, z)}{\partial z} = i\gamma(z) e^{(G(z))} F^{-1}\{F\{b_l(T, z) b_m(T, z) b_{l+m}^*(T, z)\} e^{(-i\omega^2 D(z)/2)}\} \qquad (4.11)$$

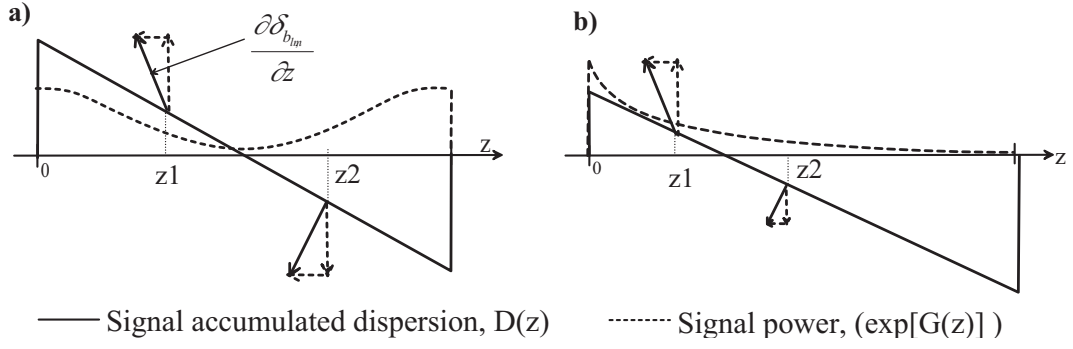[3]I.e. for weak nonlinearities, see section 3.1.2.

Figure 4.4: (a) symmetric and (b) nonsymmetric link design leading to (a) total or (b) partial cancelation of the signal Kerr-induced amplitude variations. Vertical and horizontal arrows corresponds to the real and imaginary part of $\frac{\partial \delta b_{l,m}(T,z)}{\partial z}$ respectively.

$F\{.\}$ symbolizing the Fourier-transform operator and $G(z)$ and $D(z)$ being the gain and dispersion profiles[4] of the transmission line. For unchirped Gaussian pulses, it is possible[5] to derive an analytical expression for Eq. (4.11):

$$
\begin{aligned}
\frac{\partial \delta b_{l,m}(T,z)}{\partial z} &= i\frac{A_o^3 \gamma(z) \exp\left(G(z)\right)}{\sqrt{(1-iC)(1+i3C)}} \exp\left(-\frac{3+iC}{1+i3C}\left(\frac{T}{T_o} - \frac{2(l+m)T_B}{(3+iC)T_o}\right)^2\right) \\
&\quad \exp\left(-\frac{(l^2+m^2-(1+iClm))T_B^2}{(1-iC)(3+iC)T_o^2}\right)
\end{aligned}
\tag{4.12}
$$

with A_o and T_o the peak amplitude and the pulse half-width at $1/e$ intensity point of the pulse for $z=0$. T_B is the bit-slot duration and $C(z)$ is defined as $C(z) = D(z)/T_o^2$. Writing Eq. (4.12) at positions z_1 and z_2 verifying $D(z_1) = -D(z_2)$, one obtains:

$$
\frac{\partial \delta b_{l,m}(T,z_1)}{\partial z} = -e^{(G(z_1)-G(z_2))}\frac{\partial \delta b_{l,m}^*(T,z_2)}{\partial z}
\tag{4.13}
$$

For the $G(z_1) = G(z_2)$, the amplitude perturbations (i.e. the real part of $\delta b_{l,m}$) generated at z_1 and z_2 cancel each-other. Because amplitude-modulated signals are mostly sensitive to amplitude fluctuations, it is possible to reduce intra-channel nonlinear impairments in OOK-based systems with transmission lines presenting symmetrical optical power and dispersion distribution as depicted in Fig. 4.4.a. This result was previously demonstrated analytically

---

[4]$G(z)$ and $D(z)$ are defined in Eq. (3.13).

[5]The product and convolution product of Gaussian functions remain Gaussian, simplifying the calculation.

and verified experimentally for the case of highly dispersed pulses [77]. Conversely, this solution is not optimal for a phase-modulated signal since the phase perturbations (imaginary part of $\delta b_{l,m}$) generated at z_1 and z_2 are identical and add coherently.

Symmetrical optical power distribution can be achieved with the help of forward and backward Raman pumping. However, in most current systems, optical amplification is realized with EDFAs leading to an unsymmetrical power distribution $(G(z_1) \neq G(z_2))$ and thus to an incomplete cancelation of nonlinear amplitude perturbations (Fig. 4.4.b.). It is possible to maximize this partial cancellation by optimizing the amount of pre-compensation. For single-fiber transmission with EDFA amplification, the gain and dispersion dispersion profiles are expressed as:

$$G(z) = -\alpha z$$

$$D(z) = D_o + \beta_2 z$$

Where D_o (in ps^2) is the amount of pre-compensation. In that simple case, the cancelation is maximized for (see appendix E):

$$D_o = -\frac{2ln(2)}{3}\frac{\beta_2}{\alpha} \approx -\frac{\beta_2 L_{eff}}{2} = -\frac{sign(\beta_2)}{8\pi f_d^2} \qquad (4.14)$$

L_{eff} being the effective length of the fiber. Even though derived quite differently, this result agrees well with the analytical and numerical results reported in [79] and [80]. This result can be extended to multi-span transmission system consisting of N identical spans. Noting D_o and D_{res} the amount of pre-compensation and residual dispersion per span, we show that the optimal pre-compensation verifies:

$$D_o + \frac{(N-1)}{2}D_{res} = -\frac{\beta_2 L_{eff}}{2} \Rightarrow D_o = -\frac{sign(\beta_2)}{8\pi f_{d,eq}^2} \qquad (4.15)$$

So that the optimal pre-compensation depends on the amount of residual dispersion required to achieve the desired value for the *nonlinear diffusion bandwidth*, $f_{d,eq}$.

Numerical simulations are performed in order to verify the results reported in Eq. (4.14).
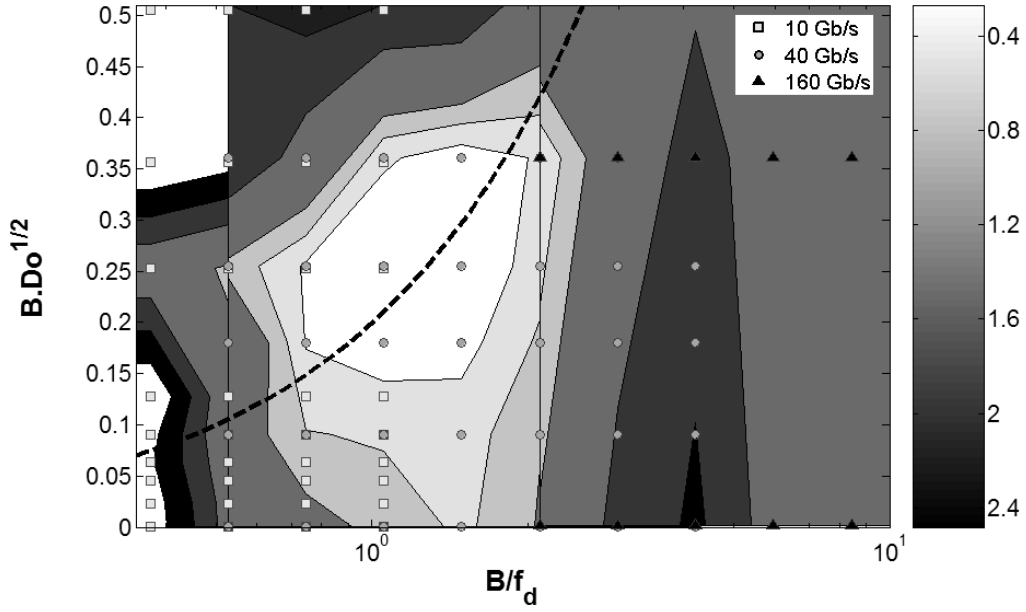
Figure 4.5: Numerical predictions for the system OSNR penalty [dB] against B/f_d and $B\sqrt{Do}$ for a single RZ channel (160 GHZ optical filter & 0.7*40 GHz electrical filter). The dotted line stands for the optimal pre-compensation according to Eq. (4.14).

The transmission of a single RZ channel at varying bit-rate (10,40 and 160 GB/s) over 80km fiber is considered. The channel input power is set to 11dBm. Both pre-compensation and *nonlinear diffusion bandwidth* have been varied. The OSNR penalty (BER=10^{-9}) is displayed against B/fd and $B.\sqrt{Do}$ in Fig.4.5. Optimal pre-compensation according to Eq. (4.14) is displayed by the dash line. Analytical prediction and numerical results agree very well.

For amplitude modulated signals at 10Gb/s systems, the optimum does not exactly correspond the one predicted in Eq. 4.15. This is because impairments due to self-pulse modulation (spectral broadening followed by FM-AM conversion) can not be neglected against impairments due to intra-bits interactions.

The transmission of 4x40Gb/s RZ channels (0.4 duty-cycle, 100GHz channel spacing, 3dBm/channel) over 4 identical sections is then considered. Each section consists of 80km of SSMF and two (linear) dispersion-compensation modules for pre and post-compensation. Full dispersion compensation is performed at receiver when necessary. Optical WDM multiplexer and de-
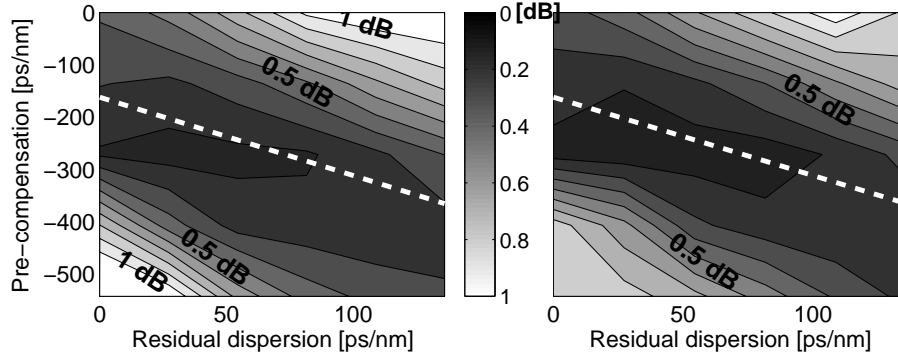
Figure 4.6: Numerical predictions for the system OSNR penalty [dB] against D_o and D_{res} for the two central channels. The dotted line stands for the optimal pre-compensation according to Eq. (4.15).

multiplexer consist of 2nd order Gaussian filters with 80GHz 3dB bandwidth. The OSNR penalty (BER=10^{-9}) for the two central channels is displayed in Fig. 4.6 against D_{res} and D_o. Optimal pre-compensation according to Eq. (4.15) coincides with the one obtained numerically.

4.2 Information distribution

Not only the transmission link but also the signal can be optimized in order to reduce nonlinear impairments. Novel modulation formats have been proposed to that end [81]. For example, RZ-DPSK takes advantage of both phase-modulation[6] and RZ pulses[7] [82]. Further improvements can be achieved using orthogonal polarizations[8] of adjacent bits [83], [84]. In this section, the issue of information encoding is tackled from a more general point of view. We examine the impact of information distribution in frequency (spectral use and granularity) and in polarization on nonlinear impairments. Their impact on the fiber maximum achievable capacity is handled in the next chapter.

---

[6]3dB gain for the receiver sensitivity with balanced detection.

[7]A pulse is sent for every bit resulting in the suppression of intra-channel cross-phase modulation due to the deterministic nature of the signal envelope.

[8]Reduction of intra-channel cross-phase modulation and four-wave mixing.

4.2.1 Information distribution in frequency

In the following section, the light is assumed to propagate over a single polarization. Under that case, the capacity of a WDM-based transmission system can be expressed as follows:

$$C = S\rho B_{tot} \tag{4.16}$$

where B_{tot} is the available bandwidth (e.g. the C-band of the optical fiber), ρ the spectral use (ratio of occupied bandwidth) and S the local spectral efficiency (i.e. the spectral efficiency of each WDM channel in bit/s/Hz). Generally, frequency guard bands are usually used in WDM transmission systems in order to reduce linear cross talk and to limit nonlinear interactions between the channels. Upgrading the system capacity is possible either by increasing the channel spectral efficiency, S (what also enables the frequency guard bands to be maintained) or by making a more efficient use of the available bandwidth (i.e. increasing ρ). Examples are illustrated in Fig. 4.7. For constant total power, these strategies consist in either splitting or bunching the power in the available bandwidth. Since our ultimate goal is to maximize the capacity transmitted in an optical fiber (see next chapter), it is of primary importance to find out which one of these strategies is the best with regard to nonlinear impairments. To that aim, we examine the OSNR as defined in Eq. (3.35):

$$OSNR = \frac{P_{tot} - P_{NL}}{P_{ase} + P_{NL}} \tag{4.17}$$

with P_{tot} the power of the aggregate WDM signal and P_{ase} and P_{NL} the amount of ASE and nonlinear noise after optical filtering falling on the photodiode. For WDM systems consisting either of a large number of channels at high granularity $(\Delta_{ch} < f_{d,eq})$[9] or of highly-dispersive channels $(B \gg f_{d,eq})$[10], it has been shown in appendix D that the entire nonlinear generated power can be considered as noise. In this case, P_{NL} is given by Eq. (3.45):

$$P_{NL} \approx \frac{2 f_{d,eq}^2}{\rho^{\chi-1}} \frac{P_{ch}^3}{\Delta_{ch}^2} N^2 \eta_0^2 \ln\left(1 + \frac{\pi}{4} \frac{B_{opt}^2}{f_{d,eq}^2}\right)$$

---

[9]Δ_{ch} is the channel spacing.
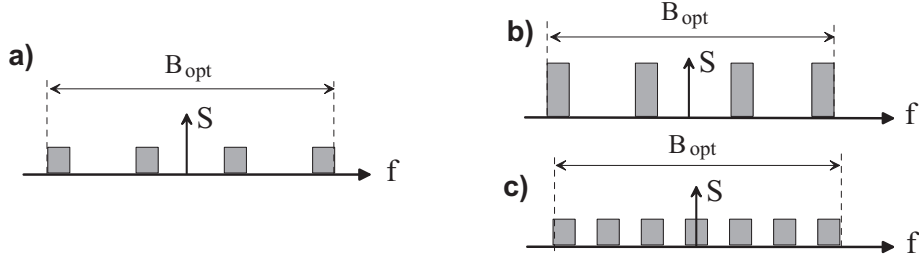[10]B is the channel baud-rate, i.e. roughly its bandwidth.

Figure 4.7: Capacity upgrade of (a) current WDM systems can be achieved with (b) higher local spectral efficiency (S in bit/s/Hz) and/or (c) larger spectral use (ρ).

with ρ the spectral use (ratio of the channel occupied bandwidth, B_{ch}, with the channel spacing, Δ_{ch}) and P_{ch} the power per WDM channel. $f_{d,eq}$ is the *equivalent nonlinear diffusion bandwidth* of the transmission line and χ is a measure of the signal granularity It was defined in Eq. (3.46) as follows:

$$\chi = \frac{1}{1 + \frac{f_{d,eq}}{\Delta_{ch} - B_{ch}}} = \frac{1}{1 + \frac{f_{d,eq}}{(1-\rho)\Delta_{ch}}} \tag{4.18}$$

i.e. χ tends towards 0 for high granularity and towards 1 for low granularity. As a consequence, the nonlinear noise depends on the spectral power (or information) distribution. Examples of possible spectral information distributions are illustrated in Fig. 4.8

Impact of the spectral use and of the granularity

The following results can be derived from Eq. (3.45):

$$\frac{\partial P_{NL}}{\partial \rho} < 0 \tag{4.19}$$

i.e. that increasing the spectral use leads to a reduction of the nonlinear noise. At constant spectral use, it can be shown that:

$$\frac{\partial P_{NL}}{\partial \chi} \geq 0 \tag{4.20}$$

so that the amount of nonlinear noise is reduced at higher granularity (low χ). These results can be intuitively understood by the fact that splitting the power in the available bandwidth reduces the local power spectral density and thus the strength of nonlinear
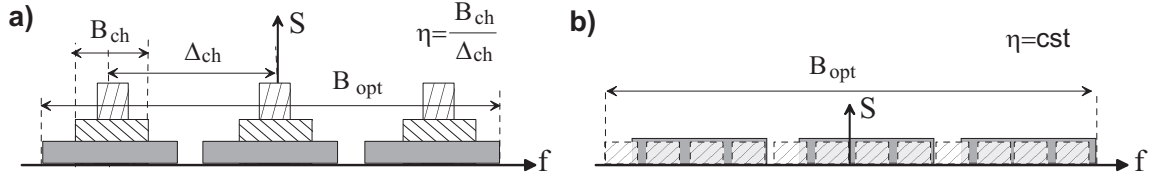
Figure 4.8: Possible information distributions of WDM-based optical transmission systems: (a) varying spectral use at constant granularity and (b) varying granularity at constant spectral use. Total system capacity ($S\rho B_{opt}$) and power remain constant.
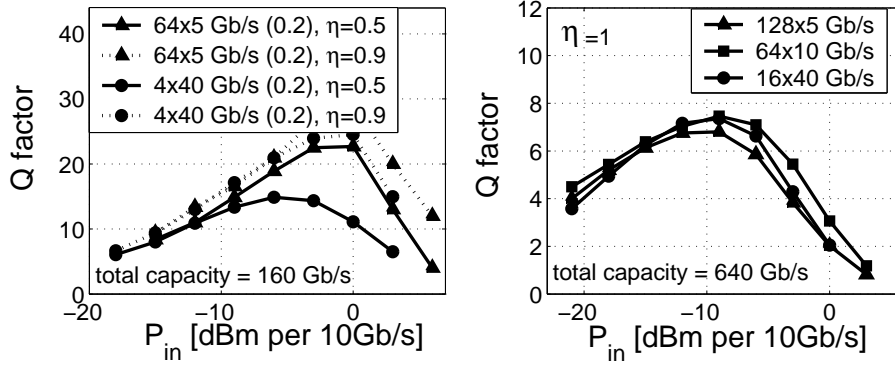
Figure 4.9: Numerical simulations. Q factor of the central channel vs. (normalized) channel input power at (a) 0.2 bit/s/Hz ($\eta = 0.5$ and 0.9) and (b) 0.8 bit/s/Hz ($\eta = 1$).

interactions. Moreover, when $\rho = 1$ (when the signal power is uniformly distributed in the frequency domain), P_{NL} is independent of the signal granularity. Thus, we expect system performance to be mainly independent of the granularity, for systems at high spectral efficiency as reported in [85] and also for systems with a high spectral use. However this result does not account for the fact that intra-channel nonlinear effects can be partially compensated with optimal pre-compensation[11], what is not the case for inter-channel effects, which are dominant at high granularity.

Numerical verification

In order to verify above statements, the following numerical simulations are performed: we consider the transmission of a total capacity of 160 Gb/s and 640 Gb/s at respective spectral efficiencies of 0.2 bit/s/Hz and 0.8 bit/s/Hz, using 5 Gb/s, 10 Gb/s or 40 Gb/s

---

[11]See previous section.

RZ channels. The transmission line consists of 4 spans, each including 80 km SSMF, an EDFA and an ideal DCF so that loss and chromatic dispersion are totally compensated in each span. No pre-compensation is considered. Optical filters (Gaussian 2nd order) are scaled with the channel bit-rate. Channels are assumed uncorrelated (unsynchronized and different PRBS sequences of 1024 bits for each channel). Q factor[12] of the central channel is reported against the input power allocated to 10 Gb/s in Fig. 4.9 for each configuration. At 0.2 bit/s/Hz, the RZ pulses are generated at 20% duty-cycle and are broadened after passing through a optical filter, whose 3dB bandwidth is varied in order to vary the channel occupied bandwidth and as a consequence the spectral use. As expected, at low spectral use high granularity seems to be beneficial in the nonlinear regime. At 100% spectral use, the system performance is roughly independent of the granularity[13]. These numerical results validate the analytical predictions.

4.2.2 Information distribution in polarization

In this section, the influence of information distribution in polarization[14] on the nonlinear impairments is investigated. Starting from the coupled nonlinear Schrödinger equations [35], we extend the analytical model presented in sections and 3.1.2 and 3.3 to the case of a birefringent optical fiber. The goal of this study is to determine the influence of polarization and fiber birefringence on nonlinear effects. Polarization-dependent loss and the frequency-dependence of polarization mode dispersion are neglected. Moreover first order PMD is assumed to be perfectly compensated at the receiver so that only nonlinear impairments remain.

Constant birefringence

We first consider the case of optical fibers with constant birefringence, i.e. with fixed Principal States of Polarization (PSP), and examine the influence of the relative power distribution in the two orthogonal propagating modes (see Fig. 4.10). Noting W_x and W_y

---

[12]See section 3.3.2.

[13]Note that no line optimization like pre-compensation is considered.

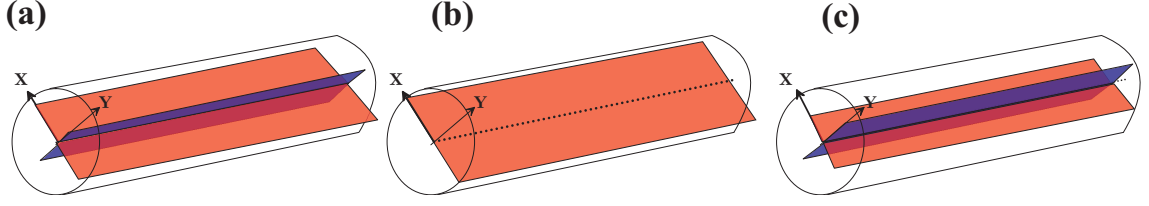[14]see *Birefringence and polarization-mode dispersion* in section 2.2.4.

Figure 4.10: (a) power distribution in polarization for a continuum spectrum. Special cases: (b) Signal propagates on a single PSP. (c) Power is equally distributed on both PSPs.

the power spectral densities[15] (in Watt/Hz) of signal propagating respectively on the x and y axis (PSPs) and assuming that the signal spectrum can be approximated by a continuum, the power spectral density of the nonlinear perturbation generated in one of the PSPs (e.g. the x-mode) is given in [86] as:

$$W_{NL,x} = 2 f_{d,eq}^2 \eta_o^2 \ln \left(1 + \frac{\pi}{4} \frac{B_{opt}^2}{f_{d,eq}^2} \right) (W_x^3 + c \frac{4}{3} W_x^2 W_y + \frac{4}{9} W_y^2 W_x) \qquad (4.21)$$

with c being the correlation ($c \in [0..1]$) product between the polarization components. it is zero when both components are de-correlate [16]. The resulting power spectral density of the nonlinear perturbation is given as $W_{NL} = W_{NL,x} + W_{NL,y}$, where $W_{NL,y}$ is obtained by inverting the x and y indices in the above expression. The analytical study - confirmed by split-step Fourier simulations - shows that nonlinear distortions are reduced up to a factor of 2/3 when the signal power is equally distributed in the PSPs (see [86]). On the contrary, the generation of nonlinear components is maximized when the signal propagates over a single PSP (Fig. 4.10.b).

In order to verify the model predictions, some numerical simulations are performed: Transmission of 15x10 Gbit/s NRZ channels at a spectral efficiency of 0.8 bit/s/Hz (12.5 GHz channel spacing) over 80km of SSMF is considered. This high spectral efficiency enables us to approximate the transmitted spectrum as a continuum, which is the condition for Eq. (4.21) to hold. Fiber's PSPs are maintained constant and the relative power distribu-

---

[15]Total signal power spectral density: $W = Wx + Wy$.

[16]i.e. when the differential group delay within the fiber effective length is more larger than the bit rate. As a consequence a large PMD reduces nonlinear impairments
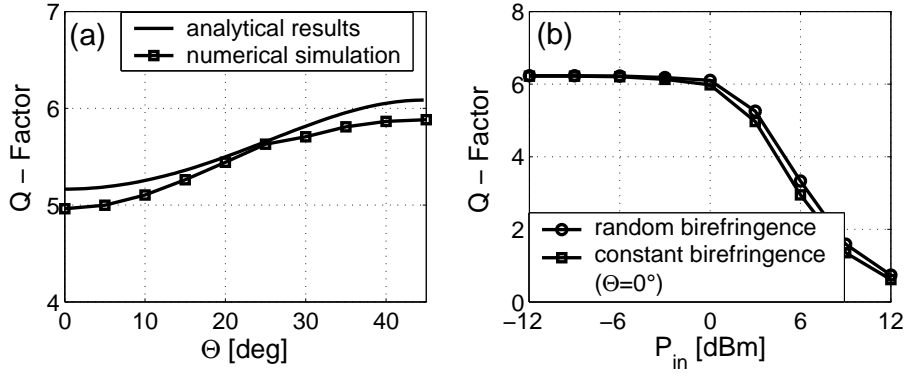
Figure 4.11: Transmission of 15x10 Gb/s NRZ channels (12.5 GHz channel spacing) over a 80 km single fiber ($D_{PMD} = 1ps/\sqrt{km}$): Q-factor of the central channel (a) against azimuth of the propagating wave (channel input power=3 dBm) (b) against channel input power for constant (worst-case, $\Theta = 0$) and random birefringence.

tion on the PSPs is varied by changing the azimuth (Θ) of coupled optical field, so that:

$$W_x = W\cos^2(\Theta)$$
$$W_y = W\sin^2(\Theta) \qquad (4.22)$$

An ideal PMD compensator is used at the receiver side so that birefringence affects only the nonlinear perturbation and not the signal[17]. The OSNR can be derived from Eq. (4.21) and is turned into Q-factor as explained in section 3.3.2. Numerical and analytical predictions for the system performance (Q-factor) depending on the azimuth of the coupled light (i.e. on the distribution of the optical power on the two PSP) are displayed in Fig. 4.11.a. Analytical predictions and numerical simulation show excellent agreement.

Randomly varying birefringence

Most fiber types are not designed to maintain polarization and exhibit a randomly varying birefringence, i.e. the orientation of the PSPs[18] is constantly changing along the fiber. As a consequence, the state of polarization (SOP) and the power distribution on the PSPs of the

---

[17]Both modes arrive simultaneously at the receiver
[18]As well as the first order PMD.

propagating wave are varying continuously. If the length scale[19] on which the PSPs vary is small compared to the fiber effective length, we can assume that all configurations of power distribution occur with the same probability (Θ uniformly distributed over $[0...\pi]$). Under this assumption, the amount of nonlinear noise generated in fibers with randomly varying birefringence is derived from Eq. (4.21):

$$W_{NL} = \frac{43}{54} 2 f_{d,eq}^2 \eta_o^2 W^3 \ln\left(1 + \frac{\pi}{4} \frac{B_{opt}^2}{f_{d,eq}^2}\right) \tag{4.23}$$

with $W = W_x + W_y$ and $W_{NL} = W_{NL,x} + W_{NL,y}$, the axis x and y being chosen arbitrarily. Note that in presence of random birefringence, the amount of generated nonlinear noise is almost as large as in the worst case (single polarization), where the 43/54 factor is replaced by 1 (see numerical results reported in Fig. 4.11). It is interesting to compare this result with the derivation of the Manakov equations proposed by Marcuse, [47] in the case of fibers with randomly varying birefringence:

$$\frac{\partial \overline{\psi}}{\partial z} + \frac{i}{2} \beta_2 \frac{\partial^2 \overline{\psi}}{\partial t^2} = i\frac{8}{9} \gamma |\overline{\psi}|^2 \overline{\psi} \tag{4.24}$$

$\overline{\psi} = f(\vec{A})$ verifies $|\overline{\psi}|^2 = A_x^2 + A_y^2$ where $\vec{A}$ is a vector standing for the slowly varying amplitude of the light in both PSPs and $f(\cdot)$ a transformation accounting for the birefringent nature of the fiber. The factor 8/9 was obtained under the assumption that the polarization evolves quickly enough (due to PMD and varying birefringence) on the Poincaré sphere so that all SOPs occur with the same probability. This normalization factor for random varying birefringence fibers has been verified experimentally in [46], [87]. Using this equation instead of the NLSE in our analysis, we obtain:

$$W_{NL} = \left(\frac{8}{9}\right)^2 2 f_{d,eq}^2 \eta_o^2 W^3 \ln\left(1 + \frac{\pi}{4} \frac{B_{opt}^2}{f_{d,eq}^2}\right) \tag{4.25}$$

Note that difference between 8/9 and $\sqrt{43/54}$ is only 0.4%. We can conclude that the present approach correctly describes the nonlinear propagation of a signal over fibers pre-

---

[19]For classical fibers, this length lays usually between 0.3 and 30 meters.

senting fix or random birefringence, even if the SOP of the light doesn't appear in our analysis.

4.3   Conclusion

In this chapter, guidelines for the design of WDM transmission systems have been proposed and verified with the help of split step Fourier simulations. These insights are applicable to a wide range of amplitude-modulated high-capacity transmission systems.

Optimal pre-compensation depending on residual dispersion effects has been derived for amplitude-modulated signals. In addition, it has been shown that distributing the optical power as uniformly as possible in the frequency (high spectral use and high granularity) and polarization domains reduces nonlinear impairments.

Chapter 5

Capacity of Fiber-Optic Transmission Systems

This chapter offers a brief overview of Shannon's information theory. Basic concepts like source entropy, mutual information and channel capacity are introduced and the fundamental limitations of fiber-optic transmission systems are briefly presented. Finally, an analytical expression for the maximum information capacity of WDM transmission systems is derived and spectral efficiencies achievable with currently available technologies are discussed.

5.1 Short introduction to Shannon's information theory

The explosion of telecommunication techniques[1] during the late 19th and the early 20th century pushed the need for a general theory of communication. Early works, such as those from Nyquist [88] and Hartley [89], laid the foundation of information theory. In the late 1940's, several theories and principles were proposed for example by Wiener [90], Tuller [91] and of course Shannon [57].

---

[1]Telegraph (Morse, 1830), Telephone (Bell, 1876), Wireless Telegraph (Marconi, 1887), AM Radio (1900), Television (1925), Frequency Modulation (Armstrong, 1936), Pulse Code Modulation (Reeves, 1937), Spread Spectrum (1940)

5.1.1 A measure of information

In Shannon's theory, a source of information is modeled as a random process. For the case of a discrete source, a symbol X_j is emitted every time unit ($j = 1, 2, ...$) with values taken form the alphabet $\{x_1, x_2, ..., x_n\}$. If the associated probability ($P\{X_j = x_i\} = p_i$) is independent of all prior symbols $X_{j-1}, X_{j-2}, ...$ this source is said to be a *discrete and memoryless source* (DMS). Following Nyquist and Hartley, Shannon proposed a logarithmic measure for the information:

$$I(x_i) = log\left(\frac{1}{p_i}\right) \tag{5.1}$$

This logarithmic definition ensures $log\left(1/(\sum p_i)\right) = 0$ and $I(x_k; x_l) = I(x_k) + I(x_l)$ so that information is additive and equal to 0 when the signal is predictable. Using Eq. (5.1), the average information in one source symbol is obtained by averaging over the source probability p_i and is denoted by:

$$H(X) = \sum_{i=1}^{n} p_i log\left(\frac{1}{p_i}\right) \tag{5.2}$$

H is called the source *entropy* and can be also referred to as *information rate* of the source in bits per symbol.

5.1.2 Channel model

Shannon extended his information analysis of the source to a general communication system by introducing the concept of *channel*, accounting for any deterministic or random transformation (noise) corrupting the transmitted signal as depicted in Fig. 5.1. A fundamental probability model for the concept of channel is the *discrete memoryless[2] channel* (DMC). Noting X and Y the input and output signals. The channel is characterized by the conditional distribution of X given Y, which is called the *channel transition probability distribution*:

$$p_{i,j} = p\left(X = x_i | Y = y_j\right) \tag{5.3}$$

---

[2]Memoryless means that the ith output depends on the ith input and not on preceding symbols.
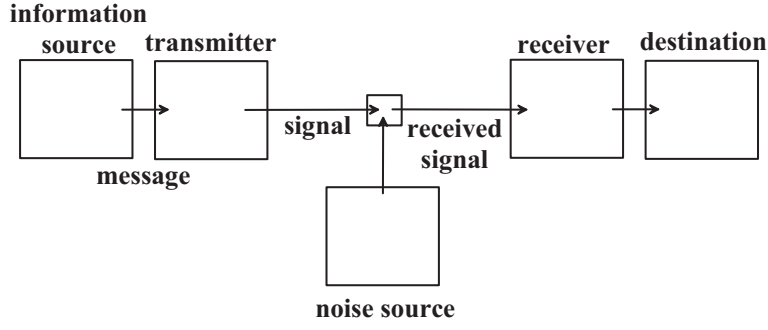
Figure 5.1: General communication system according to Shannon (from [57]).

The uncertainty about the transmitted symbol knowing the output symbol is given by the *conditional entropy*:

$$H(X|Y) = \sum_{i,j} p(x_i, y_j) log \left(\frac{1}{p(x_i|y_j)} \right) \qquad (5.4)$$

Since $H(X)$ is the average uncertainty at the input, the uncertainty resolved by seeing the output Y is obtained as:

$$
\begin{aligned}
I(X,Y) &= H(X) - H(X|Y) \\
&= \sum_{i,j} p(x_i, y_j) log \left(\frac{p(x_i, y_j)}{p(x_i)p(y_j)} \right) \\
&= H(Y) - H(Y|X) = I(Y,X) \qquad (5.5)
\end{aligned}
$$

and is called the *mutual information*. If the output is independent of the input, $H(X|Y) = H(X)$ and $I(X,Y) = 0$, whereas when the transmitted signal is perfectly restored at the output, (i.e. for a noiseless channel) $H(X|Y) = 0$ and $I(X,Y) = H(X)$.

5.1.3 Channel capacity

It is now possible to define the *capacity* (in symbols/s/Hz) of the channel as the maximum of the mutual information over all possible input distributions[3]:

$$C = max_{p(x_i)} I(X,Y) \qquad (5.6)$$

---

[3]i.e. over all possible modulation formats and encoding schemes.

70

This concept of channel capacity is the cornerstone of Shannon's fundamental theorem for a noisy channel [57]:

> *Fix $\epsilon > 0$ as desired detection error probability. Let a source have information rate R and suppose its output is to be transmitted over a channel of capacity C. If $R < C$, then there exists a coding of the source output such that the transmission of the coded output can take place with a detection error of at most ϵ. Conversely, if $R > C$, then there exists an $\epsilon' > 0$ such that the detection error will exceed ϵ' independently of the coding scheme.*

It is usually difficult to compute the channel capacity. On the one hand because $H(X|Y)$ depends on both signal and noise statistics and on the other hand because the space to explore is huge (all possible input symbol distributions have to be considered). An analytical solution of this problem has been provided by Pinsker [92] for the case that the joint probability of input and output is Gaussian. Algorithms to compute the capacity of arbitrary discrete memoryless channels have been proposed in [93] and [94].

Gaussian channel

Shannon showed that the *differential entropy* (analog to Eq. (5.2) but for a continuous variable) of a continuous random variable is maximized (under variance constraint) by the Gaussian distribution. Taking the difference between the output differential entropy, $H(Y)$, and the conditional entropy, $H(Y|X)$, he obtains the famous formula for power-constrained white Gaussian channels (here expressed in [bit/s]):

$$C = B \log_2 \left(\frac{P + N}{N} \right) \tag{5.7}$$

where B is the channel bandwidth, P the transmitted power and N the noise power within the channel band. According to Shannon, this ultimate transmission rate can be achieved if the statistical characteristics of the transmitted signal approximate those of a white noise.

5.2 Fundamental limitations

Fiber chromatic dispersion [95] and polarization mode dispersion [96], [97] can be (more or less) compensated and thus are not fundamental limitations of optical transmission systems (even if in practical case, they may cause severe signal degradation). Conversely, transmitter, receiver (see appendix F) and amplifier noise as well as some nonlinear effects can not be undone.

5.2.1 Amplifier noise

The amplification process (stimulated emission) in an EDFA is accompanied by the amplified spontaneous emission (ASE) noise. The ASE noise is neither polarized nor coherent and can be considered as a white noise. The power spectral density of ASE noise in one polarization is given by [9]:

$$W_{ASE}(f) = n_{sp}(G - 1)hf \tag{5.8}$$

with f the optical frequency and h the Planck's constant. n_{sp} is the spontaneous emission factor which depends on the electron populations in the ground ($N1$) and excited (N_2) states:

$$n_{sp} = \frac{N_2}{N_2 - N_1} \tag{5.9}$$

For high amplifier gain, the noise figure of an EDFA is given as:

$$F_{EDFA} = \frac{SNR_{in}}{SNR_{out}} \approx 2n_{sp} \tag{5.10}$$

where SNR refers to the signal-to-noise ratio. The theoretical minimum for the noise figure is 3dB. Realistic values for F_{EDFA} lay around 3.5dB for systems with 980 nm pump and 4dB at 1480nm.

5.2.2 Kerr-induced perturbations

In principle Kerr-effect is a deterministic[4] process and should not be considered as noise. A method called *optical-phase conjugation* (see [98] and [99]) has even been proposed to suppress (almost perfectly[5]) nonlinear impairments. Unfortunately, this method hugely constrains the transmission line design and requires a mid-link spectral inversion[6]. As indicated in Chapter 3 (see also [100]), impairments due to intra-channel nonlinear interactions can be (partially) canceled in RZ-based systems by a proper design of the transmission line, indicating the deterministic nature of nonlinear perturbations.

However, in WDM transmission systems with independent[7] channels, inter-channel interactions are stochastic and can be considered as noise. For a WDM system, the power of *nonlinear noise* falling in the channels can be approximated as follows:

$$P_{inter} = P_{NL} - P_{intra} \tag{5.11}$$

where P_{intra} and P_{NL} evaluated with the *continuum* and *semi-continuum* models respectively (see Eq. (3.44),(3.33),(3.45)). In the following, we first consider only inter-channel nonlinear effects and ASE as noise sources and derive the maximal capacity of WDM-based fiber-optic transmission systems. Then, we carefully extend this approach to intra-channel nonlinear interactions.

5.3 Maximum capacity of fiber-optic transmission

For a linear channel with additive white Gaussian noise, the maximum system capacity grows logarithmically with the signal to noise ratio, i.e. with the signal input power (see Eq. (5.7)). Conversely, in nonlinear media like optical fibers, increasing the signal power does not necessarily improve the system capacity, because increasing the signal power strengthen

---

[4]Kerr-effect is fully described by the NLSE. In principle the input signal can be determined by measuring the output and using inverse-scattering techniques to integrate the NLSE.

[5]If 3rd order (and all higher odd orders) dispersion can be neglected.

[6]E.g. realized through FWM in nonlinear optical fibers or semiconductor optical amplifiers.

[7]No information about the neighboring channels is available.

nonlinear impairments.

In their pioneering work [14], Stark and Mitra showed that under certain conditions, a nonlinear channel can be treated as a linear channel with multiplicative noise. Applying this idea to WDM transmission, they derived an analytical expression for the lower bound of the Shannon limit for the channel capacity, C. Nonlinear impact of ASE noise was taken into account by Tang in [20]. Using Pinsker's formalism[8] [92] and an expansion in Volterra series, he derived an accurate (but complex) expression for C for multi-span transmission with dispersion-free fibers. In [101], Turitsin et al. proposed an exact derivation of C in the case of very low dispersion fibers without the need to assume Gaussian statistics for the nonlinear noise.

In this section, a simple analytical expression for the system maximum capacity[9] is derived. This expression is valid for a wide range of WDM optical transmission systems. Unlike results reported in previous works, this expression takes the design of the transmission link into account.

5.3.1 Perturbative approach

Under the assumptions of weak nonlinearities and low ASE level (so that the nonlinear impact of ASE noise - or Gordon-Mollenauer effect [51] - can be neglected), a closed-form expression to describe signal nonlinear propagation in arbitrary transmission lines has been derived in chapter 3. This solution is given as the sum of the solution for linear transmission and a perturbation term representing nonlinear effects. Noting $\tilde{X}_j$ and $\tilde{Y}_j$ the Fourier-transforms of the amplitude envelope of jth channel at the input and output of the transmission line, one obtains after loss and dispersion compensation (see Eq. (3.15)):

$$
\begin{aligned}
\tilde{Y}_j(\omega) &\approx C_1\tilde{X}_j(\omega) + \delta_{NL}(\omega) + \delta_{OA}(\omega) \\
\tilde{Y}_j(\omega) &\approx C_1\tilde{X}_j(\omega) + \delta_{intra}(\omega) + \delta_{inter}(\omega) + \delta_{OA}(\omega)
\end{aligned}
\tag{5.12}
$$

---

[8]I.e. assuming that the joint distribution of input and output signal is Gaussian.
[9]as defined by Shannon in Eq. (5.6)

Where C_1 is a constant ensuring energy conservation (see section 3.2). δ_{OA} accounts for the noise generated during optical amplification (ASE noise) and δ_{NL} is the perturbative term describing the nonlinear spectral components falling into the channel. As discussed in 4.1.1, it can be distinguished between intra and inter-channel nonlinear contributions. The deterministic nature of intra-channel effects (here simply referred to as SPM) was discussed in the preceding section. Conversely, statistics of XPM and FWM become Gaussian with an increased number of channels[10]. The fiber maximum available bandwidth does not exceed 20 THz with classical optical amplification and since the maximum electrical receiver bandwidth of commercial systems will probably not exceed 200GHz in the near future, a large number (> 100) of WDM channels is required to approach the fiber maximum capacity. As a consequence, Gaussian statistics for δ_{inter} will be assumed in the following. Under these assumptions, Eq. (5.12) becomes:

$$
\begin{aligned}
\tilde{Y}_j &\approx C_2 F(\tilde{X}_j) + \eta_{inter} G_1 + \eta_{ASE} G_2 \\
\tilde{Y}_j &\approx C_2 F(\tilde{X}_j) + n
\end{aligned}
\tag{5.13}
$$

whit $F(\cdot)$ a bijection associated to the transmission line (accounting for the deterministic nature of SPM) and C_2 a constant ensuring energy conservation. η_{inter} and η_{ASE} are the strengths of the perturbations due to nonlinear inter-channel effects and ASE. $G_{1,2}$ are independent complex random Gaussian variables verifying:

$$
\begin{aligned}
G_j &= u_j + i v_j \\
<G_j> &= <u_j> + i <v_j> = 0 \\
<|G_j|^2> &= <|u_j|^2> + i <|v_j|^2> = 1
\end{aligned}
\tag{5.14}
$$

with $\sqrt{-1} = i$,. u and v are real random Gaussian variables with zero mean. In the case of ASE noise, u and v are identically distributed ($<|u|^2> = <|v|^2>$). This property is not always verified for the nonlinear noise. Indeed, XPM may affect the phase of the transmitted

---

[10]As a consequence of the Central Limit Theorem, see appendix D.

signal (resulting in timing jitter) more than its amplitude [23]. However, for large FM-AM conversion due to chromatic dispersion [102–104] or when FWM is the dominant nonlinear effect, we can assume the nonlinear noise to be equally distributed in phase and amplitude. Under this assumption and noting u and v the real and imaginary parts of G_j, the probability density functions associated to the inter-channel nonlinear effects and ASE contributions (noted respectively g and h) are:

$$g(u,v) \quad = \quad \frac{1}{\pi \eta_{inter}} e^{-\frac{u^2+v^2}{\eta_{inter}^2}} \tag{5.15}$$

$$h(u,v) \quad = \quad \frac{1}{\pi \eta_{ASE}} e^{-\frac{u^2+v^2}{\eta_{ASE}^2}} \tag{5.16}$$

Since ASE and nonlinear impairments are independent, the (complex) probability density function (PDF) of $n = \delta_{ASE} + \delta_{inter}$ is obtained as:

$$f(u,v) = g(u,v) * h(u,v) \tag{5.17}$$

$*$ standing for the convolution product. Since g and h are Gaussian, f remains Gaussian with zero mean and variance $\sigma_n^2 = \eta_{ASE}^2 + \eta_{inter}^2 = W_{inter} + S_{ASE}$, with W_{inter} the power spectral density of spectral components generated by nonlinear inter-channel interactions and W_{ASE} the power spectral density of ASE (in one polarization). As a consequence, the conditional probability $P(F(X_j)|Y_j)$ is obtained as:

$$P(F(X_j)|Y_j) = \frac{1}{\sqrt{2\pi}\sigma_n} e^{\frac{-|F(X_j)-Y_j|^2}{2\sigma_n^2}} \tag{5.18}$$

The knowledge of the conditional probability $P(X_j|Y_j)$ is required to calculate the channel maximum capacity. Since F is a bijection, we can write [105]:

$$P(X_j|Y_j) = P(X_j, Y_j)P(Y_j) = |J|P(F(X_j), Y_j)P(Y_j) \tag{5.19}$$

with J the Jacobian of the transformation $X \rightarrow F(X)$. For energy conservation to be ensured[11], F must conserve the norm, i.e. $|J| = 1$. As a consequence, $P(F(X_j)|Y_j) = P(X_j|Y_j)$, so that from an information theory point of view SPM does not modify system maximum achievable capacity. Using Eq. (5.7) and Eq. (5.18), the maximal achievable channel capacity, C, is obtained as:

$$C = \rho B_{opt} log_2 \left(1 + \frac{P - P_{inter}}{W_{ASE}\rho B_{opt} + P_{inter}} \right) \qquad (5.20)$$

where W_{ASE} is the spectral power density of ASE in one polarization, P, the power of the aggregate WDM signal. ρ is the spectral use, defined as the ratio of the optical bandwidth occupied by the signal and the total utilized bandwidth (gap included). The additional term in nominator ensures energy conservation of the aggregate WDM signal. According to Shannon, maximum capacity can be achieved with a modulation format having statistics similar to those of a white Gaussian noise[12].

As an example, we consider the transmission of a total aggregate bandwidth of $5\,\mathrm{THz}$ (C-band) fully filled with channels with 160GHz occupied bandwidth (no gap, $\rho = 1$) over N identical spans. Each span consists of $80\,\mathrm{km}$ SSMF (γ=1/(W-km), α=0.2 dB/km, $\beta_2 = -20\,ps^2/km$) followed by an ideal (lossless and linear) DCF and an EDFA. Fiber loss ($22\,\mathrm{dB}$ per span) is fully compensated within each span ($F_{EDFA} = 5dB$), whereas chromatic dispersion can be fully or partially compensated (100% dispersion compensation is realized at the receiver side when needed.

The system maximum achievable spectral efficiency, S ($C = B_{opt}S$), is displayed against the channel input power for one span ($N = 1$) in Fig. 5.2.a and against the number of spans in Fig. 5.2.b (optimal channel input power is derived from Eq. (5.20) for each configuration). Channel maximum capacity increases with residual dispersion per span as a result of the reduction of the *nonlinear diffusion bandwidth*, $f_{d,eq}$.

---

[11]in single-channel transmission, when the channel experiences only SPM
[12]E.g. M-QAM (Quadrature Amplitude Modulation) with M as large as allowed by the OSNR can be a good candidate.
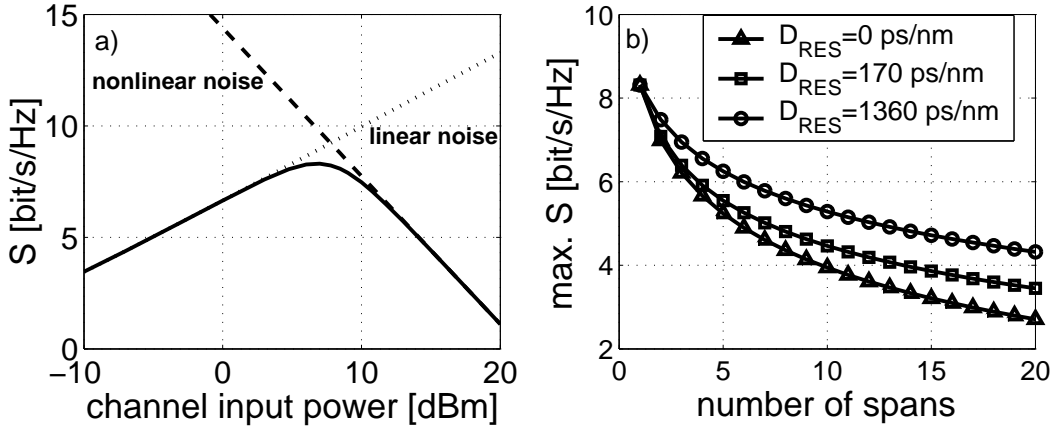
Figure 5.2: system maximum spectral efficiency in [bit/s/Hz] against a) channel input power (single-span transmission) and b) number of spans for different link design.

Impact of intra-channel nonlinear effects on the system maximum capacity

It has been argued that intra-channel nonlinear effects are deterministic effects, that can be (theoretically) undone with signal processing at the transmitter and/or receiver side. However, an optimization of the link design (see 4.1.2) is not always possible in legacy fiber plant and digital signal processing may not be easy to implement at high bit-rates. In that case, inter-pulse interactions (iXPM, iFWM) appear stochastic and have to be taken into account in calculation of the nonlinear noise ($P_{NL} = P_{inter} + P_{intra}$), which is given as in Eq. (3.45)

$$P_{NL} \approx 2f_{d,eq}^2 \rho^{1-\chi} \frac{P_{ch}^3}{B_{ch}^2} N^2 \eta_0^2 \ln \left(1 + \frac{\pi}{4} \frac{B_{opt}^2}{f_{d,eq}^2} \right)$$

Similarly to inter-channel effects, it can be shown[13] that for highly dispersive systems ($B/f_{d,eq} > 5$) intra-channel effects follow Gaussian statistics, so that the expressions for the system maximal capacity reported in Eq. (5.20) remain valid when replacing P_{inter} by P_{NL}.

---

[13]See appendix D.

5.3.2 Achievable capacity with current technologies

In the previous section, the theoretical limit for the system capacity has been derived. This limit can be achieved with optimal encoding and modulation format[14]. Such a solution is not conceivable in practicable systems. Firstly, because too long delays would be required for signal processing. Secondly because coherent detection, which is necessary to detect both phase and amplitude, necessitates an optical or electrical phase-locked loop or some other carrier recovery techniques which are complex to realize and operate.

Thus, from the system-designer point of view, the knowledge of the maximum achievable system capacity with the available technologies is at least as important as the knowledge of its Shannon limit. For example regardless of the channel quality, binary modulation formats such as On-Off Keying (OOK) or Differential Phase Shift Keying (DPSK, [3]) cannot exceed a spectral efficiency of 1 bit/s/Hz (without polarization division multiplexing). Spectral efficiencies between 1 and 2 bit/s/Hz can be achieved with Quaternary (differential) Phase Shift Keying (QPSK, [106]). Above 2 bit/s/Hz, modulation formats like Quadrature Amplitude Modulation (M-QAM, [107]) or Phase Shift Keying (M-PSK [108], [109]) with $M \geq 8$ must be employed.

For a particular modulation format (with associated probability density function, $P_x(x)$, see 5.1.1) the system maximum capacity is given as in Eq. (5.6):

$$C_s = H(Y) - H(Y|X) \tag{5.21}$$

with:

$$H(Y) = \int P_y(y) log_2 \left(P(y) \right) dy \tag{5.22}$$

$$H(Y|X) = \int \int P_x(x) P_{y|x}(y|x) log_2 \left(P_{y|x}(y|x) \right) dx dy \tag{5.23}$$

---

[14]Coherent detection and highly-efficient error-correcting codes are necessary.

with $p(y) = \int P_x(x)P_{y|x}(y|x)dx$ and the power and probability constraints:

$$\int x^2 P_x(x)dx = c < \infty \;\wedge\; \int P_x(x)dx = 1 \tag{5.24}$$

where c is a constant proportional to the channel average power. Since $P_x(x)$ is known, only the knowledge of the conditional probability $P_{y|x}(y|x)$ is required to determine C_s.

Coherent systems

In coherent systems [3], the phase and amplitude of the signal (or equivalently, its real and imaginary parts) can be modulated and detected separately. It has been shown in the previous section that the complex variables X and Y representing the envelope of the electrical field of the input and output signals verify the following relationship:

$$Y(t = t_k) = cX(t = t_k) + \delta_{NL}(t = t_k) + \delta_{OA}(t = t_k) = cX(t = t_k) + n(t = t_k) \tag{5.25}$$

where δ_{NL} and δ_{OA} account for the nonlinear and ASE noise and c is a constant ensuring energy conservation. n is a zero-mean complex Gaussian random variable with variance $\sigma_n^2 = P_{ASE} + P_{NL}$, so that $P_{y|x}(y|x)$ follows a Gaussian distribution:

$$P_{y|x}(y|x) = \frac{1}{2\pi\sigma_n^2} \exp\left(-\frac{|cx - y|^2}{2\sigma_n^2}\right) \tag{5.26}$$

Using Eq. (5.21), (5.23) and (5.23), it is possible to evaluate (numerically) C_s. As an example, the system capacity for the system described in Fig. 5.2 (transmission over a single 80km span of an aggregate bandwidth of 31x160 GHz$\approx$ 5THz with a single polarization) is reported for 4-QAM and 16-QAM in Fig. 5.3 against the channel input power. The input signal is assumed ideal (i.e. discrete), all states are assumed equally probable.

Intensity-modulated direct detection

In (ideal) intensity-modulated direct-detection (IMDD) systems, the detected signal is obtained as:

$$Y = |cX + \delta_{NL} + \delta_{OA}|^2 = |cX + n|^2 \qquad (5.27)$$

where X is the complex amplitude of the input signal and n is the perturbation standing for ASE and nonlinear noise. The conditional probability $P_{y|x}(y|x)$ is a noncentral χ^2 distribution with two degrees of freedom [110]. Noting $u = |x|$ and $v = \sqrt{y}$, the resulting conditional probability, $p(v|u)$, is shown to follow a Rice distribution [111]:

$$p(v|u) = \frac{2v}{\sigma_n^2} \exp\left(-\frac{u^2 + v^2}{\sigma_n^2}\right) I_o\left(\frac{2vu}{\sigma_n^2}\right) \qquad (5.28)$$

where $I_0(.)$ is the 0th-order modified Bessel function of the first kind. C_s as defined in (5.21) is displayed for simple OOK and multi-level (0-1/3-2/3-1) AM modulation format in Fig. 5.3 (all states are assumed equally probable). The case of constant-intensity modulation formats [112], has not been treated in this work, because it requires the use of phase modulation (e.g. DPSK) together with Dispersion-Shifted Fibers (DSF) and/or careful dispersion management[15], conditions that are unlikely to be met in commercial transmission systems. Maximum capacity for various modulation/detection techniques have been reported in [113] and other examples can be found in [111] and [114].

5.3.3   Discussion

The present approach is valid for weak nonlinearities (typically $P \geq 20\,P_{NL}$) a condition met in all transmission systems of practical interest except Soliton-transmission systems and weak nonlinear phase noise (Gordon-Mollenauer effects). This last assumption is not always verified in long haul systems where ASE accumulates along the spans and typical OSNR values lay around $10\,$dB.

Another assumption that has been made in this study is that nonlinear perturbations can

---

[15]Otherwise phase shifts are turned into amplitude variations by the fiber chromatic dispersion.
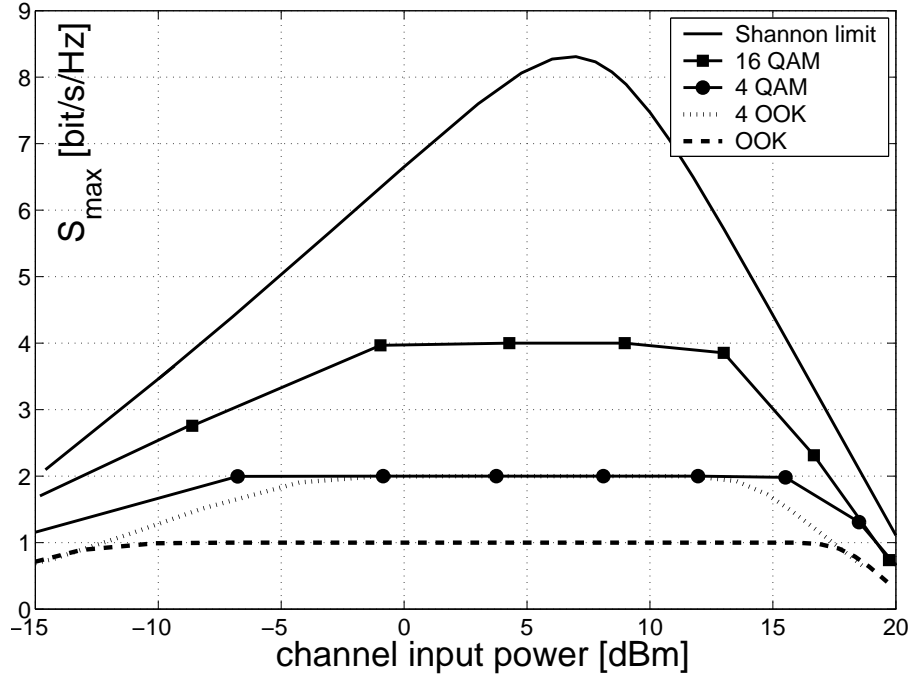
Figure 5.3: Maximal achievable spectral efficiency for different modulation formats against channel input power ($B_{ch} = 160\text{GHz}, \rho = 1$). The Shannon limit reported in figure 5.2 is shown for comparison.

be considered as Gaussian noise. We have shown (see appendix D) that the statistics of the nonlinear perturbation become Gaussian with an increasing number of co-propagating channels. As a consequence, we expect this last condition to be verified in very-high capacity transmission systems, where large number of WDM channels is assumed.

5.4 Conclusion

In this chapter, the information capacity of WDM systems in the presence of ASE noise and fiber nonlinearities has been derived as a function of the *nonlinear diffusion bandwidth*. Depending on whether intra-channel effects are considered as noise or as deterministic effects[16], this approach leads to a lower or upper bound for the system maximal achievable capacity. We have shown that this theoretical limit can be approached by coherent sys-

---

[16]They can be -theoretically- compensated with the help of (digital or analog) signal processing or optimized transmission link design.

tems (e.g. M-QAM) associated with efficient coding (e.g Turbo-codes, [115]). However, coherent detection necessitates the use of an optical or an electrical phase-locked loop, a feature usually complex to realize. Moreover, the requirements on the laser linewidth become very stringent with an increasing number of levels (e.g. 30MHz for DPSK [113], 3MHz for DQPSK, [116] and 300 KHz for 8-PSK [117] for a 10Gbaud signal). In consequence, approaching the Shannon limit of WDM-based optical transmission systems will remain a major challenge in the near future.

Chapter 6

Outlook & Conclusion

6.1 Outlook

The results reported in the present work support the idea that -even in presence of fiber nonlinearities- the capacity of today's fiber-optic transmission systems can be increased by at least an order of magnitude. Potentially, tens of Tb/s can be transmitted in the C-band for metro and even long-haul transmission without important modification of the existing fiber plant. This capacity upgrade is largely made possible by the emergence of new technologies like high-performance encoding schemes, multi-level modulation formats and electrical signal processing among others.

A wide array of options exists for the realization of these high-capacity transmission systems. For example, high bit-rates ($40\,\&\,160\,\mathrm{Gb/s}$) are of particular interest, especially with the arrival of the first $40\,\mathrm{Gb/s}$ routers. Besides possible cost savings, high bit-rate channels enable significant reduction of the number of transmitters and receivers, simplifying the network management (routing, grooming, restoring, etc.). Another benefit of high bit-rate transmission lies in the fact that impairments arising from intra-channel nonlinear interactions can be drastically reduced with appropriate transmission line design. Because the ratio of intra-channel interactions among nonlinear effects increases with the channel bandwidth, more nonlinear impairments can be potentially suppressed using 40 or $160\,\mathrm{Gb/s}$ rather than $10\,\mathrm{Gb/s}$ channels. However, this optimization is modulation format-dependent and

therefore the benefits of high bit-rates vanish while upgrading a system, for example from classical RZ to DQPSK[1]. In addition, system robustness to chromatic dispersion (GVD) and polarization-mode dispersion (PMD) is known to decrease with an increased channel bandwidth making an implementation of binary 40Gb/s systems problematic in legacy fiber plant. This problem can be overcome by using multi-level modulation formats, which offer the possibility to increase the channel bit-rate while keeping its bandwidth constant.

Increasing the transmitted bandwidth has been shown to be more advantageous with regard to nonlinear impairments than pushing the spectral efficiency in order to increase the system capacity. However, using a wider bandwidth may require additional amplifiers (for S and L bands) and other optical components, so that raising spectral efficiency may be sometimes the more economical solution. On the other hand, the complexity (and thus cost) of transmitters and receivers for multi-level modulation formats increase exponentially with the achievable spectral efficiency, so that we believe that the design of future high-capacity transmission systems will depend more on economic considerations than on technical constrains.

6.2   Conclusion

The main purpose of this work has been to examine the impact of fiber nonlinearities on the design of optical transmission systems. To that aim, a high-level analysis of WDM transmission systems has been proposed. After a brief review of the physical aspects of light propagation in optical fiber, we introduced the concepts of *nonlinear transfer function* and *nonlinear diffusion bandwidth*, both offering useful insights into nonlinear characteristics of a transmission line. Together with the *continuum* and *semi-continuum* models, they enable a rapid assessment of nonlinear impairments in WDM transmission systems. Design rules (some of them restricted to amplitude-modulated signals) for the reduction of nonlinear impairments have also been proposed. In particular, it has been shown how to reduce simultaneously intra-and inter-channel nonlinear effects. Additionally, impact of fiber bire-

---

[1]In DPSK or DQPSK transmission, phase noise degrades system performance much more than in RZ transmission leading to different optimal dispersion maps (see section 4.1.2).

fringence and of information distribution in the frequency domain on fiber nonlinearities have been investigated. Finally, the information capacity of fiber-optic transmission has been derived. Motivation for this is the ever increasing demand for more bandwidth, which could make systems operate closer and closer to this theoretical limit as it is already the case for wireless transmission systems. Since these systems will have to operate at much lower OSNR than today, we believe that high-speed electronics will play ever-increasing role in fiber-optic transmission. Not only for the implementation of efficient encoding and decoding algorithms but also for electrical mitigation of GVD, PMD and nonlinear impairments, which can provide an economic alternative to all-optical signal processing.

Appendix A

The split-step Fourier algorithm

The one method that is commonly used to solve the NLSE is the Split-Step Fourier (SSF) method [118]. Basically, it relies on the principle that linear and nonlinear effects can be considered separately form each other over short distances [119] so that the propagation equation can be written:

$$A(z + \Delta z) = \exp\left(\Delta z(\hat{N})\right) \exp\left(\Delta z \hat{D}\right) A(z) \tag{A.1}$$

with $A(z)$ the slowly varying envelope of the electrical field. $\hat{D} = -\frac{i}{2}\beta_2 \frac{\partial^2}{\partial T^2} - \frac{\alpha}{2}$ is the linear operator accounting for fiber loss and dispersion and $\hat{N} = -i\gamma|A|^2$ is the nonlinear operator accounting for Kerr-effect. $\exp\left(\Delta z \hat{D}\right)$ is usually solved in the spectral domain, whereas $\exp\left(\Delta z \hat{N}\right)$ is more favorably solved in the time domain. The Fast Fourier Transform (FFT) algorithm [120] is used to switch from one representation to another. In single channel transmission systems the computation time is roughly proportional to $N \log_2 N$, where N is the number of signal samples in time or frequency domain and to the channel peak power. In WDM systems, the signal envelope (responsible for the nonlinear modulation of the fiber refractive index) varies much more rapidly and the computation time increases on the order of at least M^3 [23], where M is the number of channels. As a consequence, if the SSF method remains suitable to predict the performance of a given WDM transmission system, it is not convenient to explore a large set of different system configurations.

Appendix B

Analytical derivation of $f_{d,eq}$

The magnitude of the *nonlinear transfer function* $|\eta(\Delta\Omega)|$ for multi-span transmission in the case of identical spans is given in Eq. (3.27) as:

$$|\eta(\Delta\Omega)|^2 = \left| \eta_s(\Delta\Omega) \frac{\sin\left(N\Delta\Omega D_{res}/2\right)}{\sin\left(\Delta\Omega D_{res}/2\right)} \right|^2$$

so that that $|\eta(\Delta\Omega)|^2$ is given as the product of two transfer functions. It has been shown in section 3.2.2 that $|\eta_s(\Delta\Omega)|^2$ can be approximated as:

$$|\eta_s(\Delta\Omega)|^2 = \frac{|\eta_o|^2}{1 + \left(\frac{\Delta\Omega}{4\pi f_d^2}\right)^2}$$

with f_d the 10dB bandwidth of $|\eta_s|^2$. Identically, when $(\Delta\Omega D_{res}/2 << \pi)$, one can write:

$$\left| \frac{\sin\left(N\Delta\Omega D_{res}/2\right)}{\sin\left(\Delta\Omega D_{res}/2\right)} \right|^2 \approx \frac{N^2}{1 + \left(\frac{\Delta\Omega}{4\pi f_a^2}\right)^2}$$

with $f_a^2 \approx \frac{1}{2\pi D_{res}(N-1)}$. finally, $|\eta(\Delta\Omega)|$ can be written as:

$$|\eta(\Delta\Omega)|^2 \approx \frac{|N\eta_o|^2}{\left(1 + \left(\frac{\Delta\Omega}{4\pi f_d^2}\right)^2\right) \left(1 + \left(\frac{\Delta\Omega}{4\pi f_a^2}\right)^2\right)}$$

keeping only the largest terms in the denominator, the above equation becomes:

$$|\eta(\Delta\Omega)|^2 \approx \frac{|N\eta_o|^2}{1 + \left(\frac{\Delta\Omega}{4\pi f_d^2}\right)^2 + \left(\frac{\Delta\Omega}{4\pi f_a^2}\right)^2} = \frac{|N\eta_o|^2}{1 + \left(\frac{\Delta\Omega}{4\pi f_{d,eq}^2}\right)^2}$$

with $1/f_{d,eq}^2 = 1/f_d^2 + 1/f_a^2$ the $10dB$ bandwidth of $|\eta(\Delta\Omega)|^2$. Thus the *equivalent nonlinear bandwidth* of a multi-span transmission line (with identical spans) is given as:

$$f_{d,eq} \approx \frac{1}{\sqrt{\frac{1}{f_{d,s}^2} + 2\pi(N-1)|D_{res}|}}$$

Appendix C

Analytical derivation of W_{NL}

Continuum model

The power spectral density of the nonlinear perturbation at the central frequency component ($f = 0$) was derived in chapter 2 as follows:

$$
\begin{aligned}
W_{NL} &= \left\langle 2\pi \left| \delta_{NL}(\omega = 0) \right|^2 \right\rangle \\
&= \left\langle 2\pi \left| \int_{-\pi B_{opt}}^{\pi B_{opt}} \int_{-\pi B_{opt}}^{\pi B_{opt}} \eta(\Delta\Omega) \tilde{A}(\omega_1) \tilde{A}^*(\omega_2) \tilde{A}(\omega - \omega_1 + \omega_2) d\omega_1 d\omega_2 \right|^2 \right\rangle \quad \text{(C.1)}
\end{aligned}
$$

where $< \cdot >$ is the mean operator. $\eta(\Delta\Omega)$, with $\Delta\Omega = \omega_1\omega_2$, is the *nonlinear transfer function* of the transmission line and $\tilde{A}(\omega)$ is the Fourier-transform of the slowly varying envelope of the electrical field. If we assume all products $\eta\tilde{A}\tilde{A}^*\tilde{A}(\omega, \omega_1, \omega_2)$ to have uncorrelated phase[1], one obtains:

$$
W_{NL} = 2\pi \int_{-\pi B_{opt}}^{\pi B_{opt}} \int_{-\pi B_{opt}}^{\pi B_{opt}} \left| \eta(\Delta\Omega) \tilde{A}(\omega_1) \tilde{A}^*(\omega_2) \tilde{A}(\omega - \omega_1 + \omega_2) \right|^2 d\omega_1 d\omega_2 \quad \text{(C.2)}
$$

If in addition the spectrum of the aggregate WDM can be approximated by a continuum (see Fig. C.1), W_{NL} can be written as:

---

[1] As a consequence of GVD and because all lasers start to emit with different optical phases.
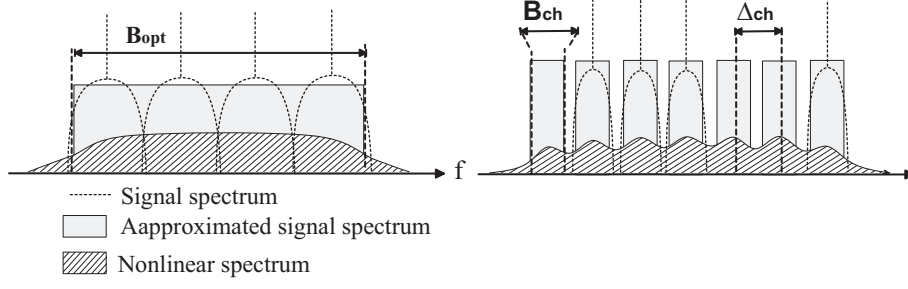
Figure C.1: Continuum (left) and semi-continuum (right) models for WDM signals.

$$W_{NL} = \frac{1}{4\pi^2} W^3 \int_{-\pi B_{opt}}^{\pi B_{opt}} \int_{-\pi B_{opt}}^{\pi B_{opt}} |\eta(\Delta\Omega)S(\omega_1,\omega_2)|^2 \, d\omega_1 d\omega_2 \qquad (C.3)$$

with $W = \frac{P_{tot}}{B_{opt}}$ the power spectral density of the input signal in W/Hz. The integration domain, $S(\omega_1,\omega_2)$, is displayed in Fig. C.2. As shown in chapter 2, η can be expressed with the help of the nonlinear diffusion bandwidth, $f_{d,eq}$. When $f_{d,eq} \ll B_{opt}$, it is roughly equivalent to integrate over S or over a square delimited by $\{\omega_1,\omega_2\} \in [-\pi B_{opt}..\pi B_{opt}]$:

$$W_{NL} \approx \frac{1}{4\pi^2} W^3 N^2 \eta_0^2 \int_{-\pi B_{opt}}^{\pi B_{opt}} \int_{-\pi B_{opt}}^{\pi B_{opt}} \frac{1}{1 + \left(\frac{\omega_1\omega_2}{4\pi f_{d,eq}^2}\right)^2} d\omega_1 d\omega_2 \qquad (C.4)$$

with N the number of spans and $\eta_0 = \frac{\gamma}{\alpha}$ (N identical spans are assumed in this example). Integrating over ω_1 leads to:

$$W_{NL} \approx \frac{1}{4\pi^2} W^3 N^2 \eta_0^2 \int_{-\pi B_{opt}}^{\pi B_{opt}} \frac{8\pi f_{d,eq} \arctan\left(\frac{B_{opt}\omega_2}{4 f_{d,eq}^2}\right)}{\omega_2} d\omega_2 \qquad (C.5)$$

setting $X = \frac{B_{opt}\omega_2}{4 f_{d,eq}^2}$, the above integral can be approximated as:

$$
\begin{aligned}
W_{NL} &\approx 2W^3 N^2 \eta_0^2 4 \frac{f_{d,eq}}{\pi} \int_0^{\frac{\pi B_{opt}^2}{4 f_{d,eq}^2}} \frac{\arctan X}{X} dX \\
W_{NL} &\approx 2 f_{d,eq}^2 W^3 N^2 \eta_0^2 \ln\left(1 + \frac{\pi}{4} \frac{B_{opt}^2}{f_{d,eq}^2}\right)
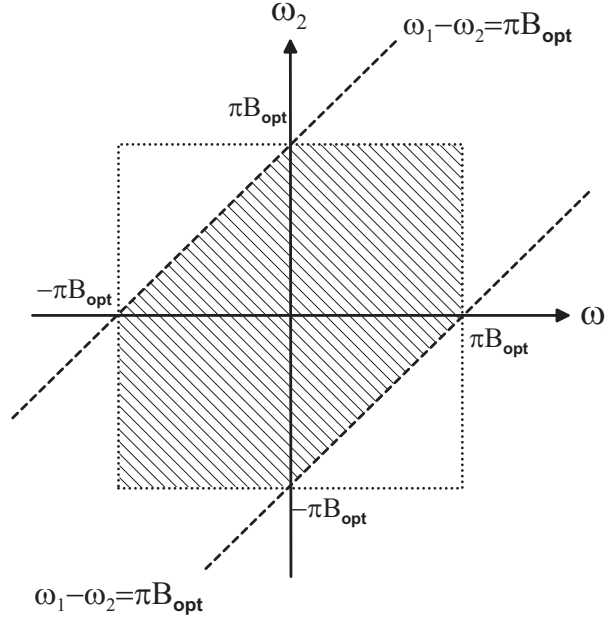\end{aligned}
\qquad (C.6)
$$

91

Figure C.2: the integration domain, $S(\omega_1, \omega_2)$ for a continuum. S=1 inside the dimmed area and 0 outside.

Semi-continuum model

The semi-continuum model accounts for the frequency gaps $\Delta G =$ is the difference between the channel spacing, Δ_{ch} and the channel occupied bandwidth, B_{ch} between the WDM channels (see Fig. C.1. $\rho = \frac{B_{ch}}{\Delta_{ch}}$ is called the spectral use. The integration domain, $S(\omega_1, \omega_2)$, for such a semi-continuum is displayed in Fig. C.3. At constant total power P (i.e. for a channel local spectral power density of $\frac{P}{\rho B_{opt}}$), the nonlinear power falling into the channels one when $\Delta G \ll f_{d,eq}$ (i.e. for high granularity) is:

$$P_{NL} =\approx (B_{opt} * \rho)\rho^3 2 f_{d,eq}^2 \left(\frac{P_{ch}}{\rho B_{ch}}\right)^3 N^2 \eta_0^2 \ln\left(1 + \frac{\pi}{4}\frac{B_{opt}^2}{f_{d,eq}^2}\right) \tag{C.7}$$

Conversely, when $\Delta G \gg f_{d,eq}$ (i.e. for low granularity), one obtains:

$$P_{NL} \approx (B_{opt} * \rho)\rho^2 2 f_{d,eq}^2 \left(\frac{P_{ch}}{\rho B_{ch}}\right)^3 N^2 \eta_0^2 \ln\left(1 + \frac{\pi}{4}\frac{B_{opt}^2}{f_{d,eq}^2}\right)$$
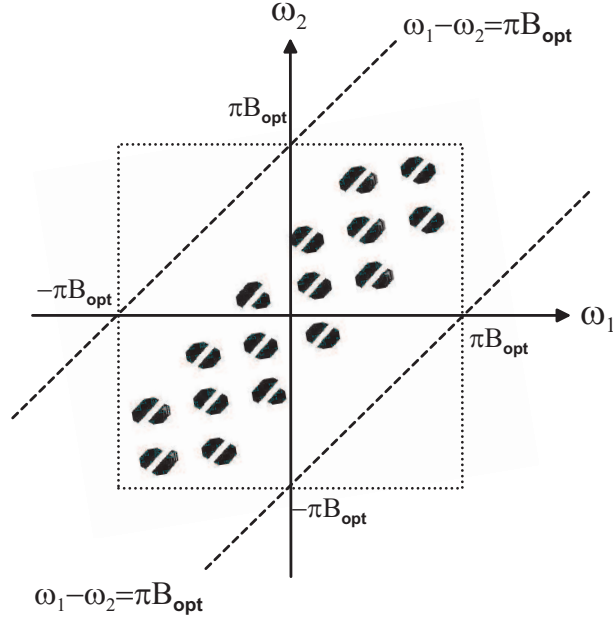
Figure C.3: the integration domain, $S(\omega_1, \omega_2)$ for a semi-continuum (7 channels, $\eta=0.5$)

The result reported in Eq. (3.45) and Eq. (3.46) verify these boundary conditions and were obtained by setting $B_{ch} = \rho \Delta_{ch}$.

Appendix D

Statistical characterization of δA_0

System model

We consider an optical signal consisting in 2N+1 co-polarized WDM amplitude-modulated channels (see Fig. D.1). We assume the channels to have the following characteristics (verified by most cases of practical interest):

> **H1**: Marks and spaces are equiprobable and the encoded signal is random.
>
> **H2**: Channels are uncorrelated (bit stream are independent) and the optical carriers (lasers) start to emit with random phases.
>
> **H3**: Channels are statically equivalent (same bit-rate, modulation format assumed) and peak-power limited.

The perturbation (see Eq. (3.15)) of the electrical field observed in the middle of the bit-slot of the central channel, $\delta A_0(t = 0)$, is obtained as follows:

$$\delta\delta A_0(t, L) = \frac{1}{\sqrt{2\pi}} \int_{-\pi B_{CH}}^{\pi B_{CH}} \delta_{NL}(\omega, L) \tag{D.1}$$

$$= X_0 + \sum_{\substack{j=-N \\ k \neq 0}}^{N} X_j + \sum_{j=-N}^{N} \sum_{\substack{k=-N \\ k \neq j}}^{N} Y_{j,k} \tag{D.2}$$

where $\delta_{NL}(\omega, L)$ is the nonlinear perturbation as derived in Eq. (3.15). X_0, X_j and $Y_{j,k}$ stand for the SPM, XPM and FWM products. X_0 is assumed to be deterministic and will not be
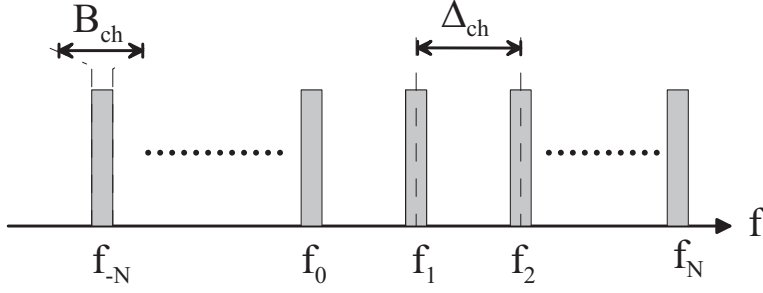
Figure D.1: Power spectral density of the considered WDM signal. B_{CH} is the channel occupied bandwidth and Δ_{CH} the channel spacing.

treated as a noise in the following discussion. For a transmission over a single span of length L verifying $e^{-\alpha L} \ll 1$, and in the limit of low dispersive systems ($\beta_2 (2\pi B_{ch})^2/\alpha \ll 1$) and large channels spacing ($B_{ch} \ll \Delta_{ch}$), the terms X_j and $Y_{j,k}$ are derived in [23] as follows:

$$X_j \quad \simeq \quad -i\gamma A_0 F_{t=0}^{-1}\{\int \frac{P_j(\omega,0)}{1 + ij\beta_2 2\pi\omega\Delta_{CH}/\alpha}d\omega\} = X_j^{Re} + iX_j^{Im} \qquad (D.3)$$

$$Y_{j,k} \quad \simeq \quad \frac{\gamma F_{t=0}^{-1}\{\int \int A_j(\omega')A_k^*(\omega'')A_{j-k}(\omega - \omega' + \omega'')d\omega'd\omega''\}}{-i + j(k-j)4\pi^2\Delta_{CH}^2\beta_2\alpha} \qquad (D.4)$$
$$\simeq \quad Y_{j,k}^{Re} + iY_{j,k}^{Im}$$

where $i = \sqrt{-1}$ and $F_{t=0}^{-1}\cdot$ is the inverse Fourier-transform operator (for t=0) and $P_j(\omega) = |A_j(\omega)|^2$ with $A_j(\omega)$ being the Fourier Transform of $A_j(t,0)$, the amplitude envelope of the jth channel at the transmitter side.

Statistical characterization of δA_0

δA_0 can be describe as a phasor (see Fig. D.2), i.e. as the sum of a real and imaginary random variable both having zero mean to ensure energy conservation ($\delta A_0 = \delta A_0^{Re} + \delta A_0^{Im}$). As a consequence of **H1**, the real and imaginary parts of X_j and $Y_{j,k}$ are random variables. Since X_j and $Y_{j,k}$ are not identically distributed, the classical formulation of the central limit theorem can not be applied.

We focus now on δA_0^{Im}. We note σ_{Im} and R_{Im} its variance and third order moment. Since
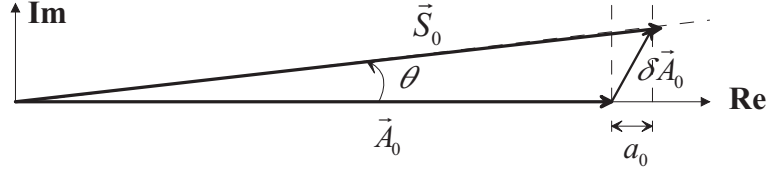
Figure D.2: θ and a_0 stand for the signal phase and amplitude variations caused by the nonlinear perturbation δA_0.

the channels are peak-power limited (**H3**), the variances (σ_i) and the third order moments (r_i) of the terms X_j^{Im} and $Y_{j,k}^{Im}$ are finite and the calculus of the covariance (see section D.10) indicates that all variables are independent. It results from **H2** and Eq. (D.5) that the PDFs of the $Y_{j,k}^{Im}$ terms are symmetrical and consequently that their third order moments are nil.

Central Limit Theorem (Lyapunov formulation) [121]

Let $z_1...z_n$ be n independent random variables not obligatory identically distributed with finite mean, μ_i, variance, σ_i, and third order moment, r_i . Noting $Z_n = \sum_{i=1}^n z_i$, $m_n = \sum_{i=1}^n \mu_i$, $S_n^2 = \sum_{i=1}^n \sigma_i^2$ and $R_n^3 = \sum_{i=1}^n r_i^3$ and if the condition

$$\lim_{n\to\infty} \frac{R_n^3}{S_n^2} = 0 \tag{D.5}$$

is verified, then

$$\frac{Z_n - m_n}{\sqrt{S_n^2}} \to N(0,1) \tag{D.6}$$

where N is the normal-centered distribution.

Application of the central limit theorem

Using Eq. (D.3), Eq. (D.5) and the results obtained in the previous section, we show that σ_{Im}^2 and R_{Im}^3 verify the following inequalities:

$$\sigma_{Im}^2 = \sum \sigma_i^2 > \left(\sum_{\substack{k=-N \\ l=k-j}}^{N} \frac{\gamma^2 P_m^3/2}{1+(lj\beta_2 4\pi^2 \Delta_{CH}^2/\alpha)^2} \right) \to I = \int \int \frac{1}{1+a^2 x^2 y^2} dx dy \quad \text{(D.7)}$$

$$R_{Im}^3 = \sum r_i^3 < \left(\sum_{j=1}^{N} \frac{2\gamma^3 P_m^3}{1+(j\beta_2 4\pi^2 B_{CH}\Delta_{CH}/\alpha)^2} \right) \to J = \int \frac{1}{1+b^2 x^2} dx \quad \text{(D.8)}$$

The integrals **I** and **J** are the continuous counterparts of the discrete summations. Since **I** diverges and **J** converges, we can conclude from the Cauchy integral test [122], that σ_{Im}^2 diverges and R_{Im}^3 converges, and finally that:

$$\lim_{N\to\infty} \frac{R_{Im}^3}{\sigma_{Im}^2} = 0 \quad \text{(D.9)}$$

what is the Lyapunov condition. Thus, for a large number of channels, the hypotheses of the central limit theorem are fulfilled and in that case δA_0^{Im} follows a Gaussian distribution with variance σ_{Im}^2. The analysis is identical for δA_0^{Re}. As a consequence, for a WDM system consisting of a large number of channels, the perturbation induced by nonlinear inter-channel interaction can be described by two random variables, both following a centered Gaussian distribution.

Discussion

In the present study, low dispersive channels and large channel spacing are assumed. These assumptions enable the derivation of simple analytical expressions for the XPM-and FWM-induced perturbations, necessary for a verification of the Lyapunov theorem. The rate of convergence is changing with higher bit-rates and/or narrower channel spacing, but the final result (convergence towards Gaussian statistics) remains the same.
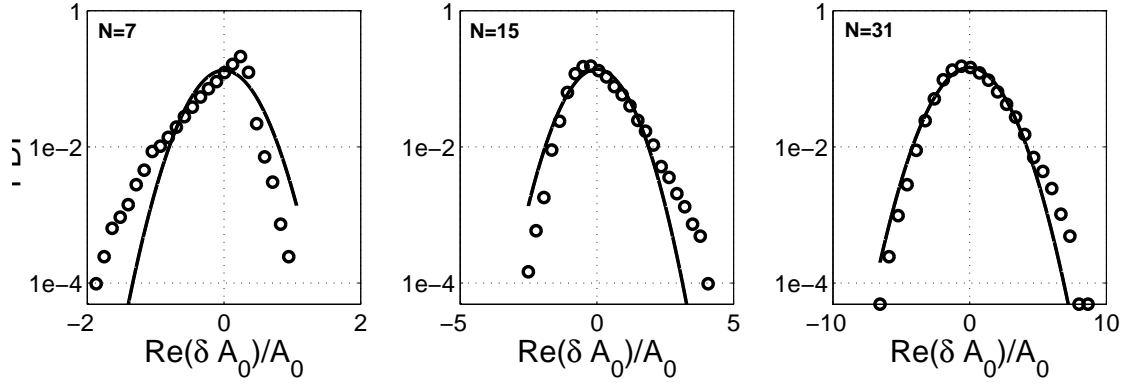
Figure D.3: PDF of δA_0^{Re} (circles) and Gaussian fitting (plenty line) for 7,15 and 31 channels.

Numerical verification

As an example, we consider the transmission of a WDM signal consisting of 7,15 or 31 2.5Gb/s NRZ channels (B_{ch}=2.5 GHz, Δ_{ch}=25 GHZ) over 80km NZ-DSF (D=8 ps/nm-km, $\alpha = 0.2$ dB/km, γ=1/W-km). For the simulation, independent sequences of 16x1204 bits per channels were considered and the emitting phase of the optical carriers were set randomly between 0 and 2π. The probability density function of δA_0^{Re} (for the central channel) as well as its Gaussian fitting are displayed in Fig. D.3. As expected, the PDF of δA_0^{Re} approaches the Gaussian distribution with an increased number of channels.

Extension to intra-channel effects

An similar study can be done for intra-channel interactions (iXPM, iFWM). Neglecting the impact of the (deterministic) self-pulse modulation, one shows that for highly-dispersive systems (i.e. for a large number of inter-bit interaction), real and imaginary parts of δA_0 follow centered Gaussian distributions.

Formulas

Let U, V be two random variables and a a real number. Noting μ the expectation (or mean) and σ the variance, it comes:

$$
\begin{aligned}
\mu(aU) &= a\mu(U) \\
\sigma^2(aU) &= a^2\sigma^2(U) \\
\mu(UV) &= \mu(U)\mu(V) + \sigma_{UV}^2 \\
\sigma_{UV}^2 &= \mu\left((U - \mu(U))(V - \mu(V))\right) \quad\quad\quad\text{(D.10)}
\end{aligned}
$$

when U and V are independent, their covariance σ_{UV}^2 is nil.

Appendix E

Optimal pre-compensation

In single-span transmission systems, the accumulated dispersion is given as :

$$D(z) = D_0 + \beta_2 z$$

D_0 being the pre-compensation and β_2 the fiber dispersion coefficient. As already discussed in 4.1.2, pre-compensation minimizing inter-bit interactions in amplitude-modulated systems, is the one maximizing the partial cancelation occurring between the real part of the nonlinear perturbations generated at z_1 and z_2 with $D(z_1) = -D(z_2)$ and $z_1 < z_2$ (see Eq. (4.13)). Noting $L_0 = -D_0/\beta_2$ so that $D(L_0) = 0$, the optimal pre-compensation is the one minimizing the following expression:

$$C(Do) = \int_0^{L_0} \left(e^{-3\alpha(L_0-x)} - e^{-3\alpha(L_0+x)} \right) dx + \int_{2L_0}^{L} e^{-3\alpha x}$$

In the above expression the fiber length L is assumed as least twice as large as L_0. The factor 3 in $e^{-3\alpha}$ accounts for the fact that the power of the generated nonlinear perturbation is proportional to $P(z)^3$, $P(z)$ being the channel power. The optimal pre-compensation is obtained by setting the derivative over Do of the above expression to zero:

$$D_{opt} \approx -\frac{2ln(2)}{3} \frac{\beta_2}{\alpha}$$

Appendix F

Transmitter and receiver noise

Transmitter noise

Most lasers used for fiber-optic communication are semiconductor lasers. The two fundamental noise mechanisms occurring during optical carrier generation are *electron-hole recombination* [3] and *spontaneous emission*, which is the dominant effect, leading to variations in the phase and intensity of the emitted light.

If low-noise lasers and ideal phase/frequency modulators are used, the transmitter noise can be neglected against receiver or optical amplifier noise in non-coherent transmission systems. Details to noise in semi-conductor laser can be found in [123] and [124].

Receiver noise

Receiver noise, leading to fluctuations in the detected current, consists mostly of two mechanisms occurring during photodetection: *thermal noise* and *shot noise* (*dark current noise* and *quantum noise*). In the following, we note $I(t) = RP_{in}(t) + i(t)$ the detected current, whit P_{in} the incident optical power, R the photodiode responsivity and $i(t)$ the current fluctuation due to noise.

Shot noise

Shot noise is noise caused by current fluctuations due to the discrete nature of charge carriers. Dark current noise and quantum noise are two types of noise that manifest themselves as shot noise. Dark current noise is independent of the optical signal and results from dark current that continues to flow in the photodiode when there is no incident light (spontaneous generation of electron-hole pairs). Quantum noise results from the random generation of electrons by the incident optical radiation and is thus signal dependent. The strength of the current fluctuations can be expressed by its variance:

$$\sigma_s^2 = <i^2(t)> = 2q(RP_{in} + I_d)\Delta_f \tag{F.1}$$

where I_d the dark current of the photodiode , Δ_f the effective noise bandwidth of the receiver (depending on the limited bandwidth of the photodiode and the electrical filter) and q the elementary electron charge. The shot-noise can be considered as a white noise[1] having the following power spectral density:

$$W_s(f) = q(RP_{in} + I_d) \tag{F.2}$$

Thermal noise

Thermal noise [125] is the noise resulting from the random motion of electrons in a conducting medium[2] leading to fluctuations in the current even in absence of applied voltage. The power spectral density of the thermal noise is given by[3]:

$$W_T(f) = 4k_B T/R_L \tag{F.3}$$

k_B is the Boltzmann's constant, T the conductor temperature and R_L the load resistor. According to Eq. (F.3), the thermal noise is a white noise giving rise to a variance of the

---

[1]Shot-noise is a stationary random Poisson process, which can be approximated by a Gaussian statistics [105].
[2]I.e. occurs in both photodetector and load resistor.
[3]for $f < 1$THz.

detected current equal to $\sigma_T^2 = S_T(f)\Delta_f$.

Publications

Conferences and workshops

K. Fischer, H. Louchet, S. Randel and K. Petermann, *A Simple Criterion for the Characterization of Nonlinear Impairments in Optical Transmission Systems*, Asia-Pacific Optical Communications, 2005 (APOC 2005)

H. Louchet, K. Petermann, A. Robinson and R. Epworth, *Introduction to the Concept of Nonlinear Diffusion Bandwidth*, 31st European Conference on Optical Communication (ECOC 2005)

H. Louchet, A. Hodzic, K. Petermann, A. Robinson and R. Epworth, *Top-Down analysis of WDM transmission systems* (invited paper), 10th OptoElectronics and Communications Conference (OECC 2005)

H. Louchet, A. Hodzic, K. Petermann, A. Robinson and R. Epworth, *Top-down analysis of high capacity optical transmission systems* (invited paper), 7th International Conference on Transparent Optical Networks (ICTON 2005)

H. Louchet and K. Petermann, *Limitation of Nonlinear Impairments in Flexible WDM Networks*, ITG Workshop Modellierung photonischer Komponenten und Systeme, Dortmund, Germany, February 2005

H. Louchet, K. Petermann, A. Robinson and R. Epworth, *On the spectral information distribution in optical fibres*, 17th Annual Meeting of the IEEE Lasers and Electro-Optics Society (LEOS 2004)

M. Malach, H. Louchet, A. Hodzic and K. Petermann, *Transmission of 10 Gb/s WDM-channels along variable line infrastructures*, 6th International Conference on Transparent

Optical Networks (ICTON 2004)

H. Louchet, A. Hodzic and K. Petermann, *Analytical Model for Nonlinear DWDM Transmissions*, 29st European Conference on Optical Communication (ECOC 2003)

H. Louchet and K. Petermann, *Analytical Model for the Design of Multi-span DWDM Systems*, ITG Workshop Modellierung photonischer Komponenten und Systeme, Backnang, Germany, November 2003

A. Hodzic, B. Konrad, H. Louchet, K. Petermann and S. Randel, *Strategies for spectrally efficient optical fiber communication systems with direct detection*, 5th International Conference on Transparent Optical Networks (ICTON 2003)

H. Louchet and K. Petermann, *Assessment of Nonlinear Impairments*, ITG Workshop Modellierung photonischer Komponenten und Systeme, Berlin, Germany, January 2003

Journals

H. Louchet, A. Hodzic, K. Petermann, A. Robinson and R. Epworth, *Simple Criterion for the Characterization of Nonlinear Impairments in Dispersion managed Optical Transmission Systems*, IEEE Photonics Technology Letters, October 2005

H. Louchet, K. Petermann, A. Robinson and R. Epworth, *Analytical model for the design of multispan DWDM transmission systems*, IEEE Photonics Technology Letters, January 2005

H. Louchet, A. Hodzic, K. Petermann, *Analytical model for the performance evaluation of DWDM transmission systems*, IEEE Photonics Technology Letters, September 2003

Bibliography

[1] K. Kao and G. Hockham, "Dielectric-fibre surface waveguides for optical frequencies," *PROC. IEE*, vol. 113, pp. 1151–1158, 1966.

[2] TIA, "Fiber Optic Network Capacity and Utilization," Telecommunications Industry Association, Tech. Rep., September 2002.

[3] G. Agrawal, *Fiber-Optic Communication Systems*.   John Wiley & Sons, 1997.

[4] E. Voges and K. Petermann, *Optische Kommunikationstechnik*.   Springer, 2002.

[5] C. Davis, *Lasers and Electro-Optics*.   Cambridge University Press, 1996.

[6] C. Silva, A. J. Seeds, and P. J. Williams, "Terahertz Span > 60-Channel Exact Frequency Dense WDM Source Using Comb Generation and SG-DBR Injection-Locked Laser Filtering," *IEEE Photonics Technol. Lett.*, vol. 13, no. 4, pp. 370–372, April 2001.

[7] J. Kim, O. Boyraz, and M. Islam, "150 channel ultra-DWDM source with N 10GHz spacing utilizing longitudinal mode slicing of supercontinuum," in *Optical Fiber Communication Conference (OFC)*, vol. 3, 2000, pp. 5–7.

[8] T. Yamanaka, "Ultrafast electroabsorption modulators with traveling-wave electrodes," in *European Conference on Optical Communication (ECOC)*, no. We.F.3.1, 2001.

[9] E. Desurvire, *Erbium-doped fiber amplifiers*.   Wiley, 2002.

[10] A. F. Evans, J. Grochocinski, A. Rahman, C. Reynolds, and M. Vasilyev, "Distributed amplification: How Raman gain impacts other fiber nonlinearities," in *Optical Fiber Communication Conference (OFC)*, vol. 1, March 2001.

[11] M. Chbat and H. A. Fevrier, "Low-cost, high-capacity ultra-long-haul WDM systems based on wide-band Raman amplification," in *European Conference on Optical Communication (ECOC)*, vol. 3, no. 3.7, September 2002.

[12] M. Islam, "Raman amplifiers for telecommunications," *IEEE J. Select. Topics Quantum Electron.*, vol. 8, p. 548–559, 2002.

[13] E. Desurvire, "Optical communications in 2025," in *European Conference on Optical Communication (ECOC)*, vol. 1, 2005, pp. 5–6.

[14] P. Mitra and J. B. Stark, "Nonlinear Limits to the Information Capacity," *Nature*, vol. 411, pp. 1027–1030, 2001.

[15] K.-P. Ho and H. Cuei, "Generation of Arbitrary Quadrature Signals Using One Dual-Drive Modulator," *IEEE J. Lightwave Technol.*, vol. 23, no. 2, pp. 764–770, 2005.

[16] J. McNicol, M. O'Sullivan, K. Roberts, A. Comeau, D. McGhan, and L. Strawczynski, "Electrical Domain Compensation of Optical Dispersion," in *Optical Fiber Communication Conference (OFC)*, no. OThJ3, 2005.

[17] H. Carrer, D. E. Crivelli, and M. R. Hueda, "Maximum-Likelihood Sequence Estimation in Dispersive Optical Channels," *IEEE J. Lightwave Technol.*, vol. 23, no. 2, pp. 749–763, 2005.

[18] J. Stark, P. Mitra, and S. Sengupta, "Information capacity of nonlinear wavelength division multiplexing fiber optic transmission line," *Opt. Fiber Technol.*, vol. 7, pp. 275–288, 2001.

[19] E. Narimanov and P. Mitra, "The channel capacity of a fiber optics communication system: Perturbation theory," *IEEE J. Lightwave Technol.*, vol. 20, pp. 530–537, 2002.

[20] J. Tang, "The multispan Effects of Kerr Nonlinearity and Amplifier Noises on Shannon Channel Capacity of a Dispersion-free Nonlinear Optical Fiber," *IEEE J. Lightwave Technol.*, vol. 19, pp. 1110–1115, 2001.

[21] ——, "The Channel Capacity of a Multispan DWDM System Employing Dispersive Nonlinear Optical Fibers and Ideal Coherent Optical Receiver," *IEEE J. Lightwave Technol.*, vol. 20, no. 7, pp. 1095–1101, July 2002.

[22] E. Desurvire, "Quantum noise model for ultimate information-capacity limits in long-haul wdm transmission," *IEE Electronics Lett.*, vol. 38, pp. 983–984, 2002.

[23] B. Xu and M. Brandt-Pearce, "Comparison of FWM-and XPM-Induced Crosstalk Using the Volterra Series Transfer Function Method," *IEEE J. Lightwave Technol.*, vol. 21, pp. 40–53, 2003.

[24] P. Diament, *Wave Transmission and Fiber Optics.* Macmillan, New York, 1990.

[25] G. Agrawal, *Nonlinear Fiber Optics*, 2nd ed. Academic Press, 1995.

[26] Y. Shen, *Principles of Nonlinear Optics.* Wiley, New York, 1984.

[27] D. Marcuse, *Theors of Dielectric Optical Waveguides.* Academic Press, San Diego, 1991.

[28] Technical Staff of CSELT, *Optical Fibre Communication.* CSELT, 1980.

[29] S. Walker, "Rapid Modeling and Estimation of Total Spectral Loss in Optical Fibers," *IEEE J. Lightwave Technol.*, vol. 4, pp. 1125–1131, 1986.

[30] E. A. J. Marcatili, "Bends in optical dielectric guides," *Bell Syst. Tech. J.*, vol. 48, p. 2103, 1969.

[31] K. Petermann, "Microbending loss in monomode fibres," *IEE Electronics Lett.*, vol. 12, pp. 107–109, 1976.

[32] U. B. Unrau, "Specialty Fibers for Optical Amplifiers in Communications," in *European Conference on Optical Communication (ECOC)*, no. Mo.B.4, 2001.

[33] I. P. Kaminov, "Polarization in optical fibers," *IEEE J. Quantum Electron.*, vol. 17, pp. 15–22, 1981.

[34] S. Huard, *Polarization of Light.* Wiley, 1996.

[35] C. Menyuk, "Pulse Propagation in an Elliptically Birefringent Kerr Medium," *IEEE J. Quantum Electron.*, vol. 25, pp. 2674–2682, 1989.

[36] I. Kaminov and T. Koch, *Optical Fiber Telecommunication IIIA.* Academic Press, 1997.

[37] I. Kaminov and L. Tingye, *Optical Fiber Telecommunications IVB Systems and Impairments.* Academic Press, 2002.

[38] A. Hasegawa and F. Taper, "Transmission of stationary nonlinear optical pulses in dispersive dielectric fibers I. Anomalous dispersion," *Appl. Physics Lett.*, vol. 23, pp. 142–144, 1973.

[39] K. Inoue, "Four wave mixing in Optical Fibers in the zero-dispesion wavelength region," *IEEE J. Lightwave Technol.*, vol. 10, pp. 1553–1561, 1992.

[40] M. Wu, "Fiber Nonlinearity Limitations in Ultra-Dense WDM Systems," *IEEE J. Lightwave Technol.*, vol. 22, pp. 1483–1497, 2004.

[41] K. Inoue, "Polarization effect on four-wave mixing efficiency in a single-mode fiber," *IEEE J. Quantum Electron.*, vol. 28, p. 883, 1992.

[42] Y. Emori, "Ultrabroadband fiber Raman amplifiers," in *European Conference on Optical Communication (ECOC)*, 2002.

[43] A. Chraplyvy, "Limitations on Lightwave Communication Imposed by Optical-Fiber Nonlinearities," *IEEE J. Lightwave Technol.*, vol. 8, p. 1548, 1990.

[44] F. Forghieri, R. Tkach, and A. Charplyvy, *Fiber Nonlinearities and Their Impact on Transmission Systems*, I. Kaminov and T. Koch, Eds. Academic Press, 1997.

[45] F. Forghieri, "Granularity in wdm networks: The role of fiber nonlinearities," *IEEE Photonics Technol. Lett.*, vol. 8, no. 10, pp. 1400–1402, 1996.

[46] S. Chernikov and J. Taylor, "Measurement of normalization factor of n2 for random polarization in optical fibers," *OSA Optics Lett.*, vol. 21, pp. 1559–1561, 1996.

[47] D. Marcuse, "Apllication of the manakov-pmd equation to studies of signal propagation in opticalfibers with randomly varying birefringence," *IEEE J. Lightwave Technol.*, vol. 15, pp. 1735–1745, 1997.

[48] M. Schetzen, *The Volterra and Wiener Theories of Nonlinear Systems.* Wiley, 1989.

[49] W. Rugh, *Nonlinear System Theory The Volterra/Wiener Approach.* Johns Hopkins University Press, 1981.

[50] K. Peddanarappagari and M. Brandt-Pearce, "Volterra Series Transfer Function of Single-Mode Fibers," *IEEE J. Lightwave Technol.*, vol. 15, pp. 2232–2241, 1997.

[51] J. Gordon and L. Mollenauer, "Phase noise in photonic communications systems using linear amplifiers," *OSA Optics Lett.*, vol. 15, pp. 1351–1353, december 1990.

[52] J. Bouteiller, K. Brar, and C. Headley, "Quasi-constant signal power transmission," in *European Conference on Optical Communication (ECOC)*, vol. 3, September 2002.

[53] J.-H. Lee, "Analysis and Characterization of Fiber Nonlinearities with Deterministic and Stochastic Signal Sources," Ph.D. dissertation, Virginia Polytechnic Institute and State University, 2000.

[54] R. Maurer and S. Narayanan, "Noise loading analysis of a third-order nonlinear system with memory," *IEEE Trans. Commun. Technol.*, vol. 16, pp. 701–712., 1968.

[55] M. Schwartz, W. Benner, and S. Stein, *Communication systems and techniques.* McGraw-Hill, 1966.

[56] TIA-EIA, "TIA/EIA-526-19 standard," http://global.ihs.com, Tech. Rep.

[57] C. E. Shannon, "A Mathematical Theory of Communication," *Bell Syst. Tech. J.*, vol. 27, pp. 379–423, 623–656, 1948.

[58] R. McDonough and A. Whalen, *Detection of Signals in Noise.* Academic Press, 1971.

[59] S. Personic, "Receiver design for digital fiber optic communications systems," *Bell Syst. Tech.*, vol. 6, July 1973.

[60] N. Bergamo, F. Kerfoot, and C. Davidson, "Margin measurements in Optical Amplifer Systems," *IEEE Photonics Technol. Lett.*, vol. 5, pp. 304–306, 1993.

[61] C. J. Anderson and J. A. Lyle, "Technique for evaluating system performance using Q in numerical simulations exibiting intersymbol interference," *IEE Electronics Lett.*, vol. 30, pp. 71–72, January 1994.

[62] D. Marcuse, "Derivation of Analytical expression for the Bit-Error Probability in lightwave Systems with optical amplifier," *IEEE J. Lightwave Technol.*, vol. 8, pp. 1816–1823, 1990.

[63] E. Desurvire, D. Bayart, B. Desthieux, and S. Bigo, *Erbium-doped Fiber Amplifiers -Device and System Developments.* John Wiley & Sons, 2002.

[64] P. J. Winzer, M. Pfennigbauer, and R.-J. Essiambre, "Coherent Crosstalk in Ultra-dense WDM Systems," *IEEE J. Lightwave Technol.*, vol. 23, pp. 1734–1744, 2005.

[65] E. Forestieri, "Evaluating the Error Probability in Lightwave Systems with Chromatic Dispersion, Arbitrary Pulse Shape and Pre- and Postdetection Filtering," *IEEE J. Lightwave Technol.*, vol. 18, pp. 1493–1503, 2000.

[66] R.-J. Essiambre, "Intra-Channel Effects in High-Speed Pseudo-Linear Transmission," in *Lasers and Electro-Optics Society (LEOS), annual meeting*, Lasers and E.-O. Society, Eds., vol. 2, 2003, pp. 840–841.

[67] *VPItransmissionMaker, VPIsystems.*

[68] B. Wichman and I. Hill, "Algorithm 183. An efficient and portable pseudo-random bit generator," *Appl. Stat.*, vol. 31, pp. 188–190, 1982.

[69] B. Konrad, "Impact of Fiber Chromatic Dispersion in High-Speed TDM Transmission Systems," *IEEE J. Lightwave Technol.*, vol. 20, no. 12, pp. 2129–2135, December 2002.

[70] A. Cauvin, "Single-channel nonlinear impairments at various bit-rate in dispersion managed systems," in *European Conference on Optical Communication (ECOC)*, 2003.

[71] A. Cauvin, Y. Frignac, and S. Bigo, "Nonlinear impairments at various bit rates in single-channel dispersion-managed systems," *IEE Electronics Lett.*, vol. 39, pp. 1670–1, 2003.

[72] A. Judy, "Optimizing fiber dispersion for DWDM systems," in *Optical Fiber Communication Conference (OFC)*, February 1997, pp. 272 – 273.

[73] Y. Frignac, "Numerical optimization of pre-and in-line dispersion compensation in dispersion-managed systems at 40 Gbit/s," in *Optical Fiber Communication Conference (OFC)*, no. ThFF5, 2004.

[74] Y. Frignac, S. Bigo, and J. Antona, "Enhanced analytical engineering rule for fast optimization of dispersion maps in 40Gb-based transmission systems," in *Optical Fiber Communication Conference (OFC)*, 2004.

[75] Y. Frignac, J.-C. Antona, S. Bigo, and J.-P. Hamaide, "Numerical optimization of pre- and in-line dispersion compensation in dispersion-managed systems at 40 Gbit/s," in *Optical Fiber Communication Conference (OFC)*, March 2002, pp. 612 – 613.

[76] Y. Frignac and S.Bigo, "Numerical optimization of residual dispersion in dispersion-managed systems at 40 Gbit/s," in *Optical Fiber Communication Conference (OFC)*, vol. 1, 2000, pp. 48–50.

[77] A. Mecozzi, C. Clausen, M. Shtaif, S.-G. Park, and H. Gnauck, "Cancellation of Timing and Amplitude Jitter in Symmetric Links Using Highly Dispersed Pulses," *IEEE Photonics Technol. Lett.*, vol. 13, pp. 445–447, May 2001.

[78] M. J. Ablowitz and T. Hirooka, "Resonant Intrachannel Pulse Interactions in Dispersion-Managed Transmission Systems," *IEEE J. Select. Topics Quantum Electron.*, vol. 8, no. 3, p. 603–615, 2002.

[79] S. Kumar, J. C. Mauro, S. Raghavan, and D. Q. Chowdhury, "Intrachannel Nonlinear Penalties in Dispersion-Managed Transmission Systems," *IEEE J. Select. Topics Quantum Electron.*, vol. 8, no. 3, p. 626–631, 2002.

[80] R. Killey, H. Thiele, V. Mikhailov, and P.Bayvel, "Reduction of Intrachannel Nonlinear Distortion in 40-Gb/s-Based WDM Transmission over Standard Fiber," *IEEE Photonics Technol. Lett.*, vol. 12, pp. 1624–1626, 2000.

[81] A. Hodzic, "Investigations of high bit rate optical transmission systems employing a channel data rate of 40 Gb/s," Ph.D. dissertation, Technische Universität Berlin, 2004.

[82] L. Xiang and al, "Performance analysis of time-polarization multiplexed 40-Gb/s RZ-DPSK DWDM," *IEEE Photonics Technol. Lett.*, pp. 302–304, January 2004.

[83] A. Hodzic, N. Hecker-Denschlag, M. Winter, S. Jansen, K. Saucke, and K. Petermann, "Performance improvement of 10 Gb/s/ch NRZ DWDM transmission using orthogonal polarizations of adjacent bits in a single wavelength channel," in *Lasers and Electro-Optics Society (LEOS), annual meeting*, 2003, pp. 845 – 846.

[84] G. Charlet, R. Ischler, A. Klekamp, P. Tran, H. Mardoyan, L. Pierre, W. Idler, , and S. Bigo, "WDM bit-to-bit alternate polarization RZ-DPSK transmission at 40x42.7 Gb/s over transpacific distance with large Q factor margin," in *European Conference on Optical Communication (ECOC)*, 2004, pp. 48–49.

[85] A. Hodzic, B. Konrad, H. Louchet, K. Petermann, and S. Randel, "Strategies for spectrally efficient optical fiber communication systems with direct detection," in *International Conference on Transparent Optical Networks (ICTON)*, 2003, pp. 58 – 63.

[86] S. Warm, "Einfluss der Polarization auf die Kapazität von optischen DWDM Übertragungsystemen," Master's thesis, Technische Universität Berlin, 2004.

[87] S. Chernikov and J. Taylor, "Measurements of n2 and normalization factor for random polarization in optical fibers," in *Optical Fiber Communication Conference (OFC)*, no. Ths5, 1996, pp. 289–290.

[88] H. Nyquist, "Certain factor affecting the telegraph speed," *Bell Syst. Tech. J*, vol. 3, pp. 324–352, 1924.

[89] R. Hartley, "Transmission of information," *Bell Syst. Tech. J.*, vol. 7, pp. 535–563, 1928.

[90] N. Wiener, *Cybernetics, Chapter III: Time Series, Information and Communication.* Wiley, 1948.

[91] W. Tuller, "Theoretical limitation on the rate of transmission of inforamtion," Ph.D. dissertation, MIT, Cambridge, 1949.

[92] M. Pinsker, *Information and Information Stability of Random Variables and Processes.* Holden Day, 1964.

[93] S. Arimoto, "An algorithm for computing the capacity of arbitrary memoryless channels," *IEEE Trans. Inform. Theory*, vol. IT-18, pp. 14–20, 1972.

[94] R. Blahut, "Computation of Channel Capacity and rate-distortion functions," *IEEE Trans. Inform. Theory*, vol. IT-18, pp. 460–473, 1972.

[95] A. Gnauck and R. Jopson, *Optical Fiber Telecommunications IIIA (Dispersion Compensation for Optical Fiber Systems)*, I. Kaminov and T. Koch, Eds. Academic Press, 1997.

[96] H. Sunnerud, C. Xie, M. Karlsson, and P. Andrekson, "Outage probability in PMD compensated transmission systems," in *European Conference on Optical Communication (ECOC)*, 2001, p. 204–205.

[97] L. Yan, Q. Yu, T. Lou, A. Willner, and X. Yao., "Compensation of higher order polarization mode dispersion using phase modulation and polarization control in the transmitter," *IEEE Photonics Technol. Lett.*, vol. 14, p. 858–860, 2002.

[98] C. Kurtzke, "Optical-phase conjugation-a new approach to future high-capacity optical communication systems," in *IEE Colloquium on High Capacity Optical Communications*, May 1994.

[99] D. Breuer, C. Kurtzke, and K. Petermann, "Upgrading the embedded standard-fibre network by optical-phase conjugation," *IEE Proceedings-Optoelectronics*, vol. 143, pp. 205 – 208, June 1996.

[100] A. Chowdhury and R.-J. Essiambre, "Optical phase conjugation and pseudolinear transmission," *OSA Optics Lett.*, vol. 29, pp. 1105–1107, 2004.

[101] K. Turitsyn, S. Derevyanko, I. Yurkevich, and S. Turitsyn, "Information Capacity of Optical Fiber Channels with Zero Average Dispersion," *Physical Review Letters*, vol. 91, pp. 203 901–1 203 901–4, 2003.

[102] J. Wang and K. Petermann, "Small signal analysis for dispersive optical fiber communication systems," *IEEE J. Lightwave Technol.*, vol. 10, pp. 96–100, 1992.

[103] S. Betti and M. Giaconi, "Analysis of the cross-phase modulation effect in WDM optical systems," *IEEE Photonics Technol. Lett.*, vol. 13, pp. 43–45, 2001.

[104] R. Hui, K. Demarest, and C. Allen, "Cross-Phase Modulation in Multispan WDM Optical Fiber Systems," *IEEE J. Lightwave Technol.*, vol. 17, pp. 1018–1026, 1999.

[105] J. Goodman, *Statistical Optics.* Wiley, 2000.

[106] P. Cho, V. Grigoryan, Y. Godin, A. Salamon, and Y. Achiam, "Transmission of 25-Gb/s RZ-DQPSK signals with 25-GHz channel spacing over 1000km over SMF-28 fiber," *IEEE Photonics Technol. Lett.*, vol. 15, pp. 473–475, 2003.

[107] C. Pi-Yang and W. Way, "Ultimate capacity of a laser diode in transporting multichannel M-QAM signals," *IEEE J. Lightwave Technol.*, vol. 15, pp. 1914 – 1924, October 1997.

[108] M. Ohm, "Optical 8-DPSK and receiver with direct detection and multilevel electrical signals," in *IEEE/LEOS Workshop on Advanced Modulation Formats*, 2004, pp. 45 – 46.

[109] M. Seimetz, "Multi-format transmitters for coherent optical M-PSK and M-QAM transmission," in *International Conference on Transparent Optical Networks (IC-TON)*, 2005.

[110] F. Abramovich and P. Bayvel, "Some Statistical Remarks on the Derivation of BER in Amplified Optical Communication Systems," *IEEE Transaction on Communications*, vol. 45, pp. 1032–1034, 1997.

[111] K.-P. Ho, "Exact Evaluation of the Capacity forIntensity-Modulated Direct-Detection Channels With Optical Amplifier Noises," *IEEE Photonics Technol. Lett.*, vol. 17, pp. 858–860, 2005.

[112] K. Ho, "Channel Capacity of WDM System Using Constant-Intensity Modulation Formats," in *Optical Fiber Communication Conference (OFC)*, no. ThGG85, 2002.

[113] J. Kahn and K. Ho, "Spectral Efiiciency Limits and Modulation/Detection Techniques for DWDM Systems," *IEEE J. Select. Topics Quantum Electron.*, vol. 10, pp. 259–272, 2004.

[114] B. Wu and E. Narimanov, "Information Capacity of Nonlinear Fiber-Optical Systems," in *Optical Fiber Communication Conference (OFC)*, 2005.

[115] C. Berrou, A. Glavieux, and P. Thitimajshima, "Near Shannon limit error-correcting coding and decoding: Turbo-codes (1)," in *Proc. IEEE Int. Conf. Communication 93*, vol. 2, 93, pp. 1064–1070.

[116] S. Savory and A. Hadjifotiou, "Laser linewidth requirements for optical DQPSK systems," *IEEE Photonics Technol. Lett.*, vol. 16, pp. 930 – 932, 2004.

[117] D.-S. Ly-Gagnon, K. Katoh, and K. Kikuchi, "Coherent Demodulation of Differential 8-Phase-Shift Keying with Optical Phase Diversity and Digital Signal Processing," in *Lasers and Electro-Optics Society (LEOS), annual meeting*, 2004.

[118] R. Hardin and F. Tappert, "Application of the Split-step Fourier Method to the Numerical Solution of Nonlinear and Variable Coefficient Wave Equation," *SIAM Rev*, vol. 15, p. 423, 1973.

[119] VPIsystems, *Photonics Module Reference Manual (FiberNLS)*.

[120] J. Cooley and J. Tukey, "An Algorithm for the Machine Calculation of Complex Fourier Series," *Math. Comput.*, vol. 19, p. 297, 1965.

[121] [Online]. Available: http://mathworld.wolfram.com/LyapunovCondition.html

[122] A. Jeffrey, *Handbook of Mathematical Formulas and Integrals*. Academic Press, 2000.

[123] C. Henry, "Theory of the linewidth of semiconductor lasers," *IEEE J. Quantum Electron.*, vol. 18, pp. 259 – 264, 1982.

[124] ——, "Theory of the phase noise and power spectrum of a single mode injection laser," *IEEE J. Quantum Electron.*, vol. 19, pp. 1391 – 1397, 1983.

[125] H. Nyquist, "Thermal Agitation of Electric Charge in Conductors," *Phys. Rev.*, vol. 32, p. 110, 1928.